

Winter 2011

A methodology for evaluating the implications of climate change on the design and performance of flexible pavements

William C. Meagher III.
University of New Hampshire, Durham

Follow this and additional works at: <https://scholars.unh.edu/thesis>

Recommended Citation

Meagher, William C. III., "A methodology for evaluating the implications of climate change on the design and performance of flexible pavements" (2011). *Master's Theses and Capstones*. 689.
<https://scholars.unh.edu/thesis/689>

This Thesis is brought to you for free and open access by the Student Scholarship at University of New Hampshire Scholars' Repository. It has been accepted for inclusion in Master's Theses and Capstones by an authorized administrator of University of New Hampshire Scholars' Repository. For more information, please contact nicole.hentz@unh.edu.

A METHODOLOGY FOR EVALUATING THE IMPLICATIONS OF CLIMATE CHANGE
ON THE DESIGN AND PERFORMANCE OF FLEXIBLE PAVEMENTS

BY

William C. Meagher III

Bachelor of Science in Civil Engineering, University of New Hampshire, 2009

THESIS

Submitted to the University of New Hampshire

In Partial Fulfillment of

the Requirements for the Degree of

Master of Science

In

Civil Engineering

December, 2011

UMI Number: 1507827

All rights reserved

INFORMATION TO ALL USERS

The quality of this reproduction is dependent upon the quality of the copy submitted.

In the unlikely event that the author did not send a complete manuscript and there are missing pages, these will be noted. Also, if material had to be removed, a note will indicate the deletion.



UMI 1507827

Copyright 2012 by ProQuest LLC.

All rights reserved. This edition of the work is protected against unauthorized copying under Title 17, United States Code.

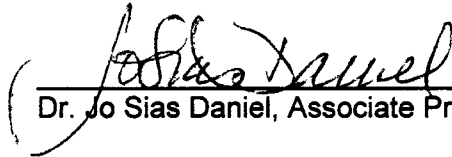


ProQuest LLC
789 East Eisenhower Parkway
P.O. Box 1346
Ann Arbor, MI 48106-1346

This thesis has been examined and approved.



Thesis Director, Dr. Jennifer Jacobs, Professor of Civil Engineering



Dr. Jo Sias Daniel, Associate Professor of Civil Engineering



Dr. Ernst Linder, Professor of Mathematics & Statistics

12/1/2011

Date

ACKNOWLEDGEMENTS

My utmost gratitude goes to my thesis advisor, Dr. Jennifer Jacobs, because without her support this work would not have been possible. Her expertise and enthusiasm were invaluable to the execution of this thesis, and her detailed and constructive comments brought forth the best in this present thesis.

I am most indebted to my committee members, Dr. Jo Sias Daniel and Dr. Ernst Linder, whose subject matter expertise and guidance helped me complete this thesis.

I would also like to thank my family for their support during the past few years. I would especially like to recognize my wife, Megan, who stood by me during my late night and weekend writing sessions. Without her support at home, I would still be writing.

TABLE OF CONTENTS

ACKNOWLEDGEMENTS.....	iii
LIST OF TABLES	vi
LIST OF FIGURES	vii
ABSTRACT.....	ix
CHAPTER I - BACKGROUND.....	1
Motivation.....	1
Mechanistic-Empirical Pavement Design Guide (M-E PDG) (Version 1.1).....	2
Principles of the Mechanistic-Empirical Approach.....	3
Climatic Modeling – Enhanced Integrated Climate Model (Version 3.2)	6
Structural Response Modeling	8
Climate Modeling.....	9
CHAPTER II - DATA & INPUTS	11
Climate Model Data.....	11
Data Structure Overview	14
Finding & Downloading Data	14
North American Regional Climate Change Program Data Overview	15
Project Data Overview	16
Variables.....	17
Temperature	17
Precipitation.....	21
Percent Sunshine	22
Pavement Model Data.....	23
CHAPTER III - METHODOLOGY	29
CHAPTER IV – RESULTS.....	41
CDF-Transformation.....	42
Model Temperature.....	56
Hindcast Model Temperature.....	56
Future Model Temperature	59
Hindcast Model Results	64
Alligator Cracking.....	64
AC Rutting	65
Future Model Results.....	74
Alligator Cracking.....	74
AC Rutting	75
Future Model versus Hindcast Model.....	84

Alligator Cracking.....	84
AC Rutting	85
CHAPTER V – SUMMARY	90
Conclusion.....	90
Future Work.....	93
LIST OF REFERENCES.....	94
APPENDIX A	96
APPENDIX B	97
APPENDIX C	99
APPENDIX D	104

LIST OF TABLES

Table 1 - NARCCAP Table 2: Primary 3-hourly Surface Fields (2-D)	14
Table 2 - Hindcast Model Data Precipitation Event Comparison	22
Table 3 - Unbound M-E PDG Material Inputs	24
Table 4 - M-E PDG Stations and Station Record Starting Date	27
Table 5 - Conversion of RCM to M-E PDG Variables	33
Table 6 - Kolomogrov-Smirnov Test Values, Critical Value (*) = 0.192. Hindcast is for 1970 to 2000. Future is for 2040 to 2070.	55
Table 7 - Difference (Model Prediction – Measured Value) in Hindcast Model Temperature.....	58
Table 8 - Difference (Model Prediction – Measured Value) in Future Model Temperature	61
Table 9 - Difference (Future - Hindcast) in Model Temperature.....	62
Table 10 - Predicted Distresses for the Hindcast Climate Scenarios.....	67
Table 11 - Hindcast Model Pavement Age (in Months) at Failure.....	67
Table 12 - Predicted Distresses for the Future Climate Scenarios	77
Table 13 - Future Model Pavement Age (in Months) at Failure	77
Table 14 - Differences in Distresses between Model Periods.....	86
Table 15 - Difference in Time to Distress (Future - Hindcast) in Months. Negative values indicate distress occurs earlier.	87

LIST OF FIGURES

Figure 1 - Schematic of the Design Process (Design Guide, 2004).....	5
Figure 2 - Study location including the center of the original Atmosphere-Ocean General Circulation Model and Regional Climate Model grid cells as well as the M-E PDG climate stations. The four study sites are Berlin, NH, Boston, MA, Concord, NH, and Portland, ME.....	13
Figure 3 – Hindcast Model Temperature Data Compared to Observed M-E PDG Station Data.....	18
Figure 4 - Typical Cumulative Distribution of Temperature Data (CRCM+CGCM3 Concord, NH).....	20
Figure 5 - Typical Application of the CDF-t Method (CRCM+CGCM3 Concord, NH).....	20
Figure 6 - Typical Pavement Cross Sections.....	25
Figure 7 - Study Sites and Associated Model Points Identified.....	28
Figure 8 - Methodology Process Chart.....	30
Figure 9 - Observed Data CDF to CRCM + CGCM3 RCM Model Overlap CDF for Concord, NH.....	37
Figure 10 - CDF-t for the CRCM + CGCM3 RCM Model Overlap for Concord, NH.....	37
Figure 11 - CDF-t for the CRCM + CGCM3 RCM Model 1970 - 2000 for Concord, NH.....	38
Figure 12 - CDF-t for the CRCM + CGCM3 RCM Model 2040 - 2070 for Concord, NH.....	38
Figure 13 - CDF-t for CRCM+CGCM3 Model 1970 - 2000 for Berlin, NH.....	43
Figure 14 - CDF-t for CRCM+CGCM3 Model 2040 - 2070 for Berlin, NH.....	43
Figure 15 - CDF-t for RCM3+CGCM3 Model 1970 - 2000 for Berlin, NH.....	44
Figure 16 - CDF-t for RCM3+CGCM3 Model 2040 - 2070 for Berlin, NH.....	44
Figure 17 - CDF-t for RCM3+GFDL Model 1970 - 2000 for Berlin, NH.....	45
Figure 18 - CDF-t for RCM3+GFDL Model 2040 - 2070 for Berlin, NH.....	45
Figure 19 - CDF-t for CRCM+CGCM3 Model 1970 - 2000 for Boston, MA.....	46
Figure 20 - CDF-t for CRCM+CGCM3 for Model 2040 – 2070 for Boston, MA.....	46
Figure 21 - CDF-t for RCM3+CGCM3 Model 1970 - 2000 for Boston, MA.....	47
Figure 22 - CDF-t for RCM3+CGCM3 Model 2040 - 2070 for Boston, MA.....	47
Figure 23 - CDF-t for RCM3+GFDL Model 1970 - 2000 for Boston, MA.....	48
Figure 24 - CDF-t for RCM3+GFDL Model 2040 - 2070 for Boston, MA.....	48
Figure 25 - CDF-t for CRCM+CGCM3 Model 1970 - 2000 for Concord, NH.....	49
Figure 26 - CDF-t for CRCM+CGCM3 Model 2040 - 2070 for Concord, NH.....	49

Figure 27 - CDF-t for RCM3+CGCM3 Model 1970 - 2000 for Concord, NH	50
Figure 28 - CDF-t for RCM3+CGCM3 Model 2040 - 2070 for Concord, NH	50
Figure 29 - CDF-t for RCM3+GFDL Model 1970 - 2000 for Concord, NH	51
Figure 30 - CDF-t for RCM3+GFDL Model 2040 - 2070 for Concord, NH	51
Figure 31 - CDF-t for CRCM+CGCM3 Model 1970 - 2000 for Portland, ME	52
Figure 32 - CDF-t for CRCM+CGCM3 Model 2040 - 2070 for Portland, ME	52
Figure 33 - CDF-t for RCM3+CGCM3 Model 1970 - 2000 for Portland, ME	53
Figure 34 - CDF-t for RCM3+CGCM3 Model 2040 - 2070 for Portland, ME	53
Figure 35 - CDF-t for RCM3+GFDL Model 1970 - 2000 for Portland, ME	54
Figure 36 - CDF-t for RCM3+GFDL Model 2040 - 2070 for Portland, ME	54
Figure 37 - Hindcast Model Mean Monthly Temperature	57
Figure 38 - Future Model Mean Monthly Temperature.....	60
Figure 39 - Hindcast Model Secondary Alligator Cracking.....	68
Figure 40 - Hindcast Model Interstate Alligator Cracking.....	69
Figure 41 - Hindcast Model Secondary AC Rutting	70
Figure 42 - Hindcast Model Interstate AC Rutting.....	71
Figure 43 - Percent Difference in Alligator Cracking from Baseline for the Hindcast Model Period	72
Figure 44 - Percent Difference in AC Rutting from Baseline for the Hindcast Model Period.....	73
Figure 45 - Future Model Secondary Alligator Cracking	78
Figure 46 - Future Model Interstate Alligator Cracking.....	79
Figure 47 - Future Model Secondary AC Rutting	80
Figure 48 - Future Model Interstate AC Rutting	81
Figure 49 - Percent Difference in Alligator Cracking from Baseline for the Future Model Period.....	82
Figure 50 - Percent Difference in AC Rutting from Baseline for the Future Model Period	83
Figure 51 - Percent Difference in Alligator Cracking between Model Periods.....	88
Figure 52 - Percent Difference in AC Rutting between Model Periods	89

ABSTRACT

A METHODOLOGY FOR EVALUATING THE IMPLICATIONS OF CLIMATE CHANGE ON THE DESIGN AND PERFORMANCE OF FLEXIBLE PAVEMENTS

By

William C. Meagher III

University of New Hampshire, December, 2011

A methodology is presented by which the implications of climate change on pavement deterioration can be assessed. This work focuses on the preparation and use of climate model datasets as inputs into the Mechanistic-Empirical Pavement Design Guide model to simulate pavement performance and deterioration over time. The methodology is illustrated using climate model temperature data from three North American Regional Climate Change Assessment Program scenarios at four sites across New England for alligator cracking and asphalt concrete rutting. The change in alligator cracking was shown to be negligible, while the difference in rutting was up to 31% between future and hindcast model periods; it suggests that climate change needs to be considered for pavement design and management. *Additional work needs to be done using the proposed methodology in converting and running the remaining deterioration relevant variables in model scenarios to fully assess the implications of climate change on pavement deterioration.*

CHAPTER I - BACKGROUND

Motivation

Climatic conditions play an important role in the properties of pavement materials and affect pavement response and performance. The changes in pavement temperature and moisture translate into changes in material moduli and other physical properties, ultimately determining the ability of the pavement to perform under given loading conditions. To date, pavement designers have considered climate based on stationary datasets derived from historical observations. The notion of climate change challenges the assumption of stationarity and therefore should be given due consideration in pavement design. Best estimates of global average annual temperature increase range from 3.2 to 7°F over the next century (*IPCC, 2007*). The Intergovernmental Panel on Climate Change (IPCC) attributes the observed pattern of change to the influence of anthropogenic forcing, stating that it is very likely that greenhouse gases caused the warming globally over the last 50 years. Consequently, much effort has been focused on understanding the contribution of road transportation and construction to the emissions of greenhouse gases. Little research has been put forth to date to understand the implications of climate change on the performance and design of the road infrastructure. The only quantitative analyses of climate change impacts on pavement performance have been conducted by Mills et al. (*2007a, 2007b*). Mills et al. concluded that forecasted temperature and precipitation changes are important considerations in several deterioration processes related to pavement performance: rutting, thermal cracking, and frost heave and thaw weakening.

Climate change forecasts raise the possibility that the frequency, duration, and severity of these deterioration processes may increase. National Research Council (2008) identified some of the potential impacts of climate change on the paved infrastructure. Those impacts include increased hot days and heat waves leading to the potential increase in rutting and the migration of liquid asphalt, later onset of seasonal freeze and earlier onset of seasonal thaw may increase pavement deterioration in response to more freeze-thaw conditions, and the increase in precipitation volumes and intensity could increase soil moisture and lower the strength in the unbound layers. A better understanding of potential modes and consequences of failure is key to informing resilient infrastructure design practices (TRB, 2009).

Recognizing that the breadth of potential research spans well beyond a single study, this study's goal was to develop a methodology to serve as the basis for broader inquiry and to demonstrate the application of that methodology. This work develops a methodology to incorporate the use of climate model forecasts in the Mechanistic-Empirical Design Guide (M-E PDG) to assess the implications of climate and climate change on pavement deterioration processes. This thesis presents the methodology then applies it at four locations in the New England region under forecasted temperature changes.

Mechanistic-Empirical Pavement Design Guide (M-E PDG) (Version 1.1)

The Mechanistic-Empirical Pavement Design Guide represents a departure from traditional pavement design. Previous to the development of the M-E PDG, design was based on limited empirical performance equations developed in the late 1950's. The need for a mechanistically based approach was recognized when the 1986 AASHTO *Guide for Design of Pavement Structures* was adopted (Design Guide, 2004). With that recognition the American Association of State Highway and Transportation Officials

(AASHTO) Joint Task Force on Pavements, in cooperation with the National Cooperative Highway Research Program (NCHRP) and the Federal Highway Administration (FHWA), sponsored the “Workshop on Pavement Design” in 1996. From which NCHRP Project 1-37A, Development of the 2002 Guide for Design of New and Rehabilitated Pavement Structures, the M-E PDG, was initiated.

Under the M-E PDG, a designer is given the flexibility to consider different pavement parameters (structure, materials, and prevailing site conditions) through an iterative process. Designs can be optimized to limit the development of pavement distresses. The mechanistic-empirical approach allows the development of a rational relationship between materials and design through the evaluation of materials and pavement performance differences. The development of a rational relationship is at the core of the M-E PDG. As Yoder and Witczak (1975) acknowledge, for a design process to be fully rational, three elements must be considered: (1) the theory used to predict the failure or distress, (2) the evaluation of pertinent material properties, and (3) the determination of the relationship between the parameter in question to the failure. The strength of the M-E PDG is that it considers all three elements.

Principles of the Mechanistic-Empirical Approach

The principles of engineering mechanics are based on explaining phenomena in purely physical or deterministic terms. That is to say, the principles are based on using a “mechanistic” approach. Using the mechanistic approach, three material behavioral response characteristics are considered in the M-E PDG. They are the relationship between stress and strain, the time dependency of strain under constant stress, and the ability of the material to recover strain after stress removal. The “empirical” approach, which is based on observation and experiment, consists of two parts. The first relates to

the characterization of materials and also to the environment and traffic inputs of the design process. The second is the relation of field performance data to accumulated damage.

The approach of the M-E PDG consists of three stages: Evaluation, Analysis, and Strategy Selection (Figure 1). Stage 1, Evaluation of the design process is the development of the input values. This includes pavement material characterization, collection/retrieval of traffic data, and the execution of the Enhanced Integrated Climatic Model (EICM). The EICM is a climatic tool used to model the temperature and moisture within each pavement layer.

Stage 2, Analysis of the design process entails an iterative analysis which consists of employing pavement and distress models incrementally over time to produce accumulated damage and smoothness outputs. If the design does not meet the set forth performance criteria, then changes can be made and the analysis can be re-run until results are satisfactory.

Stage 3, Strategy selection evaluates all the viable alternatives from Stage 2. This consists of an engineering analysis and a life cycle cost analysis of the alternatives. Externalities involved with project are also considered in this stage.

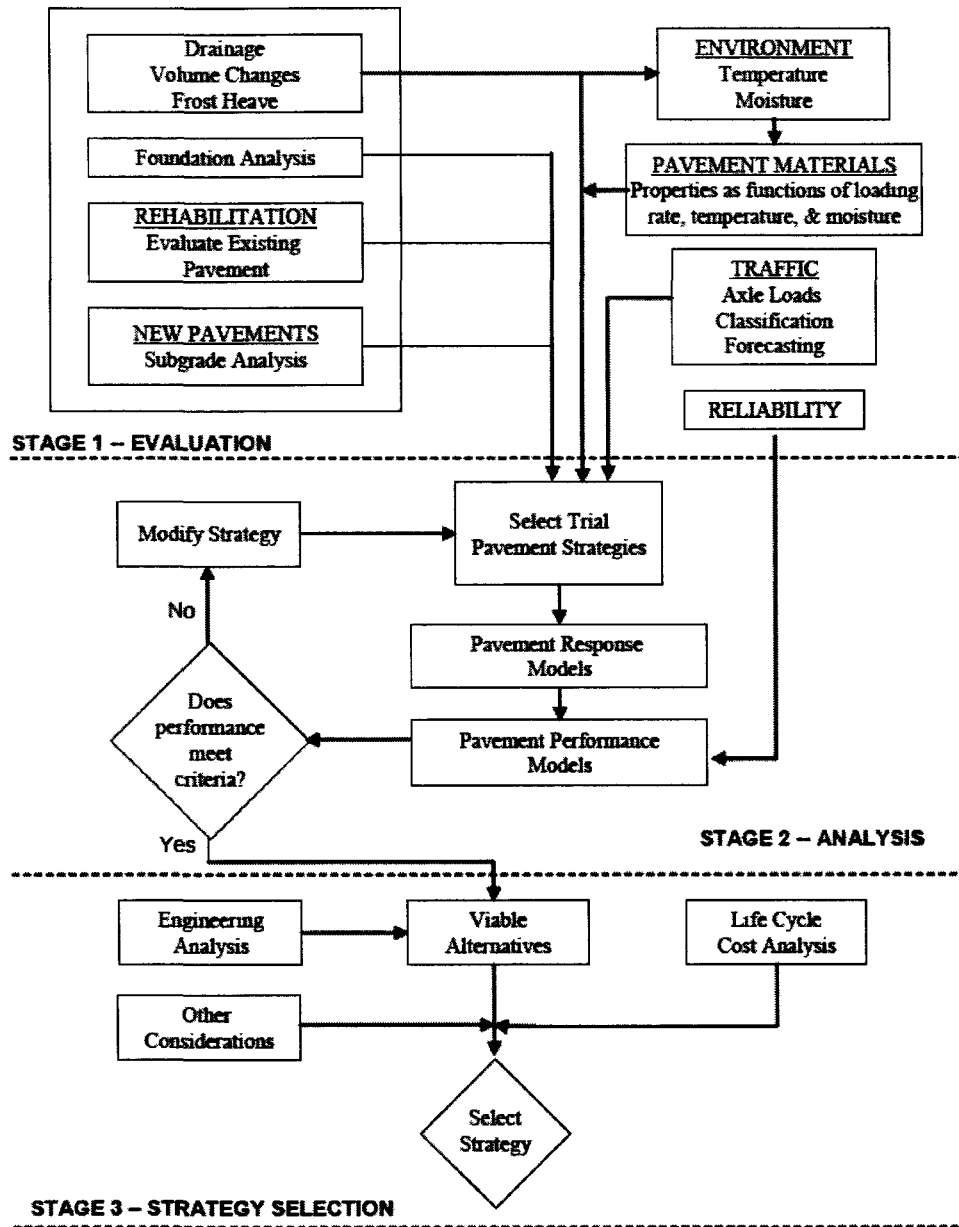


Figure 1 - Schematic of the Design Process (Design Guide, 2004)

The M-E PDG separates itself from existing AASHTO design guides in that it employs a hierarchical approach to design inputs. This allows the designer the flexibility to develop inputs based on the available resources and the importance of the design. This

approach applies to material, traffic, and environmental inputs. The hierarchy is broken down into three levels of inputs. Level 1 inputs require the highest level of accuracy and are associated with the lowest level of uncertainty. These inputs would be warranted in designs of heavily trafficked or critical pavements, where early failure would have dire consequences to safety and economics. Level 1 inputs require laboratory and field testing. Thus, obtaining these inputs requires more resources than other levels. Level 2 inputs are closest to earlier design guides and require an intermediate level of accuracy. Level 2 inputs are selected from an agency database, derived from a limited testing or estimated from correlation relationships. Level 3 inputs require the lowest accuracy and are typically the default values for an area or agency. For any design, the inputs can include a mix of these three levels. Regardless of the input level, the same models are used to predict pavement distresses.

Climatic Modeling – Enhanced Integrated Climate Model (Version 3.2)

Climate plays an important role in Mechanistic-Empirical design. Factors such as precipitation, temperature, freeze-thaw cycles, and depth to water table define the bounds of the climate on pavement performance (*Design Guide*, 2004). Temperature and moisture are two environmental variables that have a direct effect on material behavior. They are important factors that determine the pavements load carrying capacity. Moisture primarily effects unbound materials. Temperature affects both bound and unbound layers. The M-E PDG and its' companion software model dynamic temperature and moisture profiles in the pavement structure using the EICM. The EICM uses climate-related information from a database of nearly 800 U.S. weather stations to model the changing temperature and moisture profiles in the pavement and subgrade. The EICM consists of three major components: (1) the Climatic-Materials-Structural Model (CMS Model) developed at University of Illinois, (2) the CRREL Frost Heave and

Thaw Settlement Model (CRREL Model) developed at the United States Army Cold Regions Research and Engineering Laboratory (CRREL), and (3) the Infiltration and Drainage Model (ID Model) developed at Texas A&M University. These three components are combined to make the EICM a one-dimensional coupled heat and moisture flow model that is able to model pavement material characteristics over time under different climatic forcings. The CMS and CRREL models perform the heat transport needed to estimate temperature profiles. The ID model performs infiltration and drainage calculations to estimate moisture profiles.

The EICM requires hourly weather-related parameters: (1) air temperature, (2) wind speed, (3) percent sunshine, (4) precipitation, and (5) relative humidity (*Johanneck et al., 2010*). EICM uses air temperature, wind speed, and percent sunshine to compute a surface energy balance at the pavement and air interface and to force the pavement temperature profile model. Additionally, the temperature data are also used to defined freeze-thaw periods. Precipitation provides the upper boundary for infiltration of water into the pavement structure. Relative humidity is used to model the moisture gradients for rigid pavements.

Pavement temperature changes are forced by the atmospheric boundary conditions at the pavement surface. To estimate the pavement temperature profile, the CMS Model employs a one-dimensional finite difference model with two boundary conditions. The upper boundary is the pavement surface. The lower boundary temperature is a constant deep ground temperature. At the upper boundary, air temperature, wind speed, and the amount of sunshine determine the heat flux in or out of the pavement. The lower boundary is assumed to be capable of supplying an infinite amount of heat in order to keep the temperature constant. By modeling the heat flow through the pavement, the

CMS model estimates the temperature profile at the surface, at 0.5 inch, and at every inch within the asphalt layer.

The CRREL Model uses the temperature profile through the asphalt layers, as determined by the CMS model, to compute changes in the subgrade temperature profile. The depth of frost is determined by comparing the temperature profile with the freezing temperatures of the unbound materials. The temperature at which frost penetration occurs is 30°F for unbound materials. The CRREL model also estimates the vertical heave due to frost formations and soil settlement during thaw.

Several EICM outputs are used for flexible pavement design. Temperatures at the surface and midpoint of each asphalt bound layer are used in fatigue and permanent deformation prediction models. The average moisture content of each sublayer is used to predict deformation of unbound materials and the resilient modulus adjustment factor (F_{env}). F_{env} is a composite factor that accounts for the effects of the moisture content changes, freezing, thawing, and thaw recovery. The structural response model uses F_{env} to modify the unbound resilient modulus as a function of space and time.

Structural Response Modeling

Structural response models are used to compute stresses, strains, and displacements in pavement structures due to traffic and climatic factors. For flexible pavements, the M-E PDG and its companion software use two approaches for structural response modeling. The multi-layer elastic program JULEA for linear elastic analysis is used for general inputs. The 2-D finite element program DSC2D is used to conduct a finite element analysis if Level 1 inputs to characterize the non-linear response of unbound layers are provided. The response modeling is then used in field calibrated models that relate

critical stress and strains in the pavement to distress and damage experienced by the pavement.

Climate Modeling

Climate change forecasts are developed using Atmosphere-Ocean General Circulation Models (AOGCMs) which provide global climate forecasts under different greenhouse gas emission scenarios. An AOGCM consists of a three-dimensional coupled model that incorporates the physical processes in the atmosphere, oceans, and land surfaces. AOGCMs produce gridded datasets of precipitation, temperature, pressure, cloud cover, as well as of other climatic variables at daily, monthly, and semi-, and annual scales. AOGCMs have limited value to pavement design because they produce climate information at coarse scales (i.e., 250 x 250 km grid cells) with limited ability to capture local-scale variations (*Michelangeli et al., 2009*). Downscaling methods are needed to produce climate forecasts at scales which reflect site-specific conditions and uncertainty (*Rivington et al., 2008*). The two main approaches for downscaling AOGCM output to a finer resolution are dynamic and statistical. Using dynamic downscaling, Regional Climate Models (RCMs) can be produced using AOGCM output as initial and boundary conditions. This nesting produces a high-resolution model more appropriate and physically consistent for resolving the small-scale features of topography and land use, which in turn influence climate variables and can realistically simulate regional climate features, extreme physically consistent climate events, and regional scale climate anomalies (*Fowler et al., 2007, Akhtar et al., 2009*). Statistical downscaling establishes the empirical relationships between AOGCM output and local variables needed to translate the large-scale output into a finer resolution. It is a more computationally

efficient method than that of dynamic downscaling and ranges in sophistication from simple change factors to regression models, weather type schemes, and weather generators. While both approaches have advantages and disadvantages, neither method is recommended for use without appropriate expertise. Because both approaches are active research areas, there is not a single consistent approach.

Climate model output, whether from an AOGCM or RCM, is characterized by its ability to simulate key climate variables with respect to reproducing correct statistical properties. Confidence in applying climate models is based on the ability of the models to replicate key features of already observed climate. The process of assessing model performance is known as "hindcasting", which consists of using known climate forcings from historical events as inputs and testing the ability of the model to replicate the observed weather events. Models are routinely and extensively assessed by comparing their simulations with observations of the atmosphere, ocean, and land surface. There is considerable confidence that AOGCMs provide credible quantitative estimates of future climate change (*IPCC, 2007*).

CHAPTER II - DATA & INPUTS

Climate Model Data

To support intercomparisons across studies, the development of pavement community datasets would be ideal. In lieu of these datasets, the North American Regional Climate Change Assessment Program's (NARCCAP) climate change simulations provide a reasonable proxy for this methodological approach. NARCCAP is an international program whose aim is to produce high resolution climate change simulations in order to investigate uncertainties in projections of future climate and produce climate change scenarios for use in impact studies. NARCCAP provides datasets from six RCMs nested within four AOGCMs for the hindcast period 1971-2000 and for the future period 2041-2070, at a spatial resolution of 50 km. The experimental plan for NARCCAP calls for twelve RCM+AOGCM combinations to be run. Each AOGCM drives three RCMs, and each RCM is driven by two AOGCMs. A total of 52 output variables at 3-hourly temporal resolution are available through NARCCAP. The AOGCMs utilized in NARCCAP have been forced with the SRES (Special Report on Emissions Scenarios) A2 emissions scenario, which is moderately high.

For this work, three RCM+AOGCM model combinations datasets sourced from the NARCCAP climate change simulations were studied:

1. CRCM + CGCM3: Canadian Regional Climate Model (CRCM) combined with the Canadian Global Climate Model version 3 (CGCM3) AOGCM.
2. RCM3 + CGCM3: Regional Climate Model version 3 (RCM3) combined with the Canadian Global Climate Model version 3 AOGCM.

3. RCM3 + GFDL: Regional Climate Model version 3 combined with the Geophysical Fluid Dynamics Laboratory Climate Model version 2.1 (GFDL) AOGCM.

The datasets were downloaded in December, 2010.

The specifications and performance of each RCM and AOGCM, as well as more information about NARCCAP, have been well-documented elsewhere (*Mearns et al.*, 2007, updated 2011)

The three combinations were selected because the first two combinations use the same AOGCM, but a different RCM while the second two combinations use the same RCM, but a different AOGCM. Figure 2 shows the AOGCM model points, NARCCAP RCM models points, and M-E PDG climate stations for the New England region to illustrate the differences in scales.

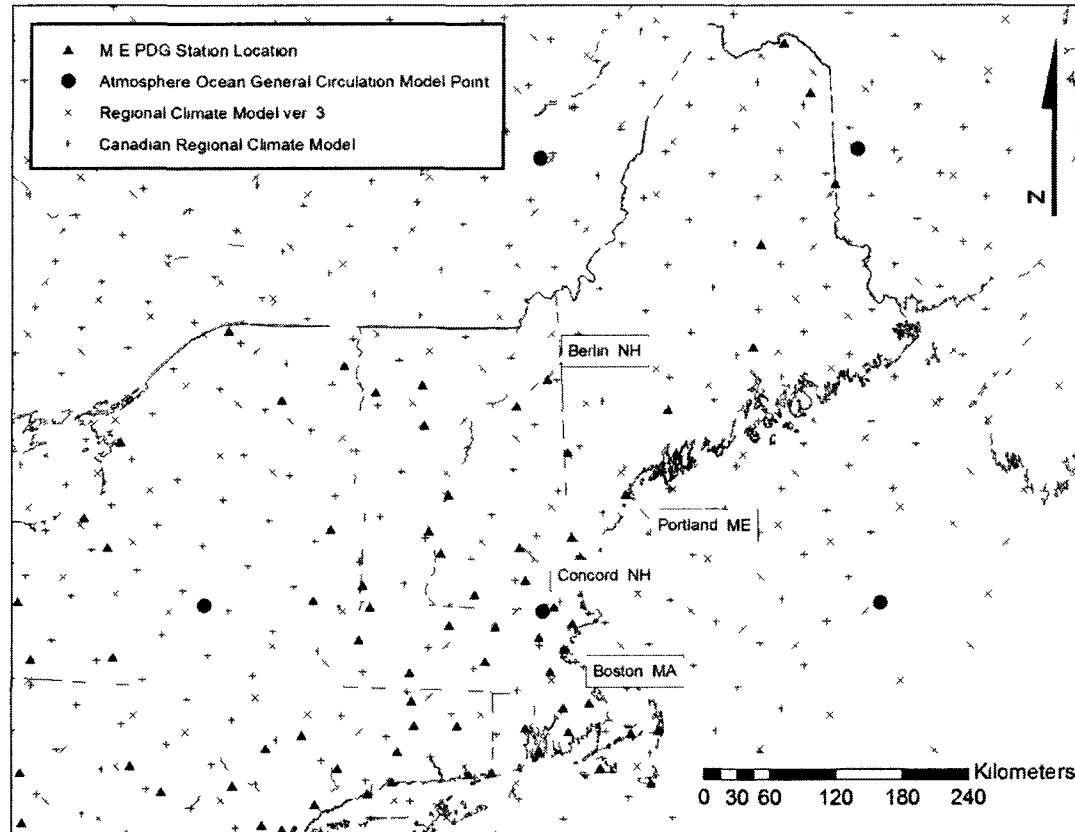


Figure 2 - Study location including the center of the original Atmosphere-Ocean General Circulation Model and Regional Climate Model grid cells as well as the M-E PDG climate stations. The four study sites are Berlin, NH, Boston MA, Concord, NH, and Portland, ME.

Data Structure Overview

Finding & Downloading Data

NARCCAP data is distributed through the Earth System Grid (ESG) – National Center for Atmospheric Research (NCAR) gateway.

<http://www.earthsystemgrid.org/project/NARCCAP.html>

The data are organized by model (RCM) and driver (GCM), and grouped into data tables. For this work, data from *Table 2: Primary 3-hourly Surface Fields (2-D)* (Table 1) were chosen. This choice was primarily based on the data availability. Because NARCCAP is an ongoing research effort, data are published as variables become available.

Table 1 - NARCCAP Table 2: Primary 3-hourly Surface Fields (2-D)

NARCCAP Table 2: Primary 3-hourly surface fields (2-D)			
Var.	Long Name	Units	Notes
huss	Surface Specific Humidity	kg/kg	Instantaneous
pr	Precipitation	kg/m*s	Average
ps	Surface Pressure	Pa	Instantaneous
rsds	Surface Downwelling Shortwave Radiation	W/m ²	Instantaneous, + Down
tas	Surface Air Temperature	K	Instantaneous
uas	Zonal Surface Wind Speed	m/s	Instantaneous, + East
vas	Meridional Surface Wind Speed	m/s	Instantaneous, + North

North American Regional Climate Change Program Data Overview

The NARCCAP data are stored in Network Common Data Form (netCDF). NetCDF consists of a set of data formats, interfaces, and software libraries for reading and writing scientific files. The netCDF data structure consists of variables, dimensions, and attributes arranged in an array-oriented dataset form that is self-describing and portable. Self-describing and portable means that the dataset includes information defining the data it contains (metadata) and is in a form that can be accessed by computers across various platforms.

NARCCAP data filenames follow the form *VariableName_ModelName_Driver_Time.nc*. Where *VariableName* is the Variable Name as listed in the data tables complicated with IPCC/CF convention, *ModelName* is the regional climate model identifier. *Driver* is identifier of the driving global climate model, and *Time* is the starting time of the file. For example, *tas_CRCM_CGCM3_1971010103.nc* contains the data for the variable *tas* (Surface Air Temperature, K as reported in Table 1) from the CRCM (Canadian Regional Climate Model) regional model driven by the CGCM3 (Canadian Global Climate Model ver. 3) boundary conditions starting at 03:00 Universal Coordinated Time (UTC) on January 1st, 1971.

The data are stored as a single variable spanning a period of five years. Files covering the beginning and ending of a model run may not contain a full five years of data. More specifically, the earliest files for the hindcast period model include data for January 1, 1968 to December 31, 1970; a three year period. The latest files for the hindcast model period include data for January 1, 1996 to November 21, 2000 or December 21, 2000, for the CRCM and RCM3, respectively, with each having roughly four years of data. The earliest files for the future period model are for the period January 1, 2038 to December 31, 2040; three years. The latest files for the future model period include data for

January 1, 2066 to November 21, 2070 or December 21, 2070, for the CRCM and RCM3, respectively, with each roughly corresponding to four years.

Project Data Overview

For this research, the data acquired through the ESG-NCAR gateway were concatenated by time period (e.g., Current or Future) for each variable, the current period being the period from January 1, 1968 to November 21, 2000 or December 21, 2000, for the CRCM and RCM3, respectively. The future period is January 1, 2038 to November 21, 2070 or December 21, 2070, for the CRCM and RCM3, respectively. Data files were concatenated using the netCDF Operators (NCO) program suite. The netCDF format is preserved through this concatenation process.

A subset of the NARCCAAP North American region data, the northeastern United States, was extracted and stored as a MATLAB MAT-file (.mat). All data variables are stored within a single file for each RCM+AOGCM combination. For example, *CRCM_CGCM3_Current.mat* contains all the variables extracted for the northeast covering the current time period associated with CRCM+CGCM3 combination.

For the M-E PDG, single model points were used. Once identified, the model points were extracted from the region of interest and the variables were converted for use by the M-E PDG. Details on the variable conversion process appear in Chapter III. These converted files contain the suffix *MEPDG* preceded by the model point. These data are also stored within a single file for each RCM+AOGCM combination. For example, *CRCM_CGCM3_Current_115_58_MEPDG.mat*, contains the variables converted to use with the M-E PDG from model point 115, 58 (x, y) for the current time period associated with CRCM+CGCM3.

During the development of this methodology, it was determined that the climate model data needed to be downscaled before use. Details on the downscaling process utilized (CDF-t) are in Chapter III. The downscaled data were stored by model (RCM), driver (AOGCM), time period, point, and variable as a DAT file (.dat). The suffix *Downscaled* denotes the actual downscaled data from the CDF-t method. The suffix *Output* describes the data necessary to construct the CDF graphs associated with the methodology used for downscaling. For example, *CRCM_CGCM3_Current_115_58_Temperature_Downscaled.dat* contains the downscaled CRCM+CGCM3 combination temperature data associated with the current time period.

Variables

This research applied the developed methodology to model temperature data. However, all available variables (Table 1) were explored to varying degrees. To serve as a reference for future work, this section describes the challenges associated with temperature, precipitation, and downwelling radiation.

Temperature

Temperature data, as distributed by NARCCAP, are in Kelvin. For use in the M-E PDG the temperature data need to be converted to degrees Fahrenheit. After the unit conversion, the hindcast model data and the station data did not match (Figure 3). The average monthly temperature from the three model data combinations did not match the observed station data, black line.

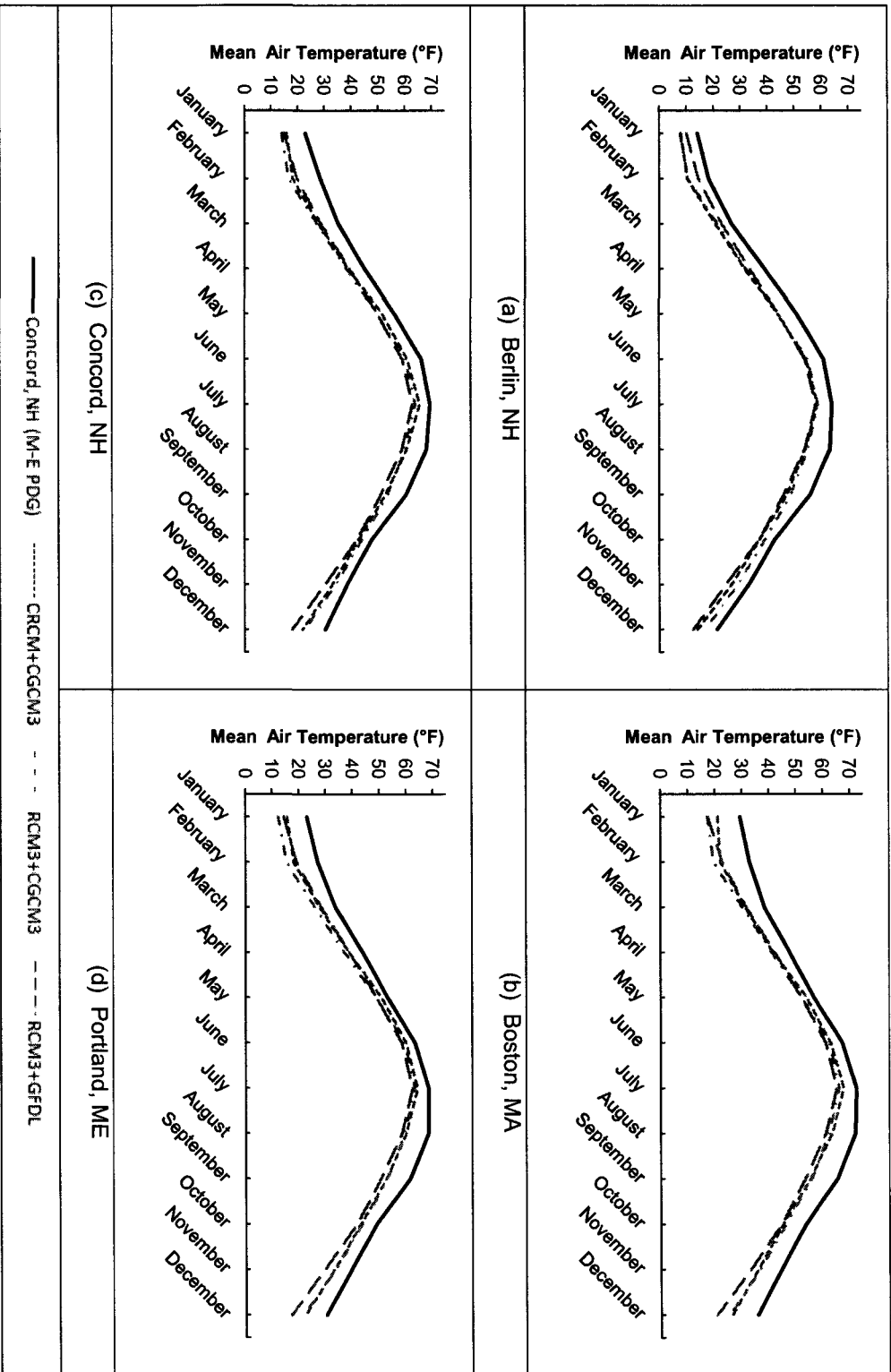


Figure 3 – Hindcast Model Temperature Data Compared to Observed M-E PDG Station Data

The cumulative distribution function (CDF) of the model data as compared to the station data shows that the model data were biased low using both the model and station overlap period and full model period as compared to that of the station data for the same period (Figure 4). This result pointed to the need for a probabilistic downscaling method to match the CDF of the M-E PDG climate data and the corresponding AOGCM+RCM CDF for the overlap period. The CDF-transformation (CDF-t), developed by Michelangeli et al. (2009), was used to downscale the model temperature data to better match the CDF of the observed data (Figure 5). The CDF-t method details appear in Chapter III.

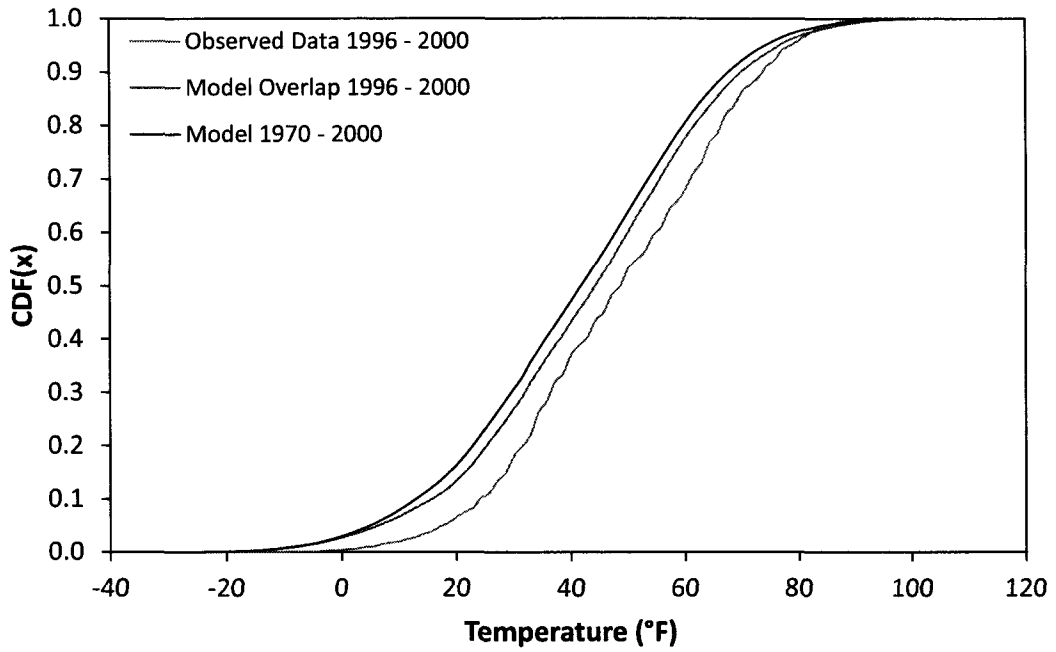


Figure 4 - Typical Cumulative Distribution of Temperature Data (CRCM+CGCM3 Concord, NH)

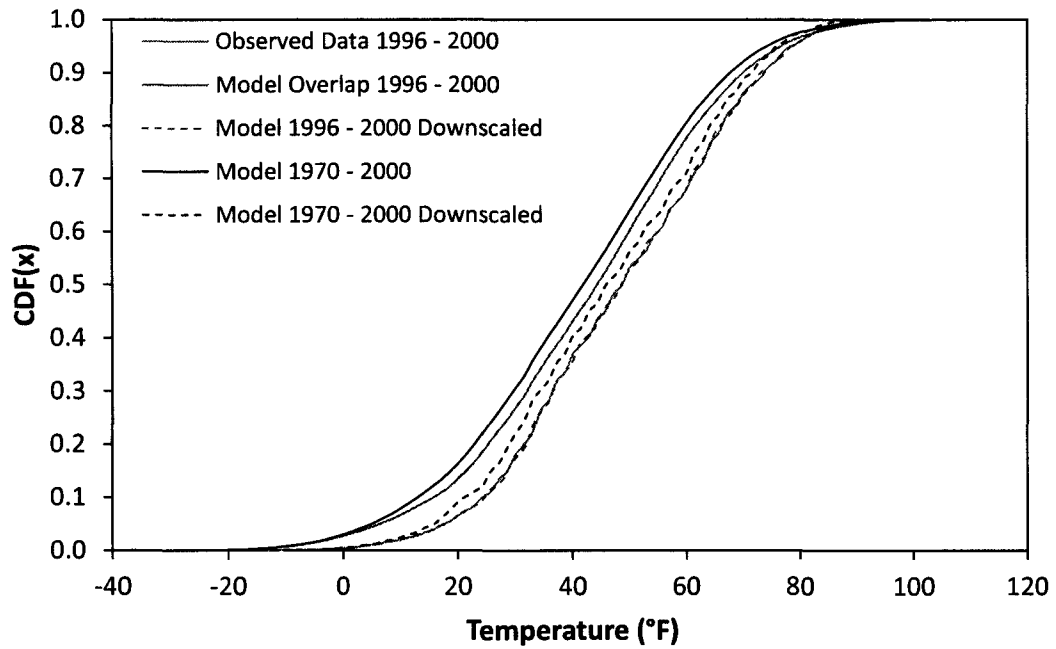


Figure 5 - Typical Application of the CDF-t Method (CRCM+CGCM3 Concord, NH)

Precipitation

The integration of the model precipitation data into the M-E PDG remains an open research question. Precipitation data, as distributed by NARCCAP, are reported as a flux with units of kilograms per square meter per second. The required units for use in the M-E PDG are inches per hours, or total accumulation per time step. The conversion from flux to total accumulation was simple, though not trivial as shown below,

$$P_T = P_F * 3600 \frac{s}{hr} * 0.0393700787 \frac{mm}{in}$$

where P_T is the total precipitation (in) and P_F is the precipitation flux ($\text{kg m}^{-2} \text{s}^{-1}$). Because water has a density of 1 gram per cubic centimeter, 1 kilogram of water equals 1000 cubic centimeters. Distributed evenly over 1 square meter, the water forms a layer with a depth equivalent to 1 millimeter. Therefore, converting the depth in millimeters to a depth in inches and multiplying by the seconds per time step, an hour in this case, gives the equivalent accumulation in inches per hour.

Differences were found between the model data and observed data for the number of precipitation events, the accumulation during each event, and the total annual average accumulation. Events refer to the data hourly time steps in which precipitation occurs. These discrepancies are illustrated in Table 2, where the number of precipitation events greatly differs between the observed station data (for Concord, NH) and associated hindcast model data. This is further illustrated in the accumulation event break down, where that majority of model events, over 50%, have between zero and 0.001 inches, while the observed data has no events within that range. Interestingly, the CRCM+CGCM3 model combination closely replicates the observed total yearly average precipitation. The remaining models grossly overestimate the yearly average precipitation by upwards of 25%.

Table 2 - Hindcast Model Data Precipitation Event Comparison

	M-E PDG	CRCM+CGCM3	RCM3+CGCM3	RCM3+GFDL
Total Events	787	33679	22945	22723
P > 1.0"	29	0	0	0
0.1" < P < 1.0"	307	147	447	594
0.01" < P < 0.1"	207	3768	3948	4482
0.001" < P < 0.01"	387	6579	6057	6075
0" < P < 0.001"	0	23332	12940	12166
P = 0"	37735	4843	15577	15799
Yearly Total Avg. (in)	37.6	36.6	50.2	60.9

Percent Sunshine

The variable percent sunshine, as required by the M-E PDG, is not directly available from NARCCAP. The *downwelling shortwave radiation* is the closest NARCCAP variable available. It has been put forth that by calculating the clear-sky radiation for a given location, which is determined by latitude and time of year, one can determine the percent sunshine using the downwelling shortwave radiation, as shown below.

$$\text{Sunshine (\%)} = \frac{\text{Downwelling Shortwave Radiation}}{\text{Clear Sky Radiation}} * 100$$

Specifically, the clear sky radiation ($\text{MJ m}^{-2} \text{hour}^{-1}$) is determined for every time step (hour). The clear sky radiation (R_{so}) is a product of the extraterrestrial radiation (R_a) multiplied by the constants "a" and "b" which account for atmospheric conditions, as shown below.

$$R_{so} = (a + b) * R_a$$

The extraterrestrial radiation ($\text{MJ m}^{-2} \text{hour}^{-1}$) is a product of the latitude and time of year, and can be expressed as follows,

$$R_a = \left(12 * \frac{60}{\pi}\right) * G_{sc} * d_r [\omega_s \sin \varphi \sin \delta + \cos \varphi \cos \delta \sin \omega_s]$$

where G_{sc} is the solar constant ($0.0820 \text{ MJ m}^{-2} \text{ min}^{-1}$), d_r is the inverse relative distance Earth-Sun, ω_s is the sunset hour angle (rad), ϕ latitude (rad), and δ solar declination (rad).

The inverse relative distance Earth-Sun is and solar declination are given as,

$$d_r = 1 + 0,033 \cos\left(\frac{2\pi}{365}J\right)$$

$$\delta = 0.409 \sin\left(\frac{2\pi}{365}J - 1.39\right)$$

where J is the Julian day.

The sunset hour angle is determined as:

$$\omega_s = \cos^{-1}[-\tan \phi \tan \delta]$$

However, this remains an open research question. As a possible substitute for downwelling shortwave radiation the variable *percent cloud cover* could be used. As NARCCAP is an ongoing effort, percent cloud cover is unavailable at this time.

Pavement Model Data

The material inputs used in this project for the M-E PDG were typical values used by the New Hampshire Department of Transportation. Two typical pavement structures shown in Figure 6 were evaluated; one representing a secondary road and the other an interstate. Typical NH initial two-way Average Annual Daily Traffic counts of 6500 and 25,000 were used for the secondary and interstate conditions, respectively. A 4% compounding traffic growth was used for each design. A PG 58-28 asphalt was selected for the secondary roadway and a PG 64-28 was selected for the interstate design. The unbound material inputs are summarized in Table 3. An annual average depth to water

table of 40.629 feet was used (USGS Site No. 431224071303601, Concord, NH; August 23, 1968 to March 25, 2011).

Table 3 - Unbound M-E PDG Material Inputs

	Crushed Gravel	Gravel	Sand	A-2-4
Avg. Modulus (psi)	30600	21150	13320	21500
Poisson's Ratio	0.35	0.35	0.35	0.35
K₀	0.5	0.5	0.5	0.5
Liquid Limit (LL)	6	6	6	14
Plasticity Index (PI)	0	0	0	2
D₆₀ (mm)	14.5	9.5	1.279	0.3476
Percent Passing No. 4	39.5	50	39	87.2
Percent Passing No. 200	6	6	6	22.4

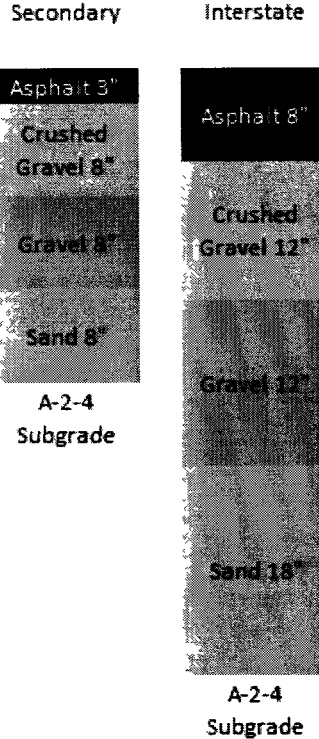


Figure 6 - Typical Pavement Cross Sections

Each pavement was evaluated at four locations: Berlin, New Hampshire; Boston, Massachusetts; Concord, New Hampshire; and Portland, Maine (Figure 7). The locations were chosen to provide geographical heterogeneity and to cover a range of the Northeast climate: central inland (Concord, New Hampshire), northern inland (Berlin, New Hampshire), southern coastal (Boston, Massachusetts), and northern coastal (Portland, Maine).

Table 4 lists the M-E PDG stations for New Hampshire, Maine, and Massachusetts, their starting date, and the number of months on record. This study's stations are shown in bold. The maximum possible overlap between RCM hindcast model and observed station data was sought. The selection of stations was limited to those whose record

began in 1996. Because the RCM hindcast model ends in 2000, this allowed for approximately four years of overlap.

The M-E PDG Version 1.1 software was run for a typical 20-year design period using the hindcast and future climate input file (only temperature changed) and the typical M-E PDG climate file based on historic records.

Table 4 - M-E PDG Stations and Station Record Starting Date

Station No.	Location (City , State)	Starting Date	Months of Record
14702	BEDFORD, MA	08/1/1998	91
54733	BEVERLY, MA	12/1/1998	87
14739	BOSTON, MA	07/1/1996	116
94624	CHATHAM, MA	07/1/1996	116
4780	FITCHBURG, MA	10/1/1997	101
94720	HYANNIS, MA	01/1/1998	98
94723	LAWRENCE, MA	06/1/1997	105
14756	NANTUCKET, MA	01/1/1998	98
94726	NEW BEDFORD, MA	07/1/1996	116
54768	NORTH ADAMS, MA	07/1/1996	116
54704	NORWOOD, MA	06/1/1998	93
54756	ORANGE, MA	07/1/1996	116
14763	PITTSFIELD, MA	02/1/1999	85
54769	PLYMOUTH, MA	07/1/1996	116
54777	TAUNTON, MA	12/1/1997	99
94724	VINEYARD HAVEN, MA	01/1/1998	98
14775	SPRINGFIELD, MA	08/1/1998	91
94746	WORCESTER, MA	07/1/1996	116
14605	AUGUSTA, ME	01/1/2001	62
14606	BANGOR, ME	04/1/1998	95
14607	CARIBOU, ME	08/1/1996	115
4836	FRENCHVILLE, ME	07/1/1996	116
54772	FRYEBURG, ME	07/1/1996	116
14609	HOULTON, ME	09/1/2000	66
14610	MILLINOCKET, ME	07/1/1996	116
14764	PORTLAND, ME	07/1/1996	116
94623	WISCASSET, ME	07/1/1996	116
94700	BERLIN, NH	07/1/1996	116
14745	CONCORD, NH	07/1/1996	116
54770	JAFFREY, NH	07/1/1996	116
94765	LEBANON, NH	05/1/1998	94
14710	MANCHESTER, NH	01/1/1998	98
54791	ROCHESTER, NH	02/1/2000	73
54728	WHITEFIELD, NH	07/1/1996	116

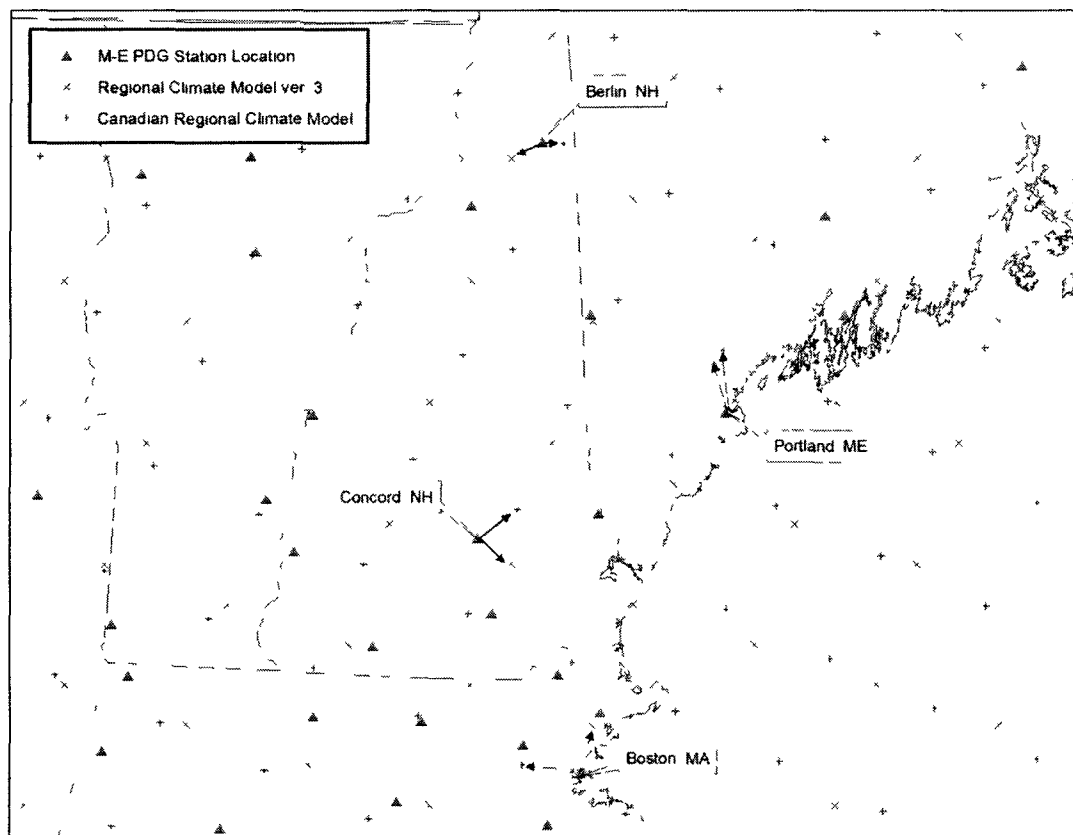


Figure 7 - Study Sites and Associated Model Points Identified

CHAPTER III - METHODOLOGY

The proposed methodology consists of a series of steps which translate the raw RCM climate datasets to data that can be combined with M-E PDG climate datasets and then used with materials and traffic properties to predict distress using the M-E PDG model. Figure 8 breaks the methodology into a five step process that uses four sets of data. Of the four datasets, three would be used for a traditional M-E PDG analysis. The new dataset is the climate model data from an RCM model. Of the five steps in the methodology, the first four are required to prepare the RCM dataset for use in the M-E PDG model. Thus, a traditional M-E PDG analysis would only require the fifth step presented in this methodology.

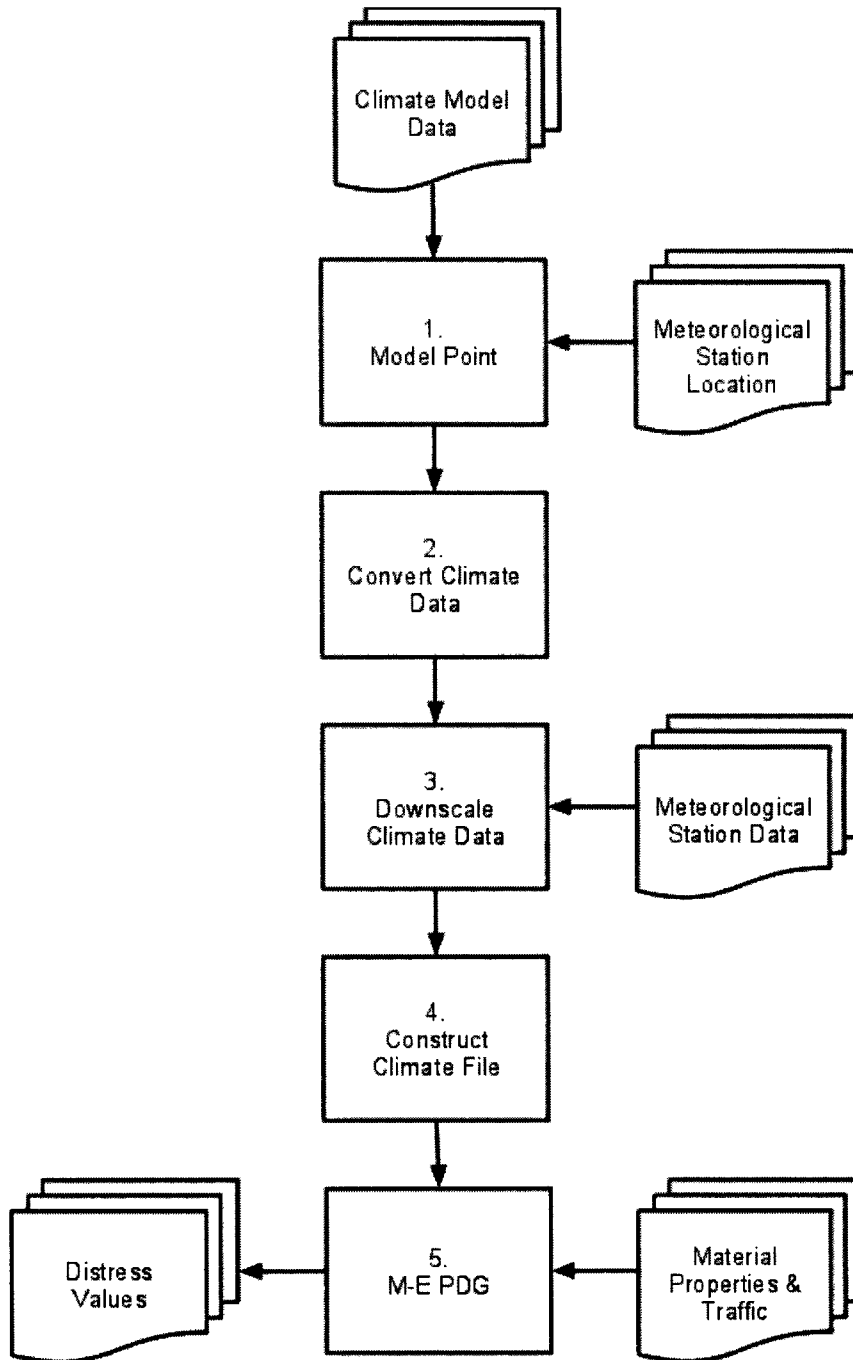


Figure 8 - Methodology Process Chart

Model Point Selection

The first step in the proposed methodology is to select the nearest RCM model point that is collocated with the pavement design location. Here, a single M-E PDG station location was selected rather than a “virtual station”. We used a nearest neighbor approach to identify the RCM cell closest to the M-E PDG station (Figure 7).

A challenge to this step is that the datasets from the two collocated points must have a period of overlap between the RCM hindcast period dataset and M-E PDG station record. For the northeast United States, the earliest M-E PDG station records begin July 1, 1996 with most stations starting later and all stations covering until February 28, 2006. For the RCM hindcast period the model output data begins January 1, 1968 and ends either November 21, 2000 or December 21, 2000, for the Canadian Regional Climate Model and Regional Climate Model version 3, respectively. With the first two years of the model data considered to be a spin-up period, a period where the models equilibrate, the hindcast model data began July 1, 1970. To achieve the maximum possible overlap period between the hindcast model data and M-E PDG station data, this study only used M-E PDG stations with data beginning on July 1, 1996. November 21, 2000 was selected as the common end point between the models and the observed data. This allowed for a minimum of a three-year overlap. Once the appropriate model point(s) were selected, the variable(s) of interest were extracted from the larger regional dataset.

Conversion of Climate Data

The second step in the proposed methodology is to extract and convert the RCM climate data to match the required M-E PDG input variables (Table 5). This involves a time conversion and a unit conversion. The data were transformed from the RCM 3-hour time step to the M-E PDG 1-hour time step. If the variable is reported as an

instantaneous value, then its value is applied to the three M-E PDG times intervals (hour) prior to, during and following the observation. In contrast, RCM average values are applied to the three intervals (hours) before the RCM reporting time. Minor conversions are required for temperature, wind speed, and precipitation. More significant conversions are needed for the relative humidity and percent sunshine. The M-E PDG relative humidity RH is calculated from the RCM specific humidity q , surface atmospheric pressure p and the air temperature T as

$$RH = 100 * \frac{e}{e_s} \quad (1)$$

where e is the vapor pressure and e_s is the saturation vapor pressure calculated as:

$$e = q * p / 0.622 \quad (2)$$

$$e_s = 611 \exp\left[\frac{(17.27 * (T - 273.15))}{(237.3 + (T - 273.15))}\right] \quad (3)$$

The conversion of RCM downwelling shortwave radiation to M-E PDG percent sunshine is an open challenge that needs to be addressed using a systematic approach. As addressed previously, it has been put forth that by calculating the clear-sky radiation for a given location, which is determined by latitude and time of year, one can determine the percent sunshine using the downwelling shortwave radiation, as shown below.

$$Sunshine (\%) = \frac{Downwelling \ Shortwave \ Radiation}{Clear \ Sky \ Radiation} * 100$$

Table 5 - Conversion of RCM to M-E PDG Variables

Regional Climate Model Output Variables		M-E PDG Climate Input Variables
Temperature (K) <i>Instantaneous</i>	→	Temperature (°F)
Precipitation (kg m ² s ⁻¹) <i>Average</i>	→	Precipitation (in)
X-Coordinate of Wind Speed (m s ⁻¹) <i>Instantaneous</i>	} →	Wind Speed (mi h ⁻¹)
Y-Coordinate of Wind Speed (m s ⁻¹) <i>Instantaneous</i>		
Downwelling Shortwave Radiation (W m ⁻²) <i>Average</i>	→	Percent Sunshine
Specific Humidity (kg kg ⁻¹) <i>Instantaneous</i>	} →	Relative Humidity (%)
Surface Pressure (Pa) <i>Instantaneous</i>		

Downscaling of Climate Data

The third step in the methodology is a probabilistic transformation of the RCM data. Because there remains a discrepancy in scale between the RCM datasets (50 x 50 km grid) and the M-E PDG pavement design site, a probabilistic transformation method is employed to match the observed statistical characteristics. The CDF-transformation (CDF-t) is one method that generates local-scale variables (site-specific) from large-scale outputs (*Michelangeli et al., 2009*). A CDF of the M-E PDG climate data is compared to the corresponding RCM CDF for the overlap period. CDF-t is based on the assumption that a relationship exists such that the CDF of an AOGCM+RCM (predictor) variable (e.g., temperature, precipitation) can be “transformed” into a CDF representing the local-scale variable (predictand) and that this relationship is constant with time. The

CDF-t is rooted in quantiles-matching approach and is a non-parametric method that makes no assumptions about the underlying distribution of the data.

The CDF-t is mathematically described as follows. F_{Sh} is the CDF of observed local data (M-E PDG Station Data), and F_{Gh} is the CDF of the RCM output at the station location for the same hindcast time period. F_{Sf} and F_{Gf} are the CDFs equivalent to F_{Sh} and F_{Gh} , respectively, but for the future time period. Assuming that F_{Gf} is known (modeled through future RCM outputs), and that a transformation T exists such that: $[0, 1] \rightarrow [0, 1]$

$$F_{Sh}(x) = T(F_{Gh}(x)) \quad (4)$$

Replace x by $F_{Gh}^{-1}(u)$, where u belongs to $[0, 1]$:

$$T(u) = F_{Sh}(F_{Gh}^{-1}(u)) \quad (5)$$

Assuming the relationship holds true in the future:

$$F_{Sf}(x) = T(F_{Gf}(x)) \quad (6)$$

The CDF for the local-scale future variable F_{Sf} is equal to:

$$F_{sf}(x) = F_{Sh}\left(F_{Gh}^{-1}\left(F_{Gf}(x)\right)\right) \quad (7)$$

The CDF-t is applied to both hindcast and future periods. The downscaled data are then used in the M-E PDG. The maximum period of overlap is desired for this downscaling method in order to capture interannual variations. In this project, the overlap period was limited to roughly three years based on the availability of measured data from the M-E PDG and the hindcast period available from the climate model data. The hindcast period of overlap consisted of the time period from July 1, 1996 to November 21, 2000.

To quantitatively assess the performance of the CDF-t method the Kolmogorov-Smirnov (K-S) test is employed. The K-S test is a non-parametric and distribution free test to determine if two dataset differ significantly. The K-S test statistic is the maximal vertical distance between the empirical cumulative distribution functions of two samples. The null hypothesis H_0 is the two datasets have the same distribution. The alternative hypothesis H_A is the datasets have different distributions. The test has an upper-tail rejection region. For large sample sizes, the approximate critical value, D_α is given by the equation

$$D_\alpha = c(\alpha) \sqrt{\frac{n_1+n_2}{n_1 n_2}} \quad (8)$$

where the coefficient $c(\alpha)$ equals 1.36 at α of 0.05, n_1 is the size of first sample, and n_2 is the size of the second sample.

An example of the CDF-t method using the CRCM + CGCM3 model scenario is shown in Figures 9 to 12 for the Concord, NH site. The CDF of the observed temperature data for 1996-2000 for the M-E PDG climate data for Concord, New Hampshire and the CDF for the CRCM + CGCM3 RCM model hindcast over the same time period are shown by the red and green solid lines, respectively. In Figure 9, the CRCM + CGCM3 RCM temperatures hindcast are biased low compared to the observed temperatures.

The CDF-t method is applied to these two datasets to transform, or downscale, the CRCM + CGCM3 RCM hindcast overlap CDF to match the observed CDF (Figure 10). A successful transformation of the CDF of the CRCM + CGCM3 RCM hindcast overlap matches the CDF of the observed data for the same period. It can be seen in Figure 10 that the CRCM + CGCM3 RCM hindcast overlap CDF follows the CDF of the observed temperature data for 1996-2000 for the M-E PDG climate data for Concord, New Hampshire, therefore indicating a transformation exists as required for Equation 5.

This transform is then applied to the large-scale hindcast dataset (Model 1970 – 2000) to develop the local-scale dataset (Model 1970 – 2000 downscaled) (Figure 11). The transformation applied to the hindcast dataset shows a low bias indicating lower temperatures. However, this is still an improved fit as compared to the non-transformed hindcast data. The same transformation is applied to the future dataset (Model 2040 – 2070) to develop the local-scale dataset (Model 2040 – 2070 downscaled) (Figure 12). In contrast to the hindcast data the transformed future temperature shows higher temperatures than that of the observed. This is in agreement with the best estimates of global average annual temperature change for the next century (*IPCC, 2007*).

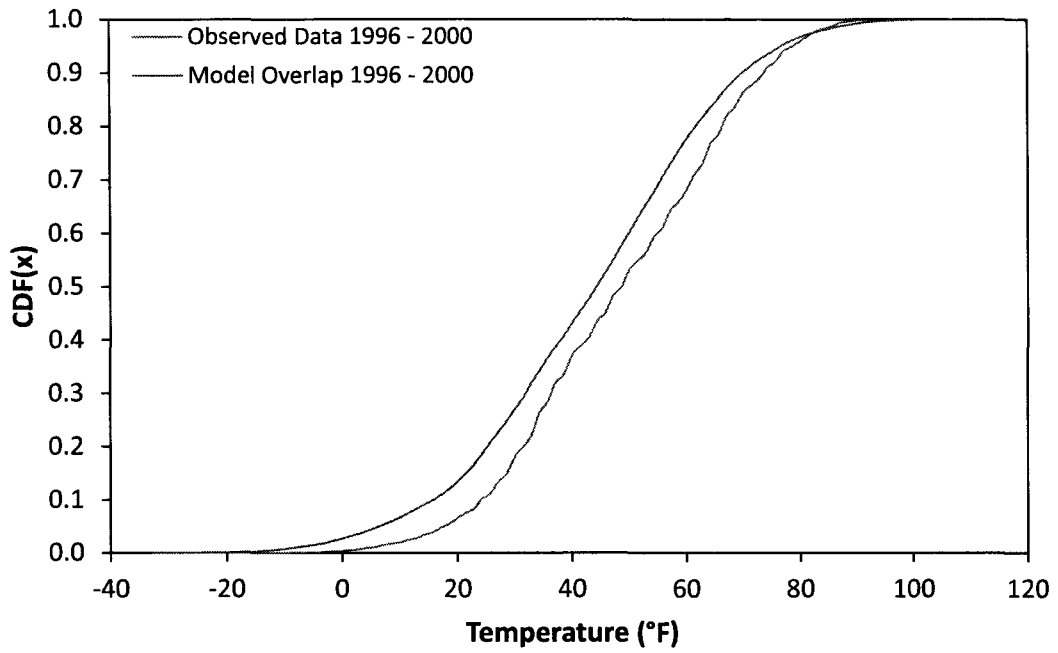


Figure 9 - Observed Data CDF to CRCM + CGCM3 RCM Model Overlap CDF for Concord, NH

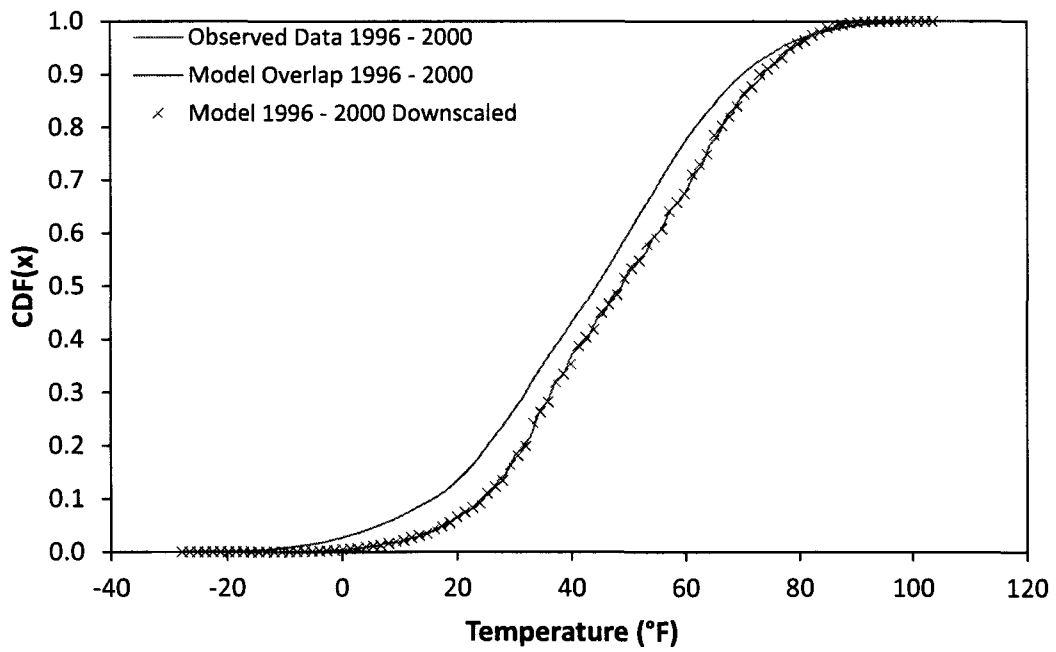


Figure 10 - CDF-t for the CRCM + CGCM3 RCM Model Overlap for Concord, NH

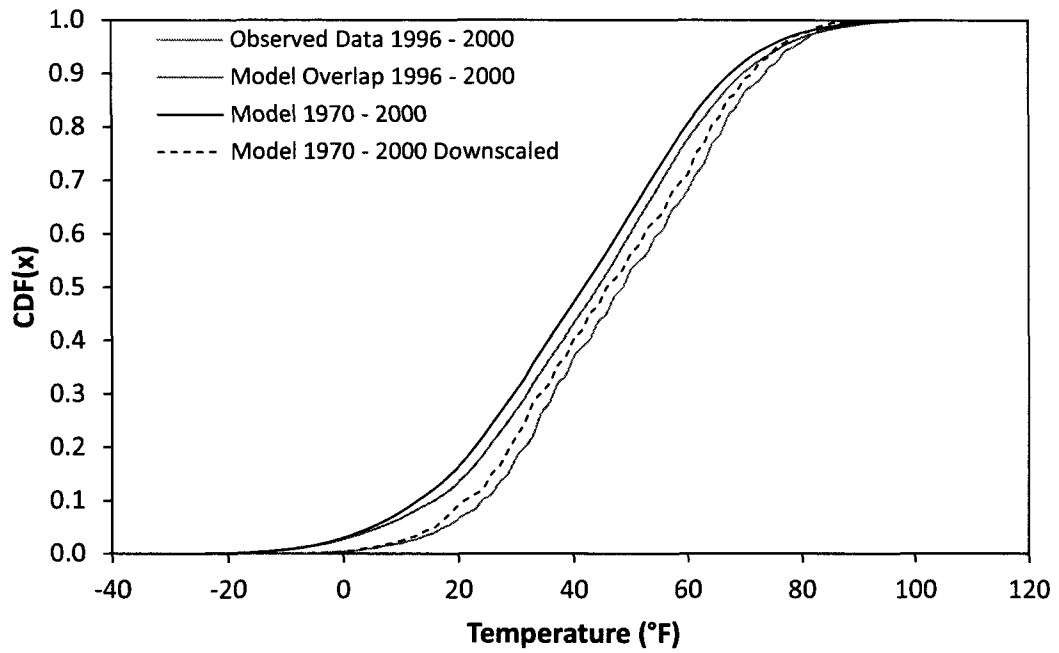


Figure 11 - CDF-t for the CRCM + CGCM3 RCM Model 1970 - 2000 for Concord, NH

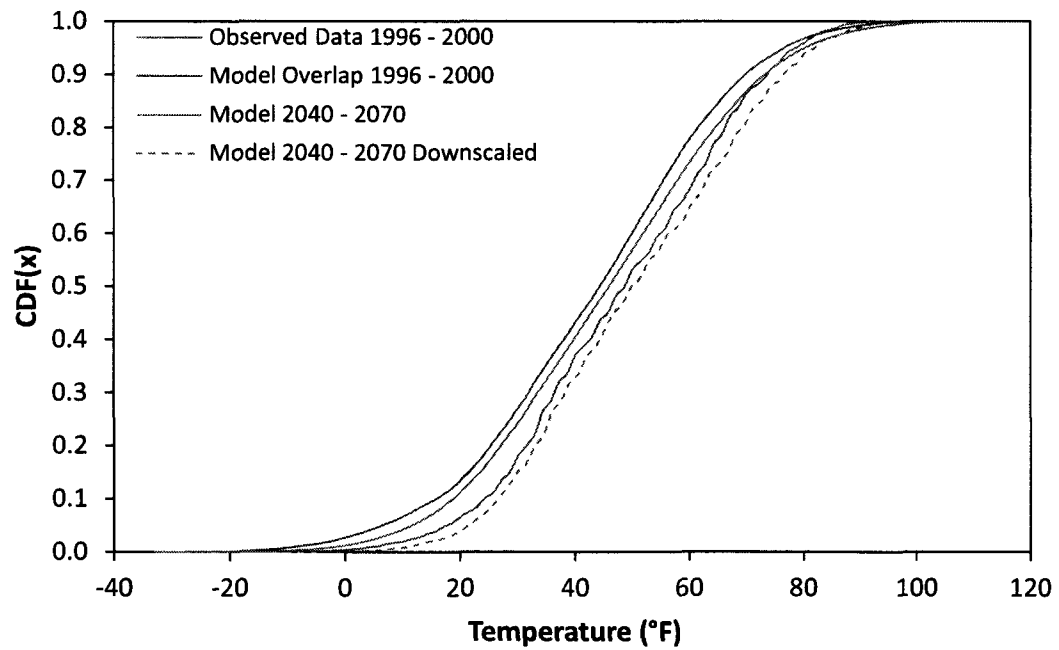


Figure 12 - CDF-t for the CRCM + CGCM3 RCM Model 2040 - 2070 for Concord, NH

Construction of M-E PDG Climate Data Files

Once the RCM data have been converted and downscaled, they must be reformatted to match the M-E PDG *Hourly Climatic File (.hcd)* (Step 4 in Figure 1). These files use comma separated value fields in order of the date (YYYYMMDDHH), temperature, wind speed (mph), percent sunshine, precipitation, and relative humidity in columns. For this study, only the temperature data were modified for the hindcast and future climate scenarios; all remaining climate data are from the original M-E PDG station. The hindcast temperature data were obtained from the RCM model data for the period of July 1, 1970 to June 31, 2000 and the future temperature data were obtained from the RCM model data for the period July 1, 2040 to June 31, 2070. For the hindcast time period (1970 – 2000) and the future time period (2040 – 2070) construction of the *Hourly Climatic File* both required the remaining climate variables for the obtained from the M-E PDG station data for the period of July 1, 1996 to June 30, 2000. These data were replicated 7.5 times to create a “virtual” station record with an equivalent 30 year length. This cycling follows the M-E PDG method used when the design period is longer than the station record (*Johanneck et al., 2010*). For example, if the design analysis is to be 10-years and the 4-year station data are available, the software would use the station data 2.5 times (the 5th and 9th years of the analysis would have the same climate as the 1st year).

For the hindcast period, July 1, 1996 to June 30, 2000 was matched and the data were copied backwards in time. The last cycle was truncated by cutting off the first two years, July 1, 1998 to June 30, 1999, of overlap to match the 30-year record length. For the future time period, the remaining variables from the period of July 1, 1996 to June 30, 2000 were cycled forward, so that the first time period in the future July 1, 2040 to June 20, 2044 matched July 1, 1996 to June 30, 2000. The last cycle was truncated by

cutting off the last two years of the station data, July 1 1999 to June 20, 2000. The reason for the difference was to match the leap years in the station data, and assure that every July 1 matched.

Before the climate data file can be read into the M-E PDG software, it must be assigned an unused station number in the station.dat file. For example, if the station number 00001 was available, then the file would be saved as 00001.hcd. The number is then added to the station.dat file list. The entry follows the format below,

Station No., City|State, Name, Latitude, Longitude, Elevation, Start Date

where *Station No.* is the assigned station number, *City|State* is the location, *Name* is the convention by which the station is identified, *Latitude* and *Longitude* are the geographic coordinates of the station, *Elevation* is the elevation in feet of the station, and *State Data* is the date of the first entry in the climate file following the YYYYMMDD format.

After constructing the M-E PDG climate data files, the M-E PDG is run as a standard analysis. It uses the required material properties and traffic inputs. The only change is that the climatic file is the one associated with the respective RCM scenario of interest.

CHAPTER IV – RESULTS

This section presents results for the methodology. The probabilistic transformation of the AOGCM+RCM data using the CDF-t method are presented for the hindcast climate model conditions and anticipated future climate model conditions. The model temperature, both hindcast and future, and observed temperature data are accompanied by location. Finally, alligator cracking and AC rutting results are presented for the hindcast climate model conditions, anticipated future climate model conditions, and the baseline (observed) conditions by study.

Three comparisons are made in this work. The first comparison is between the hindcast and observed/baseline conditions. The difference in this comparison provides a measure of the minimal error that one can expect from the climate model forecasts of future conditions based on how well it reproduces historic conditions. The second comparison is between the future and observed/baseline conditions. The difference in this comparison represents the change from using the standard design approach to one that incorporates climate change forecasts. Lastly, the third comparison examines the difference between the hindcast and future conditions. By removing errors between modeled hindcast and observed conditions, this comparison provides a consistent means to understand the relative impact due to climate change.

CDF-Transformation

Figures 13 to 36 show the CDF-transformations for hindcast and future temperature data by location. The Kolmogorov-Smirnov test results for both the hindcast model period data and future model period data are presented in Table 6. As shown in the odd numbered figures, the model hindcast temperature data are typically biased low compared to the observed data during both the overlap and hindcast periods. When transformed, the hindcast time series data is cooler than the observed data. However the CDF-t improves the fit of the CDF as compared to the non-transformed model hindcast data. The K-S test indicates that only the RCM3+GFDL model scenario for Boston, MA was significantly different from that of the observed station data. However, for every case the K-S results show that downscaled model data agrees better with the observed than the non-downscaled model data. Thus, the downscaled data are a better match of the observed data for all locations. K-S results are quite similar across sites and models for the hindcast period.

Future temperature data are warmer than the hindcast data for the overlap period. However, the model future temperature data are cooler than the observed data, but are biased high relative to the model hindcast data overlap. When transformed, the model future temperature CDFs are warmer than the observed data. Given the prediction for increased temperature in the future, the warmer data are to be expected. At each location, the model data for both non-downscaled and downscaled has a lower K-S value for the future period. As seen from the even number figures, the CDF-t changes the future temperature values from cooler than the observed to warmer. Despite this shift, the K-S statistics indicated these downscaled values are more similar to the observed values than the non-downscaled values. In fact, the CDF agreement is nearly identical to the hindcast values.

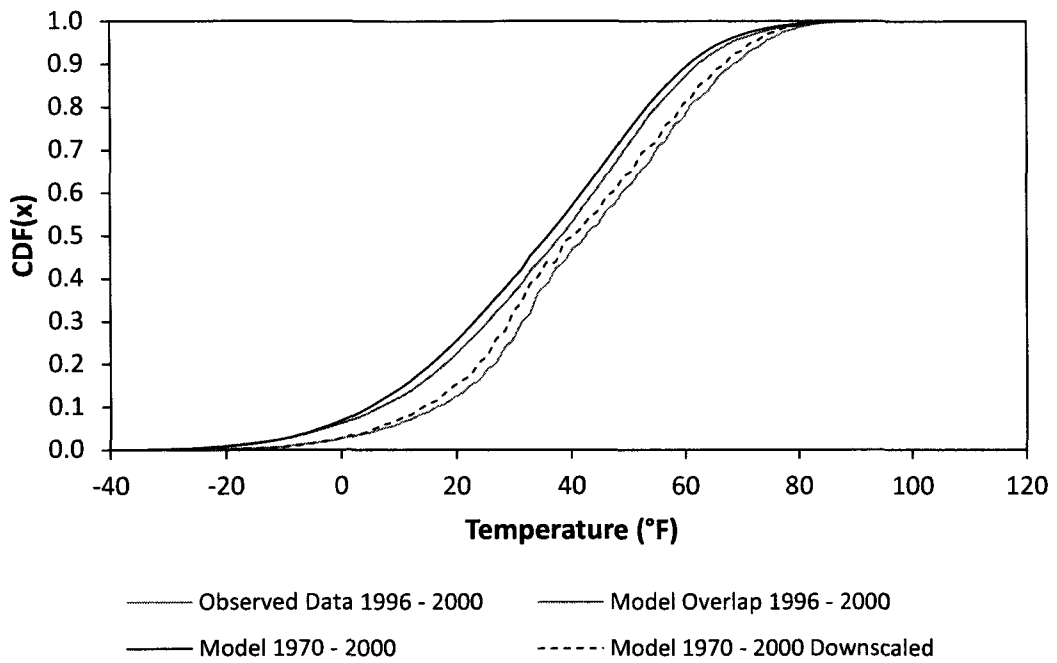


Figure 13 - CDF-t for CRCM+CGCM3 Model 1970 - 2000 for Berlin, NH

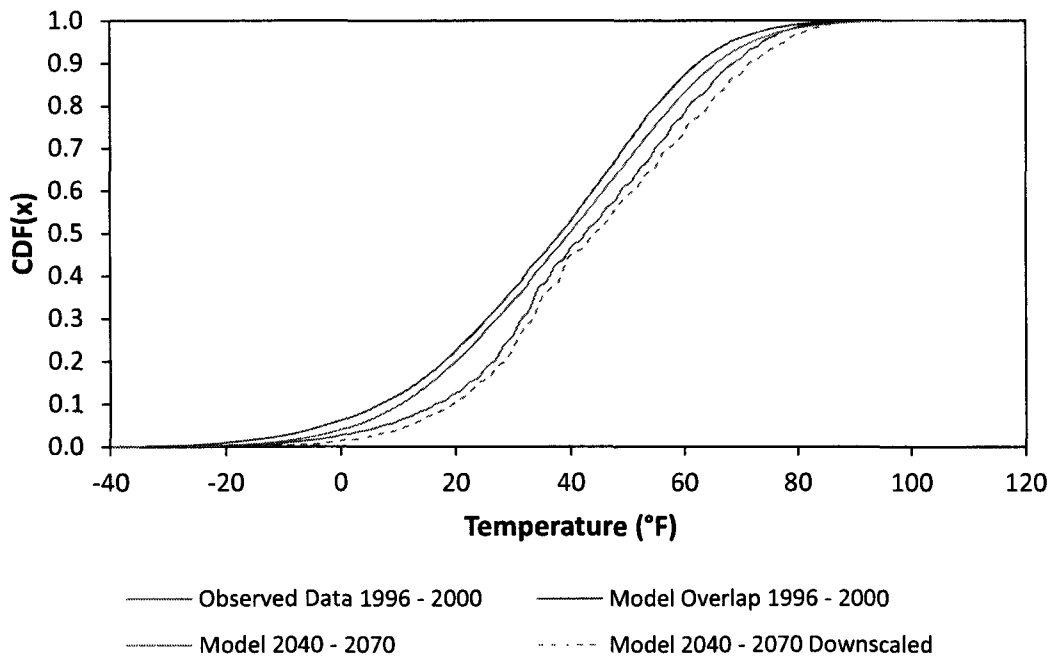


Figure 14 - CDF-t for CRCM+CGCM3 Model 2040 - 2070 for Berlin, NH

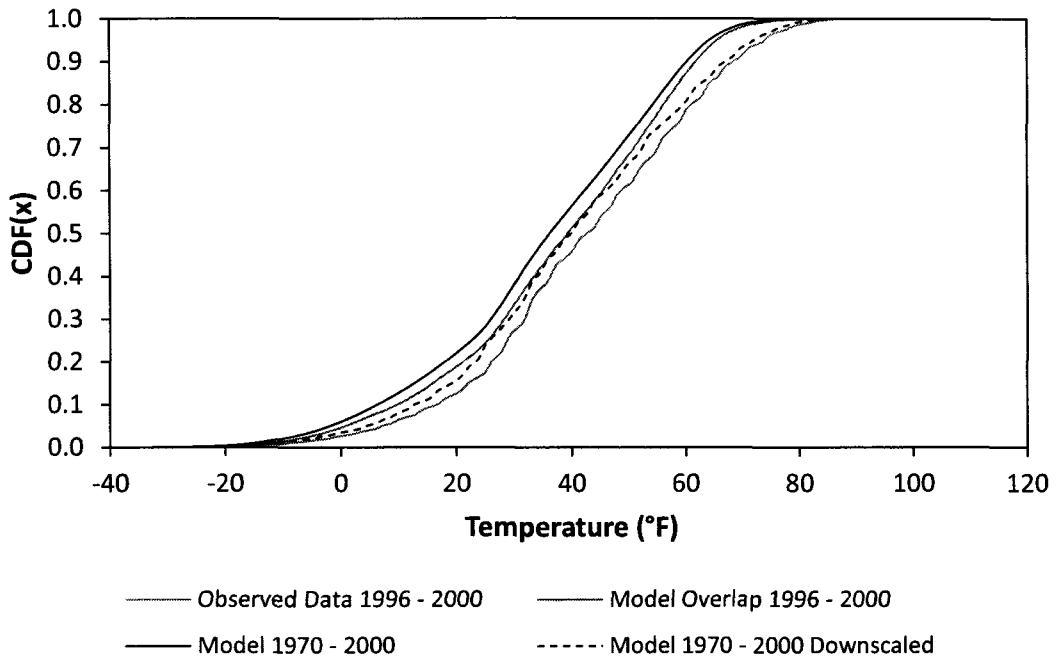


Figure 15 - CDF-t for RCM3+CGCM3 Model 1970 - 2000 for Berlin, NH

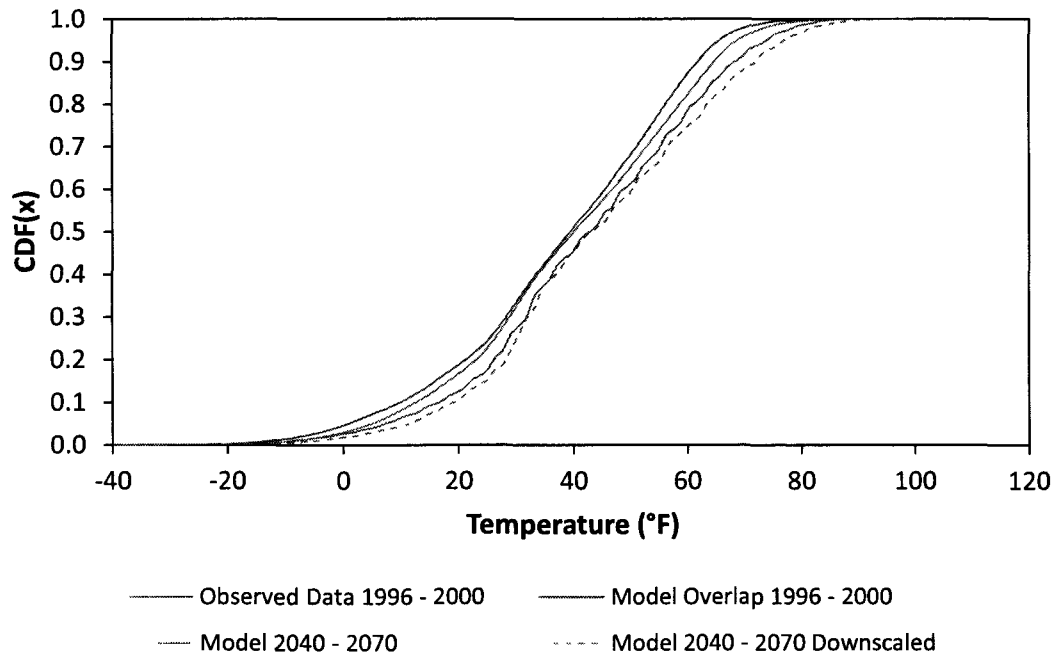


Figure 16 - CDF-t for RCM3+CGCM3 Model 2040 - 2070 for Berlin, NH

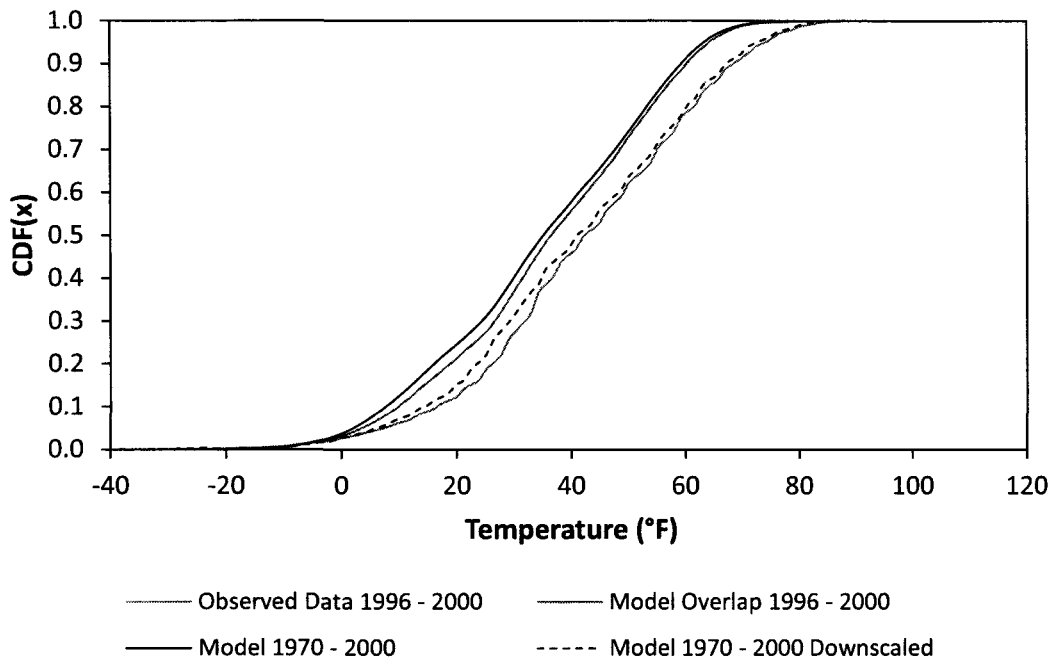


Figure 17 - CDF-t for RCM3+GFDL Model 1970 - 2000 for Berlin, NH

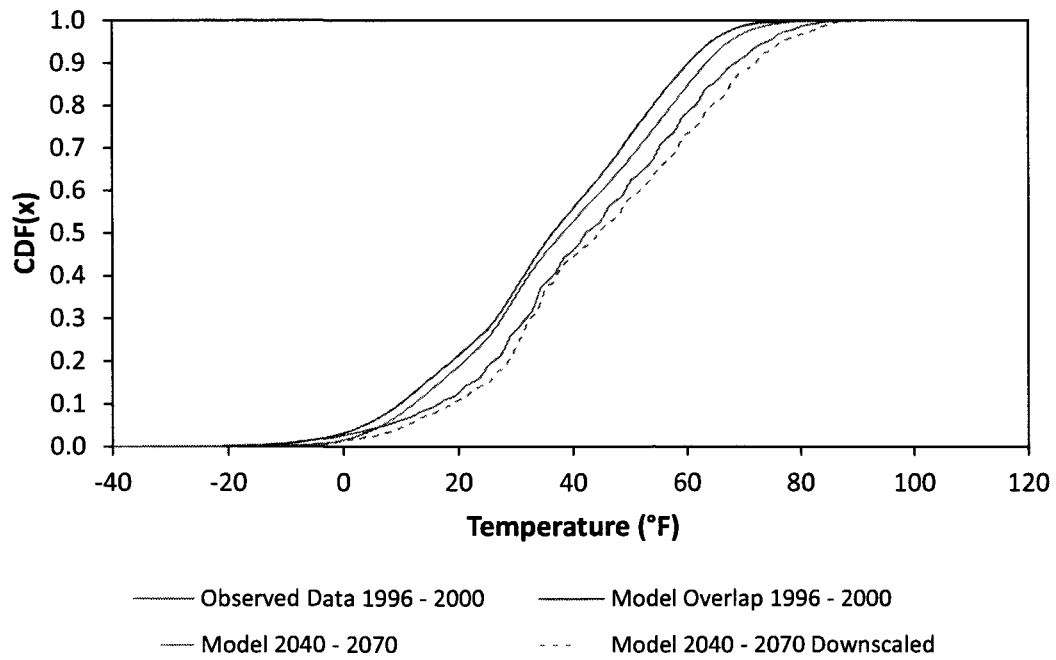


Figure 18 - CDF-t for RCM3+GFDL Model 2040 - 2070 for Berlin, NH

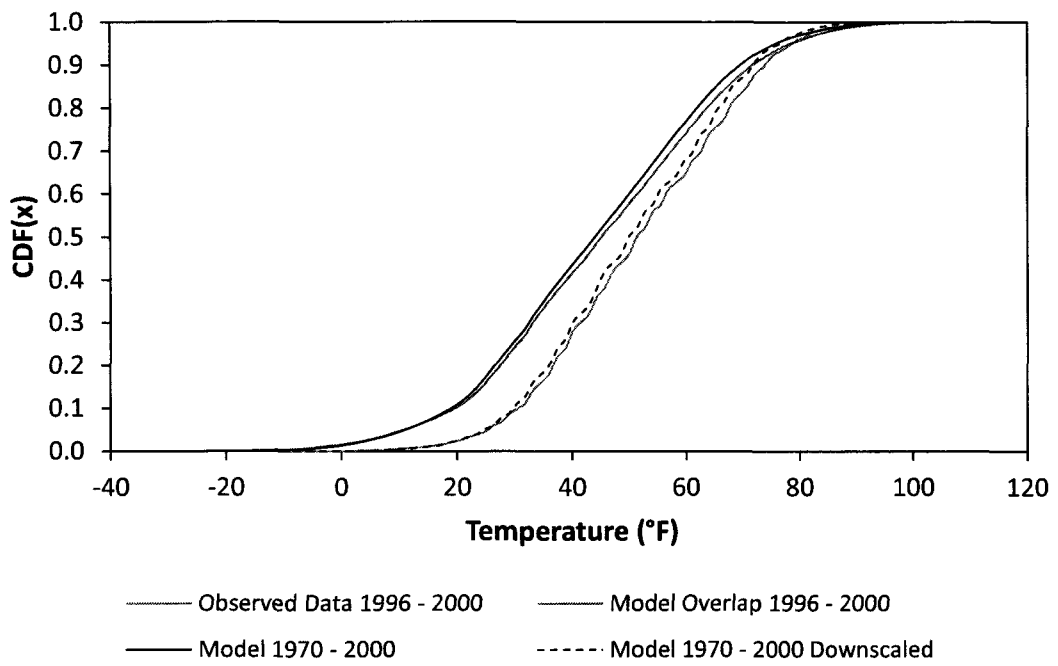


Figure 19 - CDF-t for CRCM+CGCM3 Model 1970 - 2000 for Boston, MA

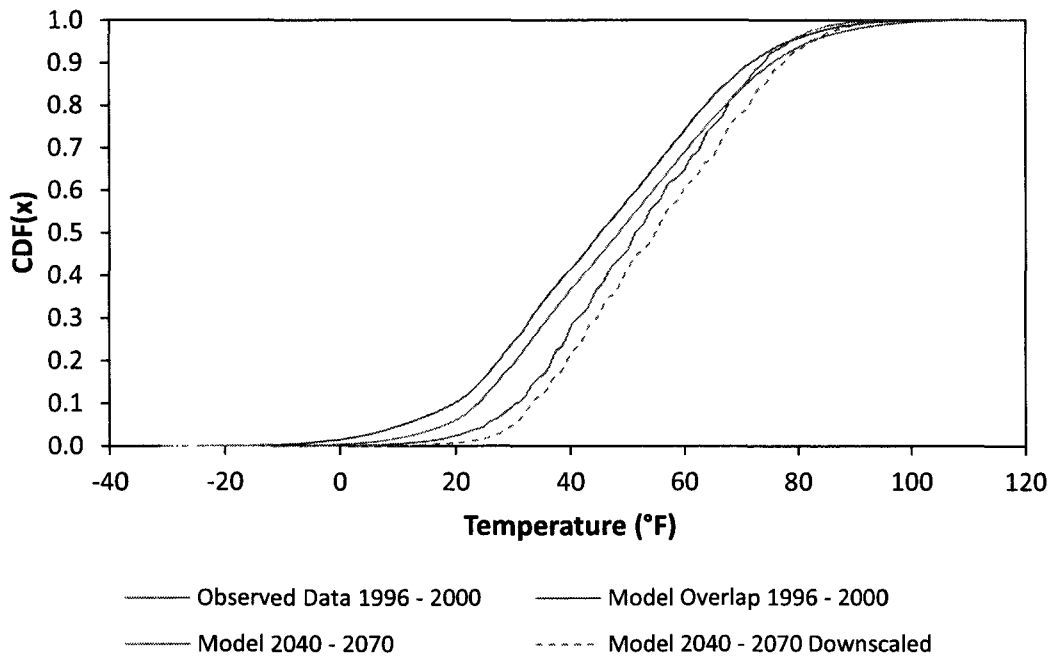


Figure 20 - CDF-t for CRCM+CGCM3 for Model 2040 - 2070 for Boston, MA

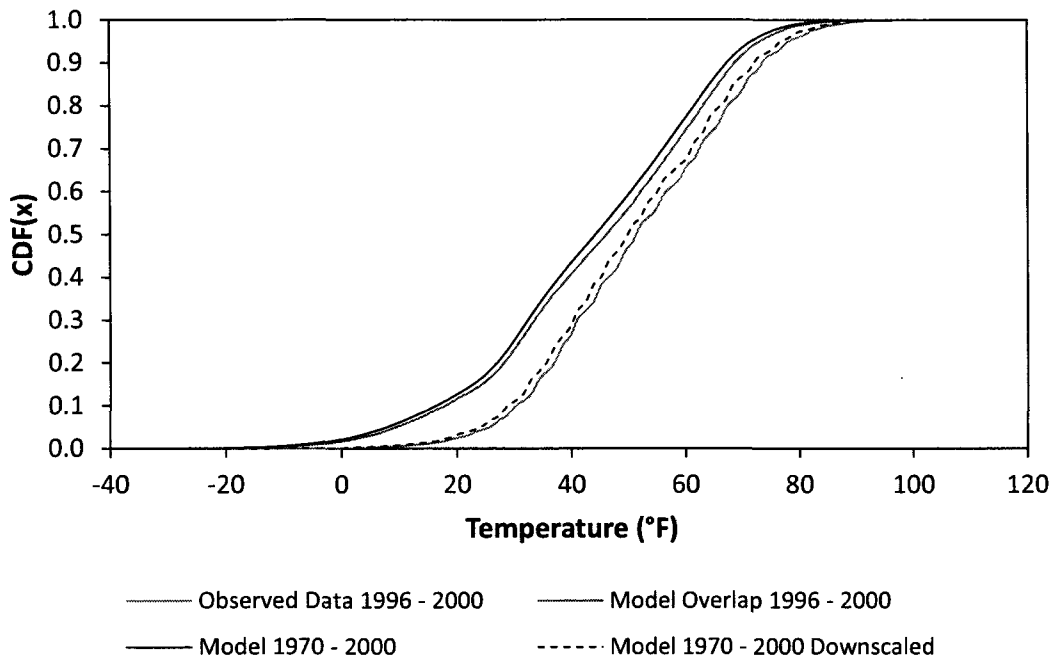


Figure 21 - CDF-t for RCM3+CGCM3 Model 1970 - 2000 for Boston, MA

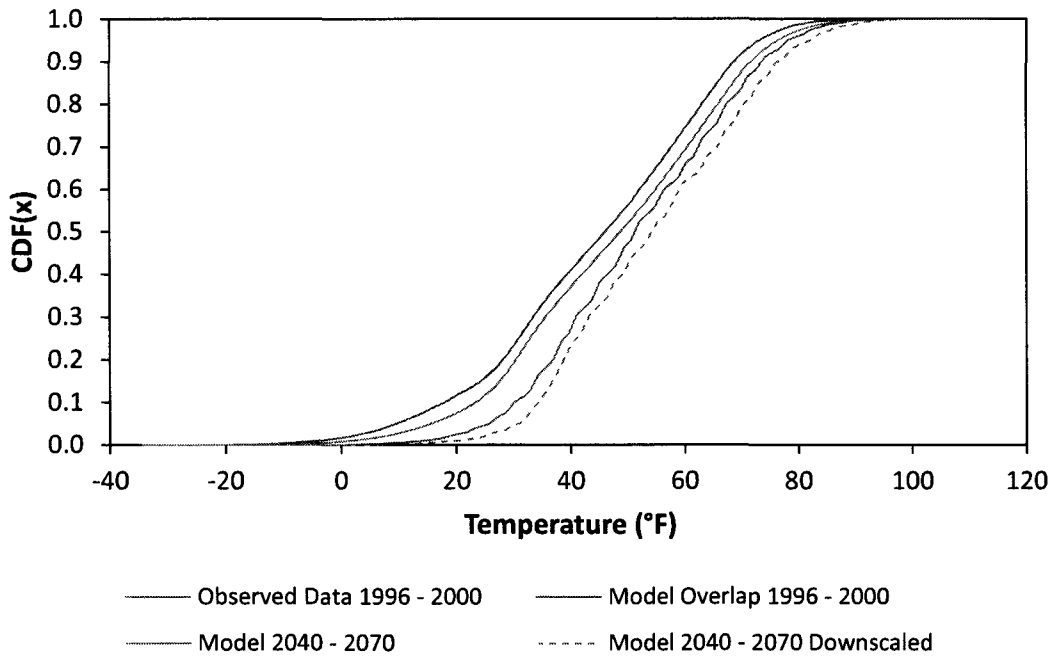


Figure 22 - CDF-t for RCM3+CGCM3 Model 2040 - 2070 for Boston, MA

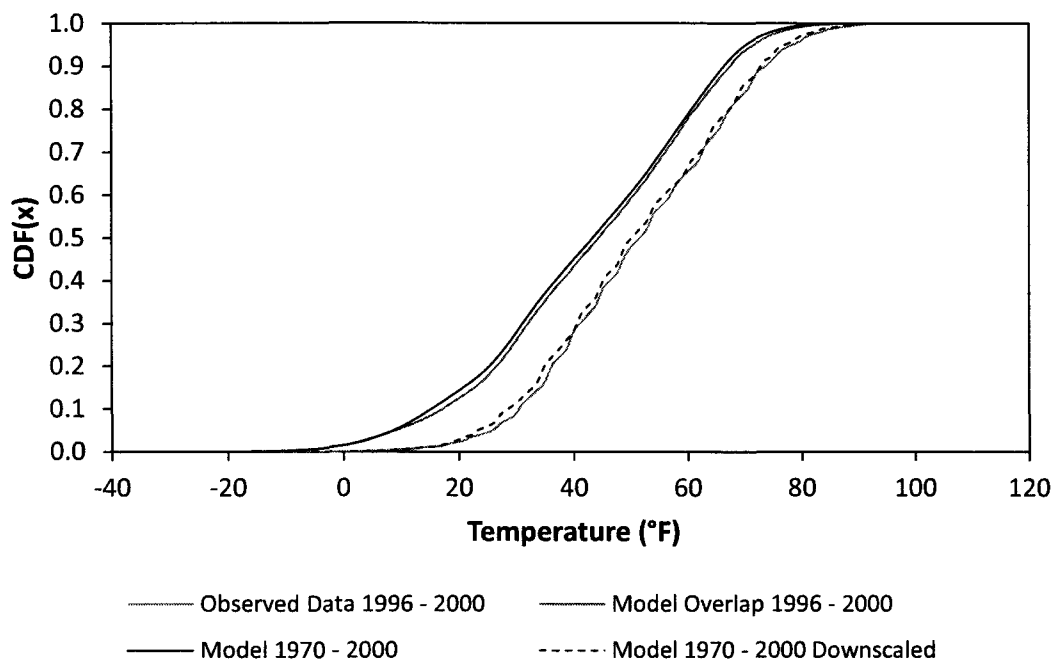


Figure 23 - CDF-t for RCM3+GFDL Model 1970 - 2000 for Boston, MA

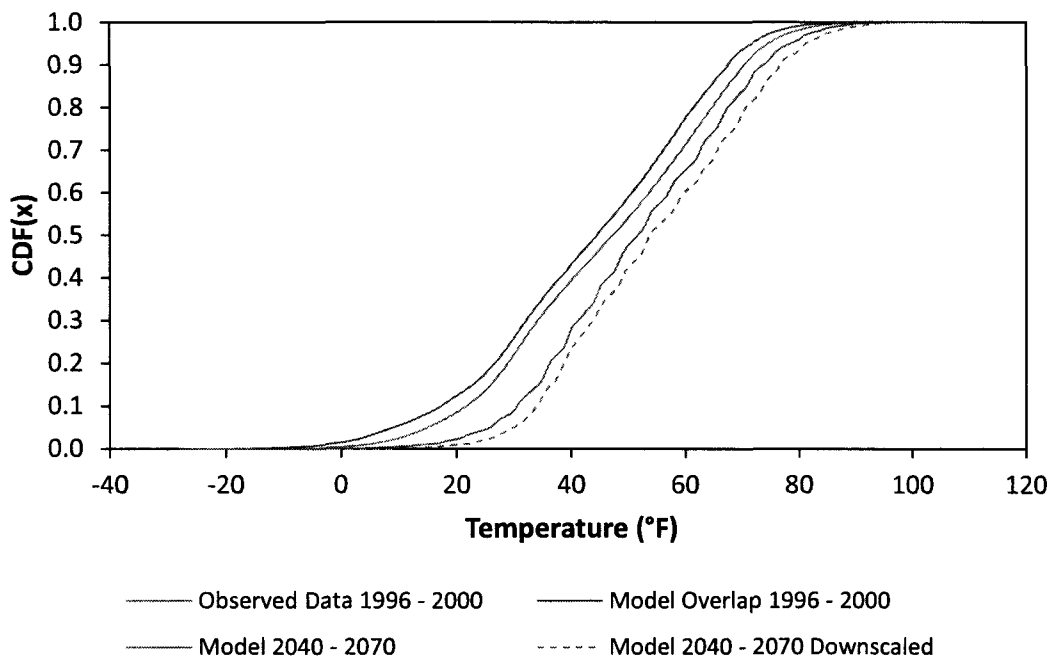


Figure 24 - CDF-t for RCM3+GFDL Model 2040 - 2070 for Boston, MA

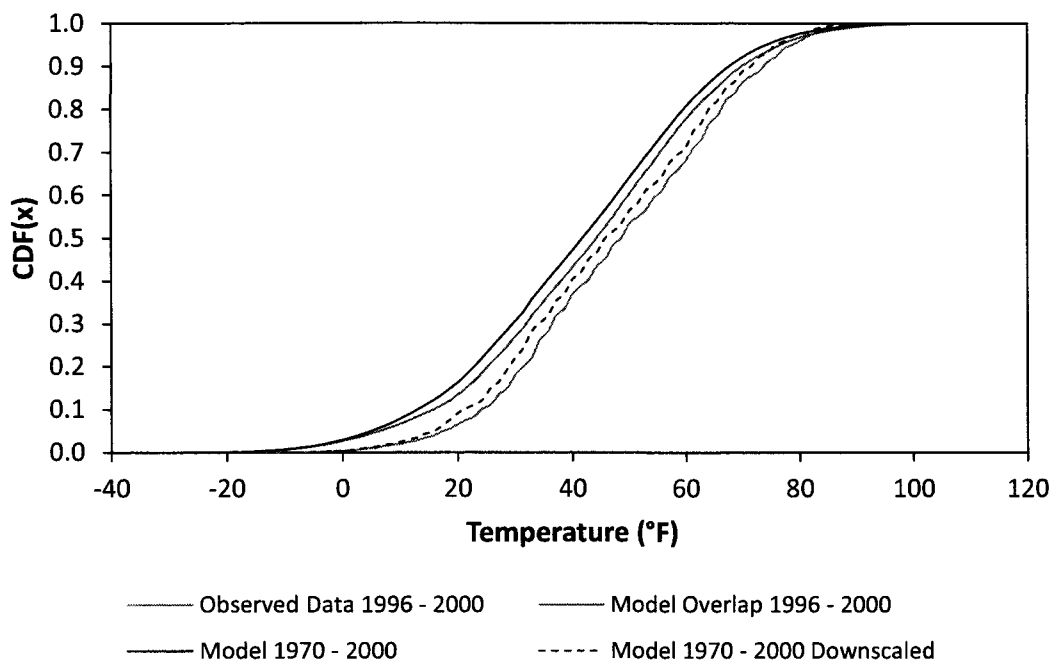


Figure 25 - CDF-t for CRCM+CGCM3 Model 1970 - 2000 for Concord, NH

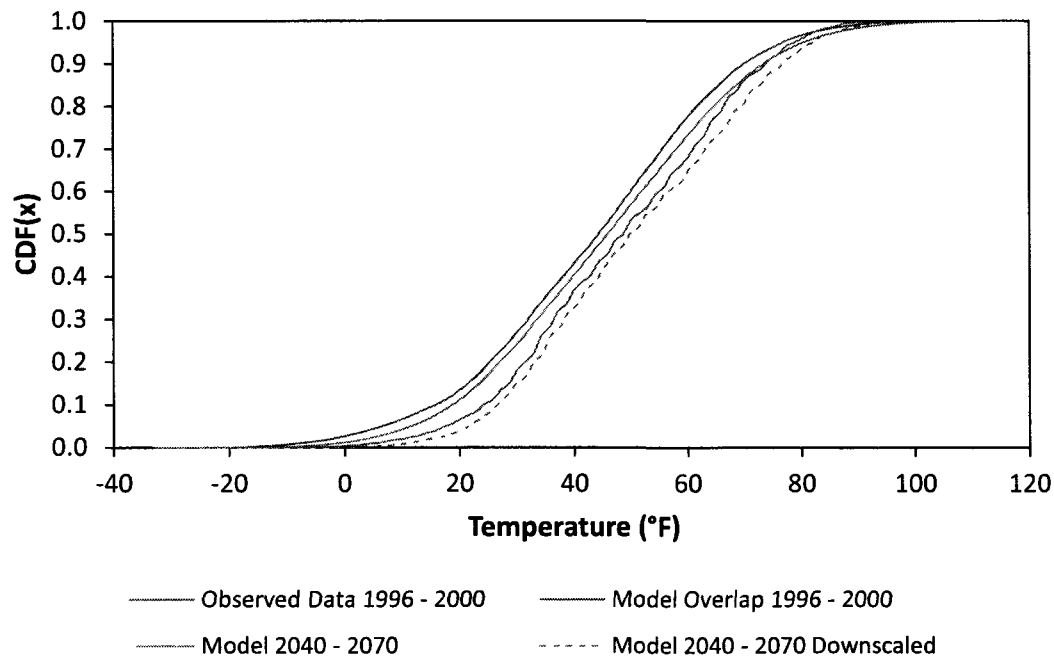


Figure 26 - CDF-t for CRCM+CGCM3 Model 2040 - 2070 for Concord, NH

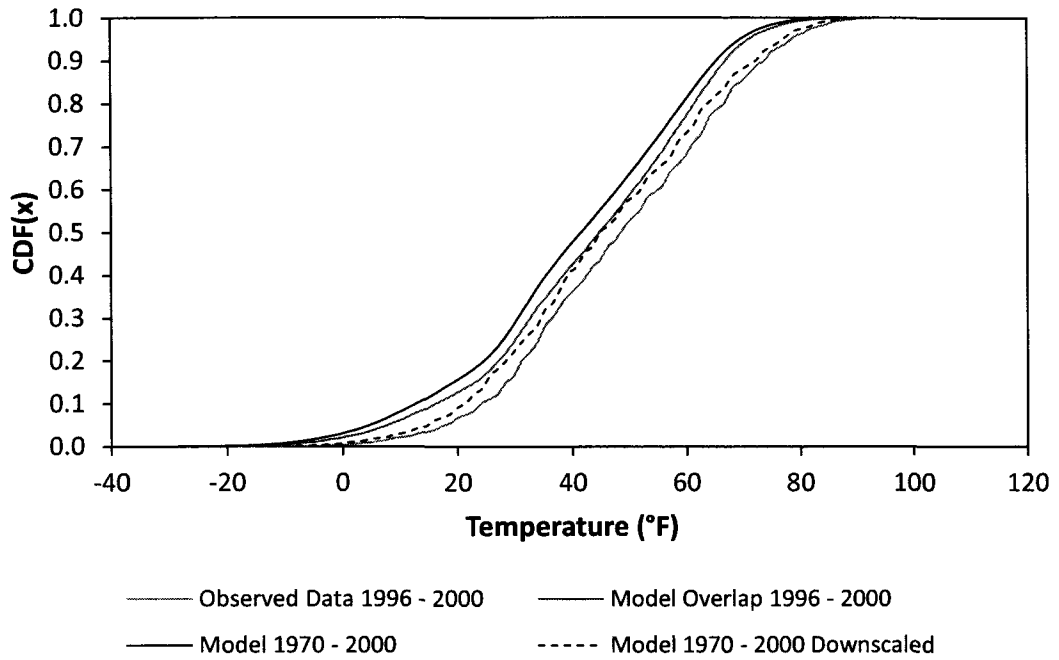


Figure 27 - CDF-t for RCM3+CGCM3 Model 1970 - 2000 for Concord, NH

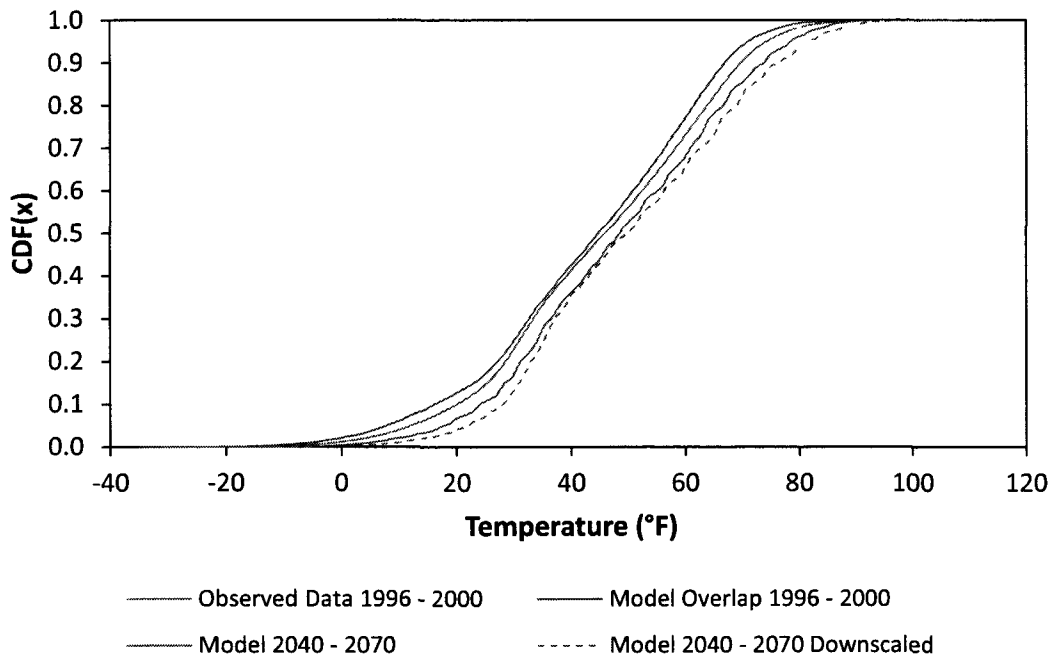


Figure 28 - CDF-t for RCM3+CGCM3 Model 2040 - 2070 for Concord, NH

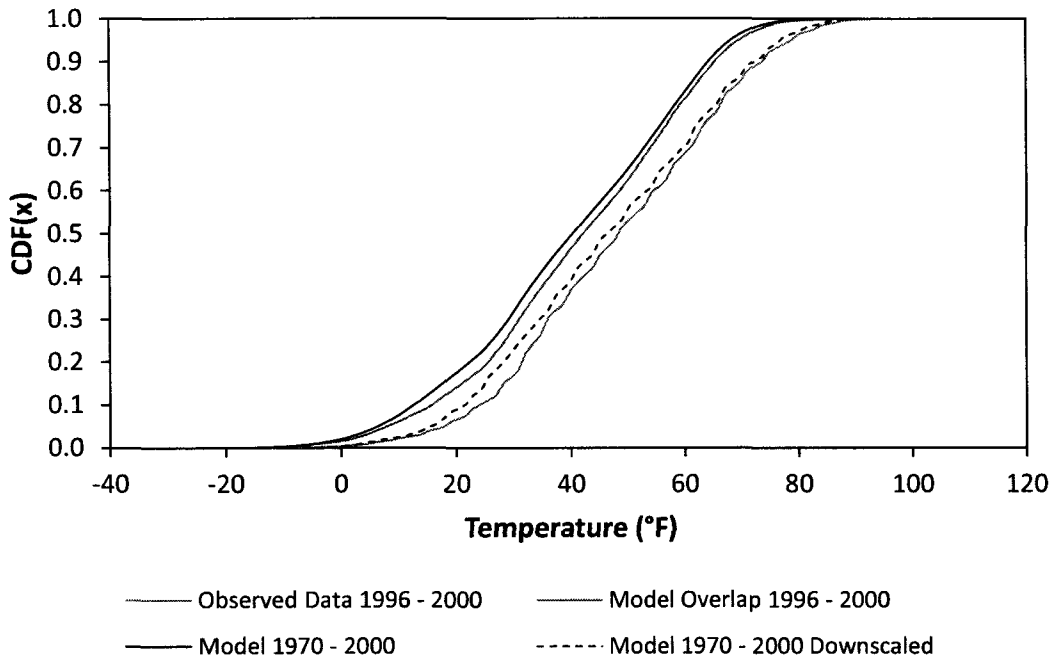


Figure 29 - CDF-t for RCM3+GFDL Model 1970 - 2000 for Concord, NH

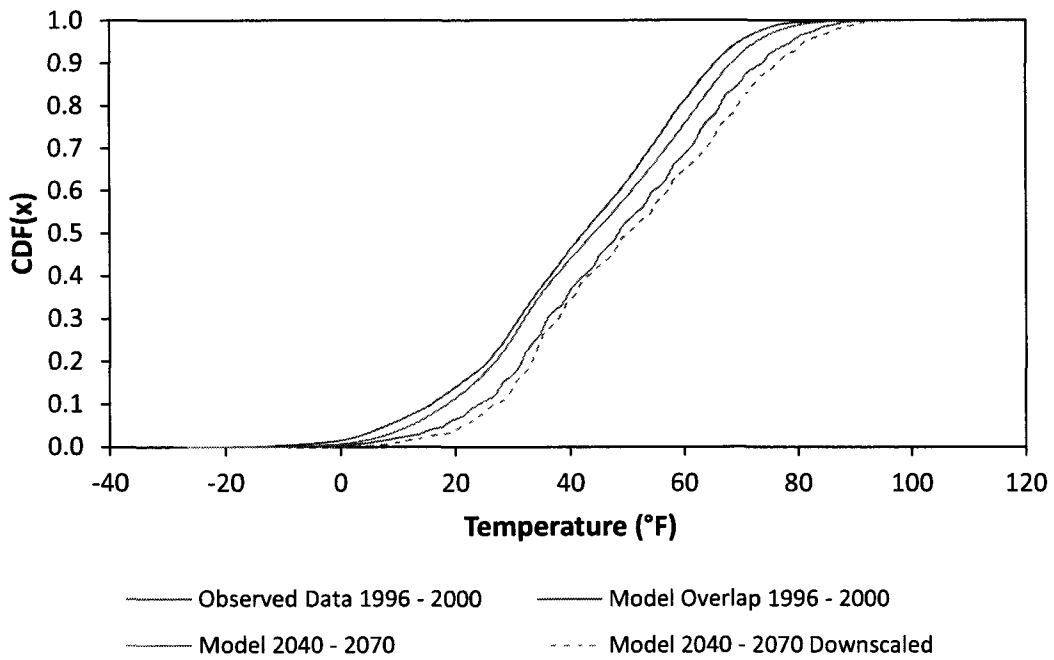


Figure 30 - CDF-t for RCM3+GFDL Model 2040 - 2070 for Concord, NH

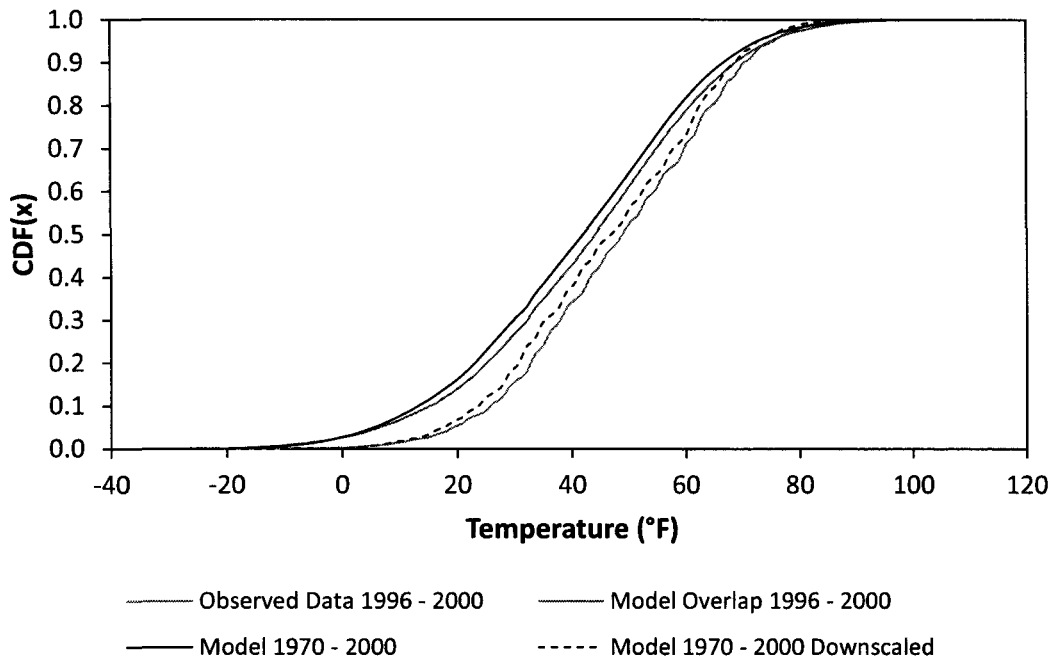


Figure 31 - CDF-t for CRCM+CGCM3 Model 1970 - 2000 for Portland, ME

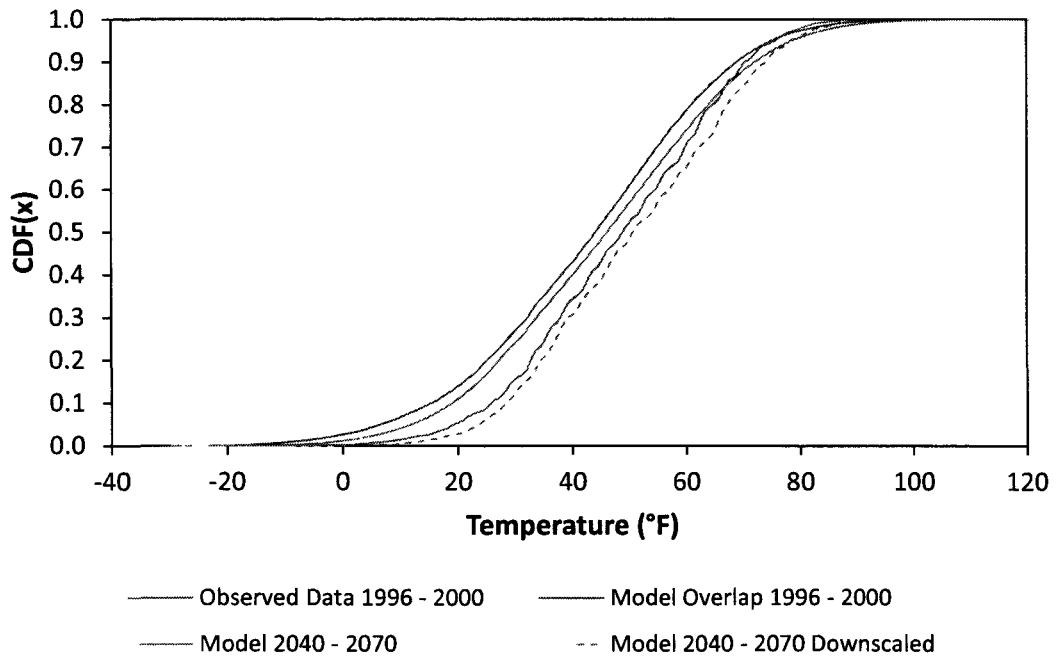


Figure 32 - CDF-t for CRCM+CGCM3 Model 2040 - 2070 for Portland, ME

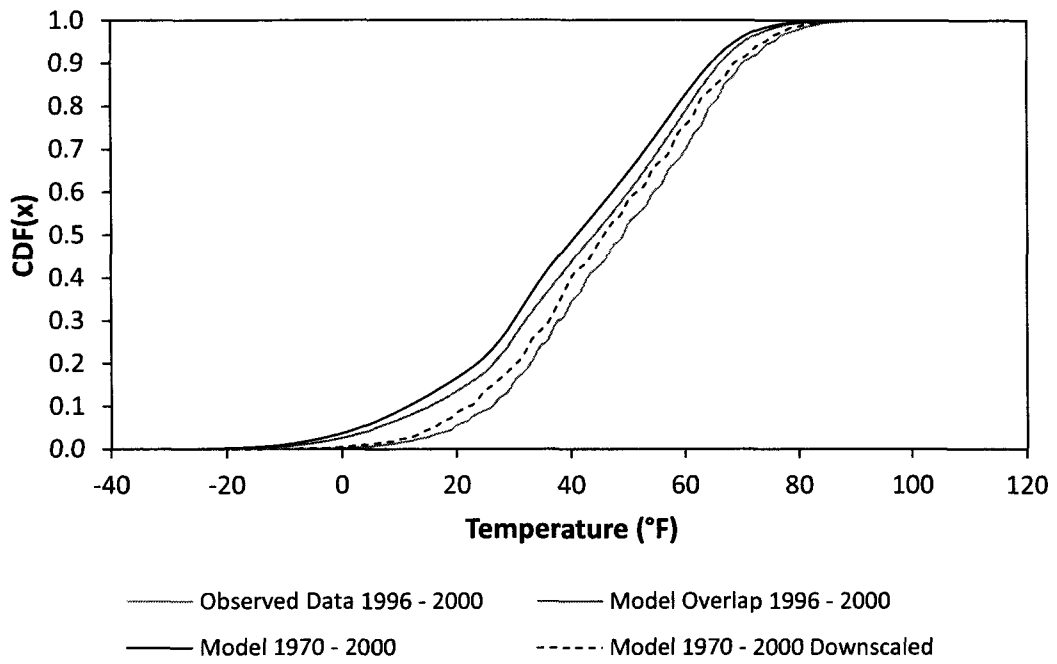


Figure 33 - CDF-t for RCM3+CGCM3 Model 1970 - 2000 for Portland, ME

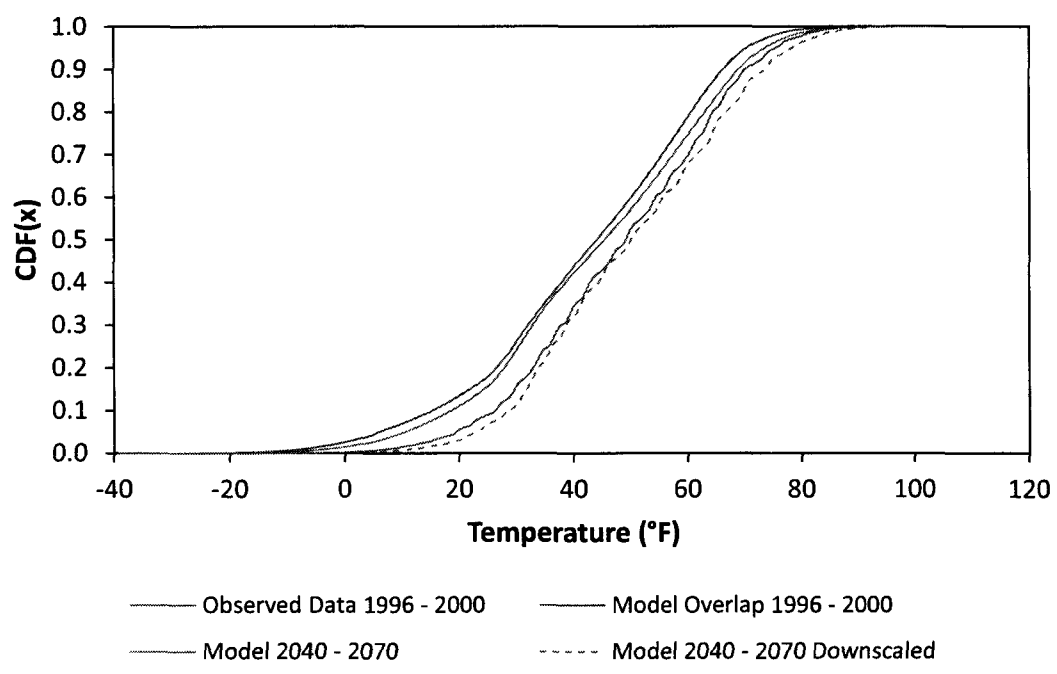


Figure 34 - CDF-t for RCM3+CGCM3 Model 2040 - 2070 for Portland, ME

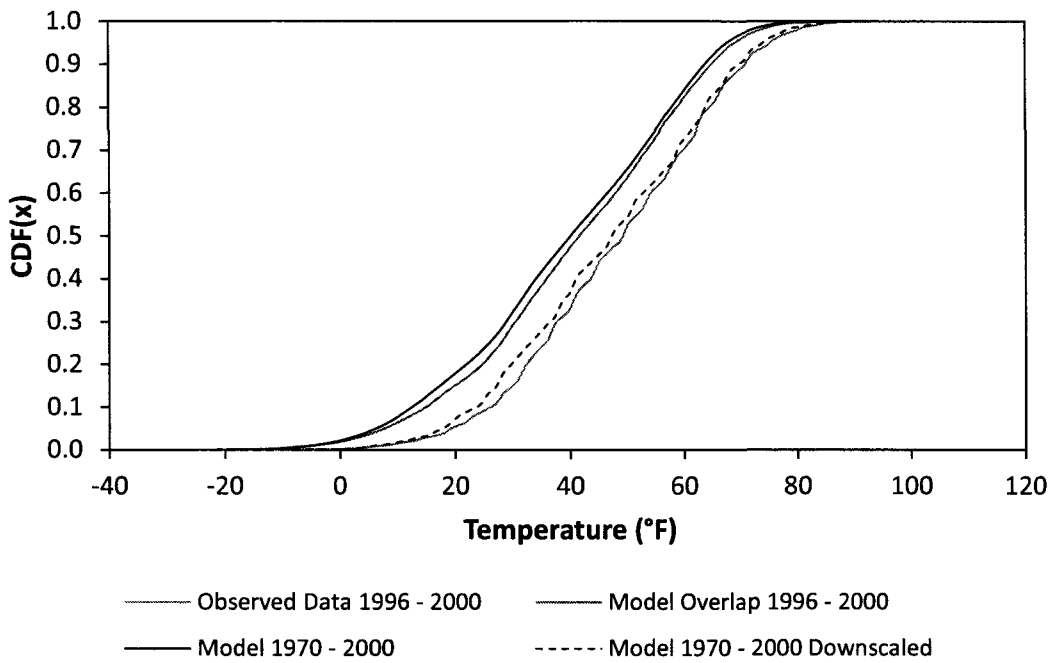


Figure 35 - CDF-t for RCM3+GFDL Model 1970 - 2000 for Portland, ME

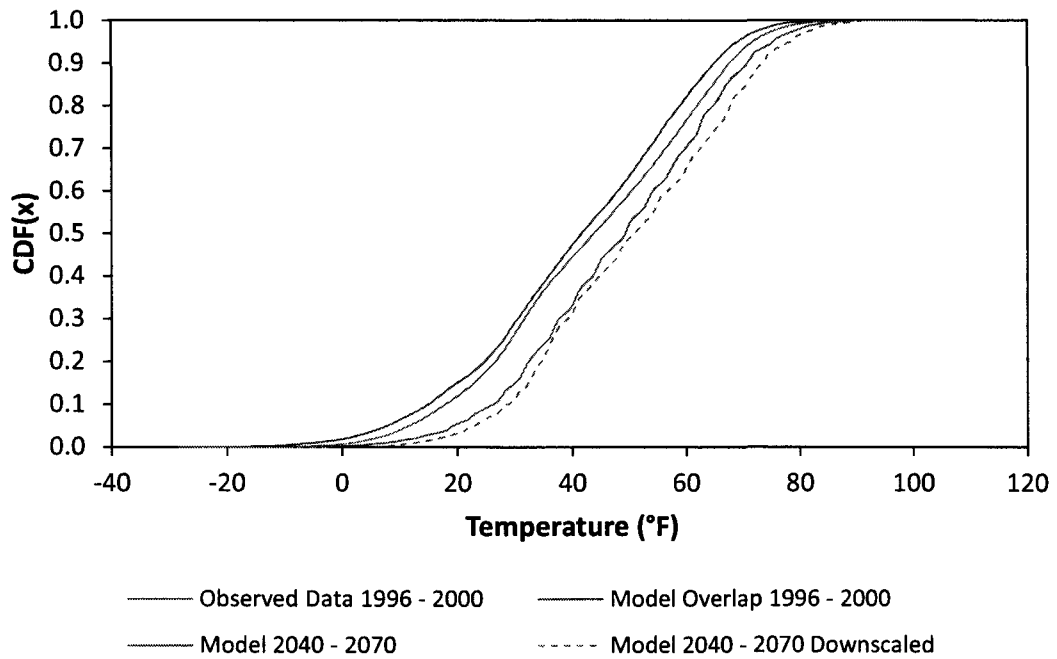


Figure 36 - CDF-t for RCM3+GFDL Model 2040 - 2070 for Portland, ME

Table 6 - Kolomogrov-Smirnov Test Values, Critical Value (*) = 0.192 Hindcast is for 1970 to 2000. Future is for 2040 to 2070.

	Model Scenario	Berlin, NH		Boston, MA		Concord, NH		Portland, ME	
		Model	Downscaled	Model	Downscaled	Model	Downscaled	Model	Downscaled
Hindcast	CRCM+CGCM3	0.152	0.063	0.184	0.045	0.139	0.058	0.156	0.057
	RCM3+CGCM3	0.122	0.063	0.187	0.043	0.130	0.058	0.160	0.066
	RCM3+GFDL	0.142	0.058	0.206*	0.036	0.149	0.059	0.180	0.057
Future	CRCM+CGCM3	0.093	0.057	0.116	0.078	0.076	0.063	0.093	0.076
	RCM3+CGCM3	0.061	0.050	0.125	0.070	0.067	0.056	0.101	0.061
	RCM3+GFDL	0.092	0.065	0.152	0.072	0.096	0.068	0.127	0.075

Model Temperature

This section presents the downscaled (transformed using CDF-t) model temperatures, hindcast and future, and observed temperatures by location.

Hindcast Model Temperature

The mean monthly air temperatures for the hindcast model scenarios and the measured station data (from the M-E PDG climate files) are presented in Figure 37. The models do a good job reproducing the temperature at each location for the spring and the winter months, but they slightly underpredict the temperature in August and September. The deviations in the months of August and September were initially thought to have occurred because of a difference in the timing of the peak mean monthly temperatures between the observed data and the model data. A comparison of the non-downscaled data and downscaled data showed this is not to be the case (Figures 3 and 37). The discrepancy may be in part due to model parameterization.

All model temperatures are cooler than the observed average annual temperature for all locations (Table 7). Typically, the average difference is less than 1°F. Concord, NH had the poorest agreement with two of the three models cooler by more than 1°F. The RCM3+GFDL model produces the closest average annual temperature at each location. The RCM3+CGCM3 exhibits the worst agreement at all locations. August and September temperatures were much cooler than the observed mean, with the coastal locations experiencing the biggest difference. Thus, Boston, MA and Portland, ME August and September temperatures were cooler by more than 4°F as compared the observed average monthly temperatures.

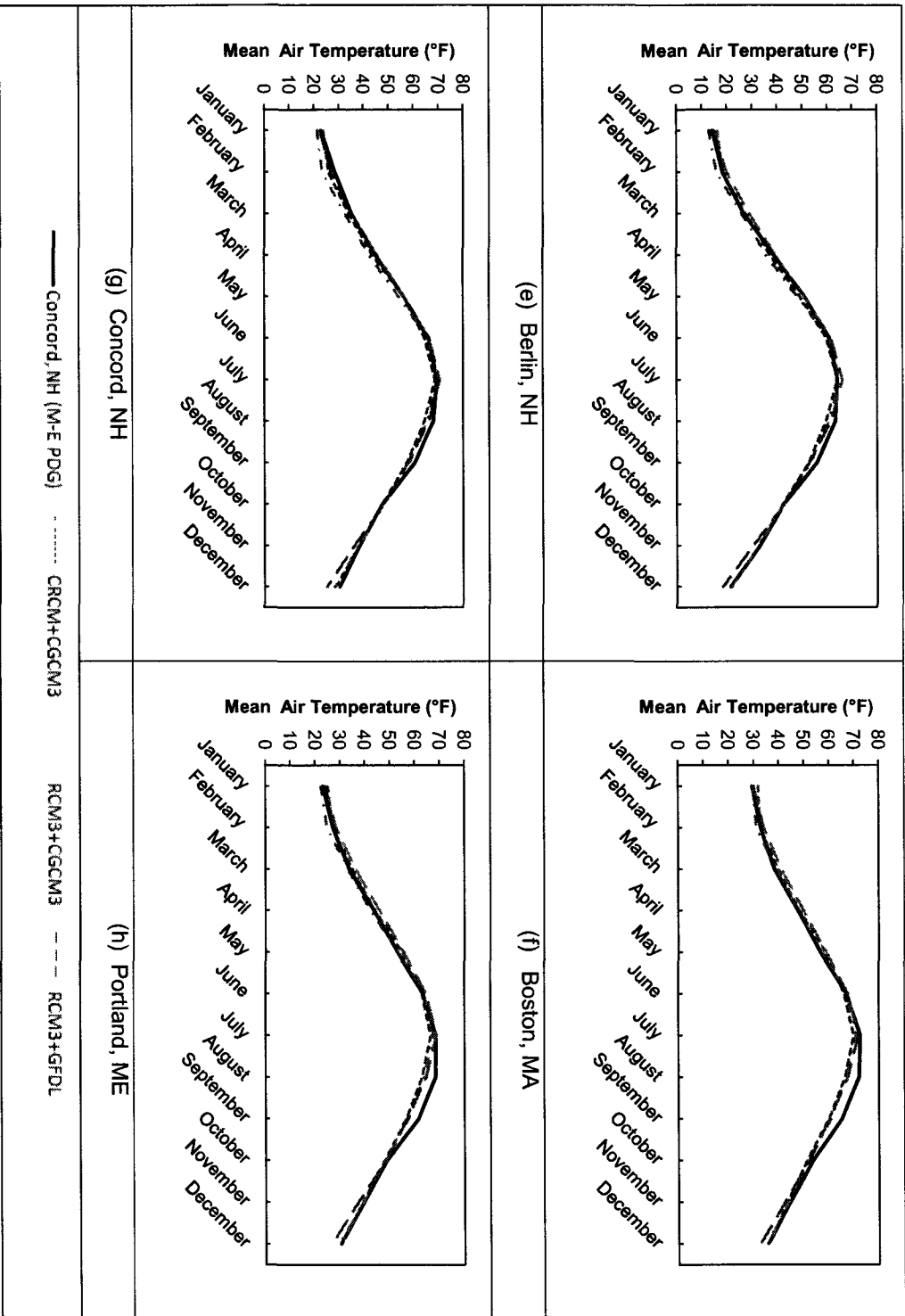


Figure 37 - Hindcast Model Mean Monthly Temperature

Table 7 - Difference (Model Prediction – Measured Value) in Hindcast Model Temperature

	Diff. Annual Air Temperature (°F)	Difference (Model - Obs.) in Air Temperature (°F)											
		January	February	March	April	May	June	July	August	September	October	November	December
Berlin, NH (M-E PDG)	40.97	14.31	18.36	26.91	39.04	51.12	61.05	64.11	63.34	56.00	42.76	33.25	21.35
CRCM+CGCM3	-0.75	2.08	0.07	0.75	-1.53	-1.84	-1.20	0.00	-3.70	-3.22	-0.42	-0.51	0.55
RCM3+CGCM3	-1.28	-1.39	-2.45	-0.92	-3.20	-2.99	-0.30	1.04	-2.63	-2.49	0.19	-0.54	0.34
RCM3+GFDL	-0.20	0.89	1.75	2.19	0.50	-0.25	0.71	2.09	-1.72	-2.98	0.22	-2.76	-3.03
<i>Model Average</i>	<i>-0.74</i>	<i>0.53</i>	<i>-0.21</i>	<i>0.67</i>	<i>-1.41</i>	<i>-1.69</i>	<i>-0.26</i>	<i>1.04</i>	<i>-2.68</i>	<i>-2.89</i>	<i>0.00</i>	<i>-1.27</i>	<i>-0.71</i>
Boston, MA (M-E PDG)	51.39	29.54	33.01	38.47	47.78	56.73	67.21	72.54	72.12	65.37	53.69	44.48	35.74
CRCM+CGCM3	-0.93	2.47	-0.15	1.45	0.58	2.11	-1.02	-2.51	-5.51	-5.32	-2.32	-1.02	0.07
RCM3+CGCM3	-1.16	0.09	-1.79	0.64	-0.08	0.74	0.12	-1.54	-4.94	-4.41	-1.61	-0.66	-0.44
RCM3+GFDL	-0.60	0.62	1.28	2.74	2.27	2.25	0.62	-0.81	-4.35	-5.08	-1.53	-2.07	-3.12
<i>Model Average</i>	<i>-0.90</i>	<i>1.06</i>	<i>-0.22</i>	<i>1.61</i>	<i>0.93</i>	<i>1.70</i>	<i>-0.09</i>	<i>-1.62</i>	<i>-4.93</i>	<i>-4.94</i>	<i>-1.82</i>	<i>-1.25</i>	<i>-1.16</i>
Concord, NH (M-E PDG)	47.49	23.04	28.65	35.36	45.13	56.37	66.31	69.51	68.14	60.69	47.75	38.52	30.39
CRCM+CGCM3	-1.28	0.89	-2.72	-1.23	-1.20	-0.14	-1.56	-0.69	-3.48	-3.25	-0.07	-0.28	-1.62
RCM3+CGCM3	-1.72	-1.68	-5.17	-2.77	-2.67	-1.95	-0.43	0.52	-2.55	-2.18	0.50	-0.11	-2.09
RCM3+GFDL	-0.94	-0.48	-1.64	-0.27	0.60	0.25	0.21	1.22	-1.81	-2.77	0.69	-2.08	-5.19
<i>Model Average</i>	<i>-1.31</i>	<i>-0.42</i>	<i>-3.18</i>	<i>-1.42</i>	<i>-1.09</i>	<i>-0.61</i>	<i>-0.59</i>	<i>0.35</i>	<i>-2.61</i>	<i>-2.73</i>	<i>0.37</i>	<i>-0.82</i>	<i>-2.97</i>
Portland, ME (M-E PDG)	46.90	23.22	27.32	33.96	44.01	53.30	63.49	68.51	68.43	61.59	48.91	39.67	30.42
CRCM+CGCM3	-0.69	2.09	-0.01	1.19	0.29	1.89	-0.46	-1.91	-5.35	-4.84	-0.85	-0.38	0.08
RCM3+CGCM3	-1.30	-0.77	-2.47	-0.52	-1.45	0.19	0.48	-0.82	-4.58	-4.05	-0.49	-0.25	-0.91
RCM3+GFDL	-0.27	1.12	1.24	2.65	2.17	2.49	1.29	0.22	-3.67	-4.40	-0.34	-2.24	-3.73
<i>Model Average</i>	<i>-0.75</i>	<i>0.81</i>	<i>-0.41</i>	<i>1.11</i>	<i>0.34</i>	<i>1.53</i>	<i>0.43</i>	<i>-0.83</i>	<i>-4.53</i>	<i>-4.43</i>	<i>-0.56</i>	<i>-0.96</i>	<i>-1.52</i>

Future Model Temperature

For the future time period, the models predict higher temperatures for much of the year, with larger differences in the spring and early summer months and minimal differences in the late summer and fall (Figure 38). August and September exhibit the smallest difference, indicating that there is a chance that the summer extremes are not being correctly captured. The summer extremes may not be correctly captured due to an insufficient overlap period between the observed data and hindcast model data or due to model parameterization. Table 8 shows that the average annual temperature change between the future period and the observed data for 10 of the 12 cases fall within the IPCC range (3.2 to 7°F) of the best estimates of global average annual temperature increase over the next century (*IPCC, 2007*). The two cases where the annual average temperature change is lower than the IPCC estimates are the RCM3+CGCM3 scenarios for Concord, NH and Portland, ME. However, when the model scenarios are averaged at each location, Portland, ME falls within the global average annual range and Concord, NH only falls 0.02°F below the IPCC estimates.

Table 9 shows that the average annual temperature changes between the future and hindcast periods for all cases fall within IPCC range (3.2 to 7°F) of the best estimates of global average annual temperature increase over the next century (*IPCC, 2007*). The GFDL AOGCM produces the lowest temperature change for all locations. The coastal locations, Boston, MA and Portland, ME, have less change than that of the inland locations, Concord, NH and Berlin, NH. The RCM3+CGCM3 model has the largest temperature difference in January. The RCM3+GFDL has the largest difference occurring in December. The CRCM+CGCM3 model has two of the four locations, Berlin, NH and Portland, ME, experiencing the largest difference in the winter months, and the remaining locations, Concord, NH and Boston, MA, with the largest difference in July.

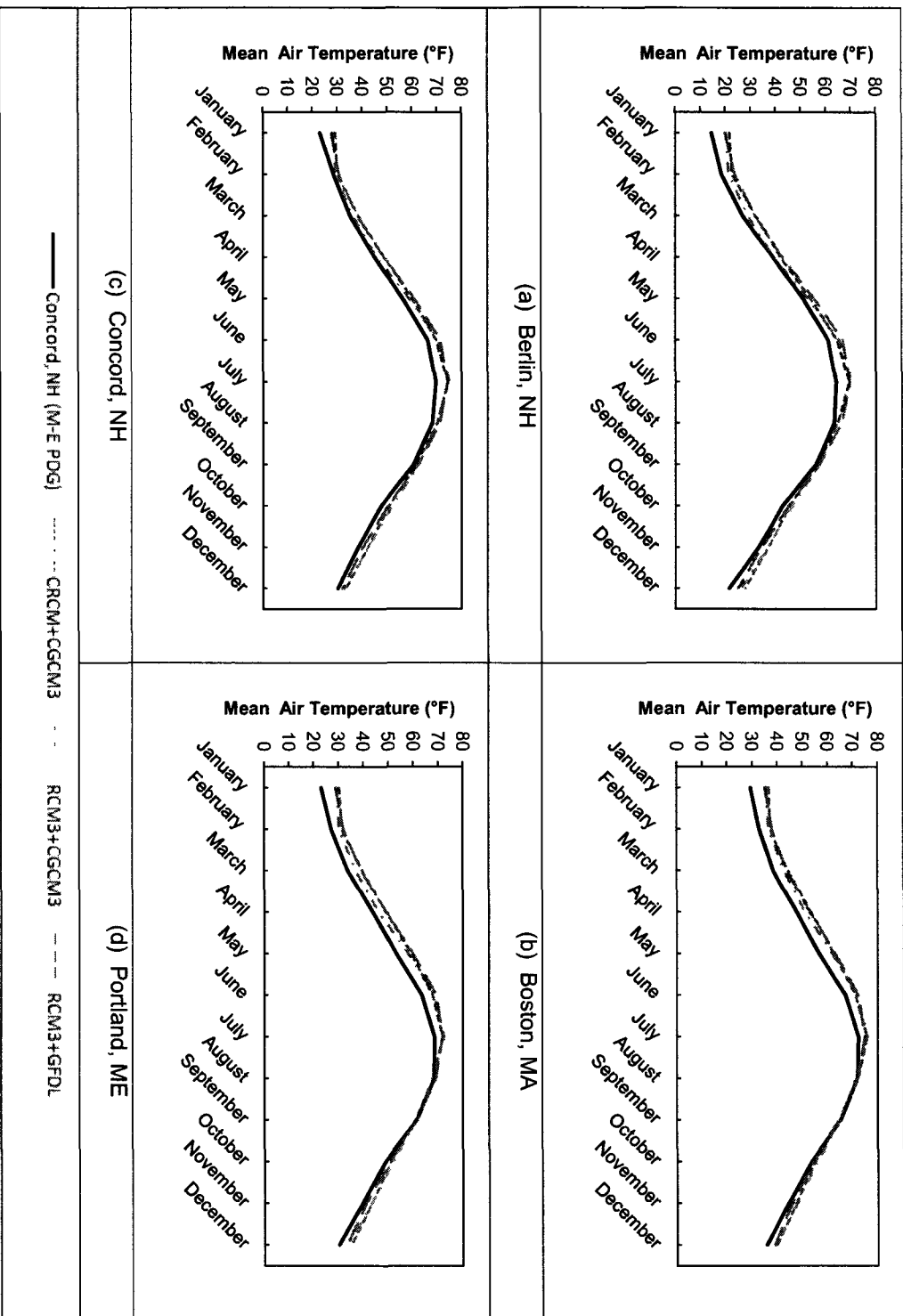


Figure 38 - Future Model Mean Monthly Temperature

Table 8 - Difference (Model Prediction – Measured Value) in Future Model Temperature

	Diff. Annual Air Temperature (°F)	Difference (Model - Obs.) in Air Temperature (°F)											
		January	February	March	April	May	June	July	August	September	October	November	December
Berlin, NH (M-E PDG)	40.97	14.31	18.36	26.91	39.04	51.12	61.05	64.11	63.34	56.00	42.76	33.25	21.35
CRCM+CGCM3	3.88	7.32	4.25	5.10	3.04	2.85	3.62	5.21	1.50	0.65	2.82	3.76	6.41
RCM3+CGCM3	3.24	5.91	2.86	2.09	0.14	1.88	4.40	6.35	1.33	1.59	4.00	3.51	4.82
RCM3+GFDL	3.92	5.48	5.36	5.08	3.74	4.39	5.84	5.39	3.12	1.49	2.42	1.15	3.58
<i>Model Average</i>	<i>3.68</i>	<i>6.24</i>	<i>4.16</i>	<i>4.09</i>	<i>2.31</i>	<i>3.04</i>	<i>4.62</i>	<i>5.65</i>	<i>1.98</i>	<i>1.24</i>	<i>3.08</i>	<i>2.81</i>	<i>4.94</i>
Boston, MA (M-E PDG)	51.39	29.54	33.01	38.47	47.78	56.73	67.21	72.54	72.12	65.37	53.69	44.48	35.74
CRCM+CGCM3	3.74	7.08	4.20	5.89	5.75	5.92	4.07	3.38	0.24	-0.33	1.43	2.99	4.29
RCM3+CGCM3	3.33	6.23	3.49	4.57	3.27	5.27	4.82	3.43	-0.67	-0.01	2.35	3.46	3.68
RCM3+GFDL	3.34	5.65	4.97	5.47	5.33	6.40	5.21	2.46	0.22	-0.62	0.47	1.41	3.14
<i>Model Average</i>	<i>3.47</i>	<i>6.32</i>	<i>4.22</i>	<i>5.31</i>	<i>4.79</i>	<i>5.86</i>	<i>4.70</i>	<i>3.09</i>	<i>-0.07</i>	<i>-0.32</i>	<i>1.42</i>	<i>2.62</i>	<i>3.70</i>
Concord, NH (M-E PDG)	47.49	23.04	28.65	35.36	45.13	56.37	66.31	69.51	68.14	60.69	47.75	38.52	30.39
CRCM+CGCM3	3.35	6.18	1.51	3.21	3.82	3.71	3.43	4.94	1.99	1.11	3.18	3.82	3.32
RCM3+CGCM3	2.94	5.45	0.69	1.04	0.77	2.64	4.24	5.53	1.75	2.16	4.43	4.10	2.48
RCM3+GFDL	3.24	4.62	2.16	2.75	3.83	4.57	5.16	4.74	3.01	1.84	2.59	1.85	1.80
<i>Model Average</i>	<i>3.18</i>	<i>5.42</i>	<i>1.45</i>	<i>2.34</i>	<i>2.81</i>	<i>3.64</i>	<i>4.28</i>	<i>5.07</i>	<i>2.25</i>	<i>1.70</i>	<i>3.40</i>	<i>3.26</i>	<i>2.53</i>
Portland, ME (M-E PDG)	46.90	23.22	27.32	33.96	44.01	53.30	63.49	68.51	68.43	61.59	48.91	39.67	30.42
CRCM+CGCM3	3.85	7.39	4.29	5.86	5.13	5.91	4.24	3.30	-0.25	-0.53	2.21	3.80	4.87
RCM3+CGCM3	3.19	6.28	3.14	3.23	2.15	4.69	4.95	3.97	-0.64	0.12	3.24	3.71	3.39
RCM3+GFDL	3.69	5.89	4.90	5.38	5.32	6.59	5.84	3.39	0.66	-0.08	1.77	1.49	3.10
<i>Model Average</i>	<i>3.57</i>	<i>6.52</i>	<i>4.11</i>	<i>4.82</i>	<i>4.20</i>	<i>5.73</i>	<i>5.01</i>	<i>3.55</i>	<i>-0.08</i>	<i>-0.16</i>	<i>2.40</i>	<i>3.00</i>	<i>3.79</i>

Table 9 - Difference (Future - Hindcast) in Model Temperature

	Diff. Annual Air Temperature (°F)	Difference (Future - Hindcast) in Air Temperature (°F)											
		January	February	March	April	May	June	July	August	September	October	November	December
Berlin, NH													
CRCM+CGCM3	4.63	5.24	4.18	4.35	4.57	4.70	4.83	5.21	5.20	3.87	3.24	4.28	5.87
RCM3+CGCM3	4.52	7.30	5.32	3.01	3.34	4.87	4.70	5.31	3.96	4.08	3.81	4.05	4.47
RCM3+GFDL	4.12	4.60	3.61	2.89	3.24	4.64	5.13	3.29	4.84	4.46	2.20	3.91	6.61
<i>Model Average</i>	4.42	5.71	4.37	3.42	3.72	4.74	4.89	4.60	4.67	4.14	3.09	4.08	5.65
Boston, MA													
CRCM+CGCM3	4.67	4.61	4.35	4.44	5.17	3.81	5.09	5.89	5.75	4.99	3.74	4.00	4.22
RCM3+CGCM3	4.48	6.14	5.29	3.93	3.35	4.53	4.69	4.97	4.28	4.40	3.96	4.12	4.12
RCM3+GFDL	3.94	5.04	3.69	2.73	3.06	4.15	4.59	3.27	4.57	4.46	2.00	3.48	6.26
<i>Model Average</i>	4.37	5.26	4.44	3.70	3.86	4.17	4.79	4.71	4.87	4.62	3.24	3.87	4.87
Concord, NH													
CRCM+CGCM3	4.63	5.30	4.23	4.45	5.02	3.85	4.99	5.63	5.48	4.36	3.25	4.10	4.94
RCM3+CGCM3	4.66	7.13	5.87	3.82	3.44	4.59	4.67	5.01	4.30	4.34	3.93	4.21	4.56
RCM3+GFDL	4.18	5.10	3.80	3.02	3.23	4.31	4.95	3.52	4.82	4.61	1.90	3.93	6.99
<i>Model Average</i>	4.49	5.84	4.63	3.76	3.89	4.25	4.87	4.72	4.87	4.44	3.03	4.08	5.50
Portland, ME													
CRCM+CGCM3	4.54	5.31	4.30	4.67	4.84	4.02	4.71	5.21	5.10	4.31	3.05	4.18	4.79
RCM3+CGCM3	4.49	7.05	5.61	3.75	3.60	4.50	4.47	4.79	3.93	4.18	3.73	3.96	4.31
RCM3+GFDL	3.95	4.77	3.66	2.73	3.15	4.10	4.55	3.16	4.33	4.32	2.11	3.73	6.83
<i>Model Average</i>	4.33	5.71	4.52	3.72	3.86	4.21	4.58	4.39	4.45	4.27	2.96	3.96	5.31

M-E PDG

The M-E PDG model was run by modifying only the temperature variable. The three model scenarios correspond to the CRCM + CGCM3, the RCM3 + CGCM3, and the RCM3 + GFDL combinations of AOGCM and RCM simulations. The hindcast climate model conditions and anticipated future climate model conditions are presented in comparison to the baseline (observed) conditions for alligator cracking and AC rutting at each of four study sites in the Northeast. The predicted amount of distress at the end of the pavements design life, the accumulation of distress over the design life of the pavement, and percent differences between the models and baseline are shown for each time period. In the accumulation of distress over the design life of the pavement, the timing of acceptable levels of distress is noted. Beyond these levels, the pavement fails to meet its' performance criteria and is in need of rehabilitation. The levels of acceptable of distress are 20 and 50 percent for alligator cracking, and 0.25 and 0.50 inches for AC rutting. The pavements age in months at each failure level for both alligator cracking and AC Rutting are also presented. Here, percent difference is defined as:

$$\% \text{ Difference} = 100 * (\text{Model distress} - \text{Baseline distress}) / \text{Baseline distress} \quad (9)$$

Hindcast Model Results

Table 10 shows the predicted magnitude of alligator cracking and AC rutting at the end of the 20 year design life for both pavement structures by location from the M-E PDG analysis using the historic ME-PDG climate files and the hindcast temperature scenarios from the three AOGCM+RCM forecasts. Figures 39 to 42 show the accumulation of distress over the design life of the pavement. In Figures 39 to 42, horizontal lines at 20% and 50%, and 0.25 inch and 0.50 inch indicate acceptable levels of distress for alligator cracking and AC rutting, respectively. Table 11 summarizes the pavement age in months at failure. Figure 43 and Figure 44 present the percent difference from baseline in the predicted amount of distress using the three hindcast climate scenarios.

Alligator Cracking

The total alligator cracking for all three models for both secondary and interstates cases is less than baseline conditions for all study sites (Table 10). All three hindcast models followed a similar trend compared to baseline for secondary alligator cracking over the design life of the pavement (Figure 39). The models exhibited alligator cracking within 1% of the baseline for the interstate cases (Figure 40). The secondary pavements under baseline and hindcast model conditions exceeded the acceptable distress limits for alligator cracking; with the exception of the model conditions for Boston, MA that did not exceed 50% (Table 11). In all secondary cases, the hindcast models reached 20% and 50% alligator cracking at the same time or slightly later than baseline. No cases for the interstate pavement exceeded the distress limits for alligator cracking. The percentage difference in alligator cracking between the hindcast model and baseline is less than 5% (Figure 43). In 10 of the 12 secondary cases the difference was less than 3%. For Portland, ME there was no difference in secondary alligator cracking for the CRCM+CGCM3 model scenario. For nine of the 12 interstate cases the percentage

difference was greater than 5%, and, three of the 12 secondary cases were greater than 10% different. For interstate alligator cracking the CRCM+CGCM3 consistently had the largest departure from baseline. No pattern was evident for the secondary cases.

AC Rutting

For AC rutting, the hindcast model temperature data exhibited less rutting than baseline, with the CRCM+CGCM3 model scenario showing the least (Table 10). The three hindcast models experienced a lower rate of rutting over the design life of the pavement across the study sites for both secondary and interstate pavements (Figure 41 and Figure 42). The coastal locations showed the lowest rate in rutting for secondary pavements. In all but the CRCM+CGCM3 model for Boston, MA the baseline and hindcast models exceeded 0.25 inches and 0.50 inches of rutting for the interstate and secondary pavement. (Table 11) The hindcast model temperature data reaches both 0.25 inches and 0.50 inches of AC rutting at the same or later baseline for all cases. Figure 44 show that AC rutting differences ranged from 0.013 inches to 0.123 inches (6.24% to 16.30%). The greatest difference for both secondary and interstate cases was for the CRCM+CGCM3 model. The RCM3+GFDL model exhibited the least difference for all the secondary cases and 11 of the 12 interstate cases. Many state agencies would consider differences less than 0.1 inches to be insignificant. Increases at and greater than 0.1 inches could be significant depending upon the total magnitude and the specific location. The CRCM+CGCM3 exceeds the 0.1 inches threshold in three of the four locations for both secondary and interstate pavements. Four of the 12 interstate cases a change greater than 0.1 inches was predicted. No apparent pattern was exhibited in the changes that exceeded 0.1 inches in magnitude.

The hindcast model temperature data had a moderate difference in AC rutting compared to baseline. For alligator cracking, the secondary case exhibited a negligible change,

while the interstate case showed a modest departure from that of the observed temperature data. No model exactly reproduced the observed conditions for using the hindcast model temperature data.

Table 10 - Predicted Distresses for the Hindcast Climate Scenarios

	Alligator Cracking (%)		AC Rutting (in)	
	Secondary	Interstate	Secondary	Interstate
Berlin, NH (M-E PDG)	57.0	8.73	0.927	0.838
CRCM+CGCM3	55.9	7.61	0.813	0.715
RCM3+CGCM3	55.5	7.68	0.828	0.736
RCM3+GFDL	55.5	7.87	0.861	0.770
Boston, MA (M-E PDG)	51.1	6.18	0.681	0.600
CRCM+CGCM3	49.8	5.49	0.577	0.492
RCM3+CGCM3	50.0	5.65	0.597	0.517
RCM3+GFDL	50.0	5.80	0.623	0.542
Concord, NH (M-E PDG)	56.3	8.62	0.933	0.900
CRCM+CGCM3	54.8	8.14	0.820	0.872
RCM3+CGCM3	53.9	8.28	0.848	0.887
RCM3+GFDL	54.0	8.18	0.873	0.875
Portland, ME (M-E PDG)	53.4	7.27	0.769	0.718
CRCM+CGCM3	53.4	6.68	0.676	0.601
RCM3+CGCM3	52.8	6.77	0.698	0.626
RCM3+GFDL	52.7	6.93	0.721	0.659

Table 11 - Hindcast Model Pavement Age (in Months) at Failure

	Alligator Cracking				AC Rutting			
	20%		50%		0.25 in		0.50 in	
	Secondary	Interstate	Secondary	Interstate	Secondary	Interstate	Secondary	Interstate
Berlin, NH (M-E PDG)	94	--	206	--	25	25	85	97
CRCM+CGCM3	95	--	215	--	25	36	109	133
RCM3+CGCM3	96	--	216	--	25	36	108	122
RCM3+GFDL	95	--	215	--	24	25	97	121
Boston, MA (M-E PDG)	105	--	236	--	36	48	144	180
CRCM+CGCM3	107	--	--	--	48	62	194	--
RCM3+CGCM3	106	--	--	--	48	60	182	229
RCM3+GFDL	108	--	--	--	37	51	178	217
Concord, NH (M-E PDG)	95	--	214	--	23	25	82	85
CRCM+CGCM3	96	--	217	--	24	24	107	96
RCM3+CGCM3	96	--	221	--	23	25	97	86
RCM3+GFDL	96	--	219	--	15	25	87	96
Portland, ME (M-E PDG)	98	--	227	--	26	36	111	133
CRCM+CGCM3	98	--	225	--	37	49	146	181
RCM3+CGCM3	98	--	228	--	36	49	134	170
RCM3+GFDL	98	--	228	--	26	37	133	157

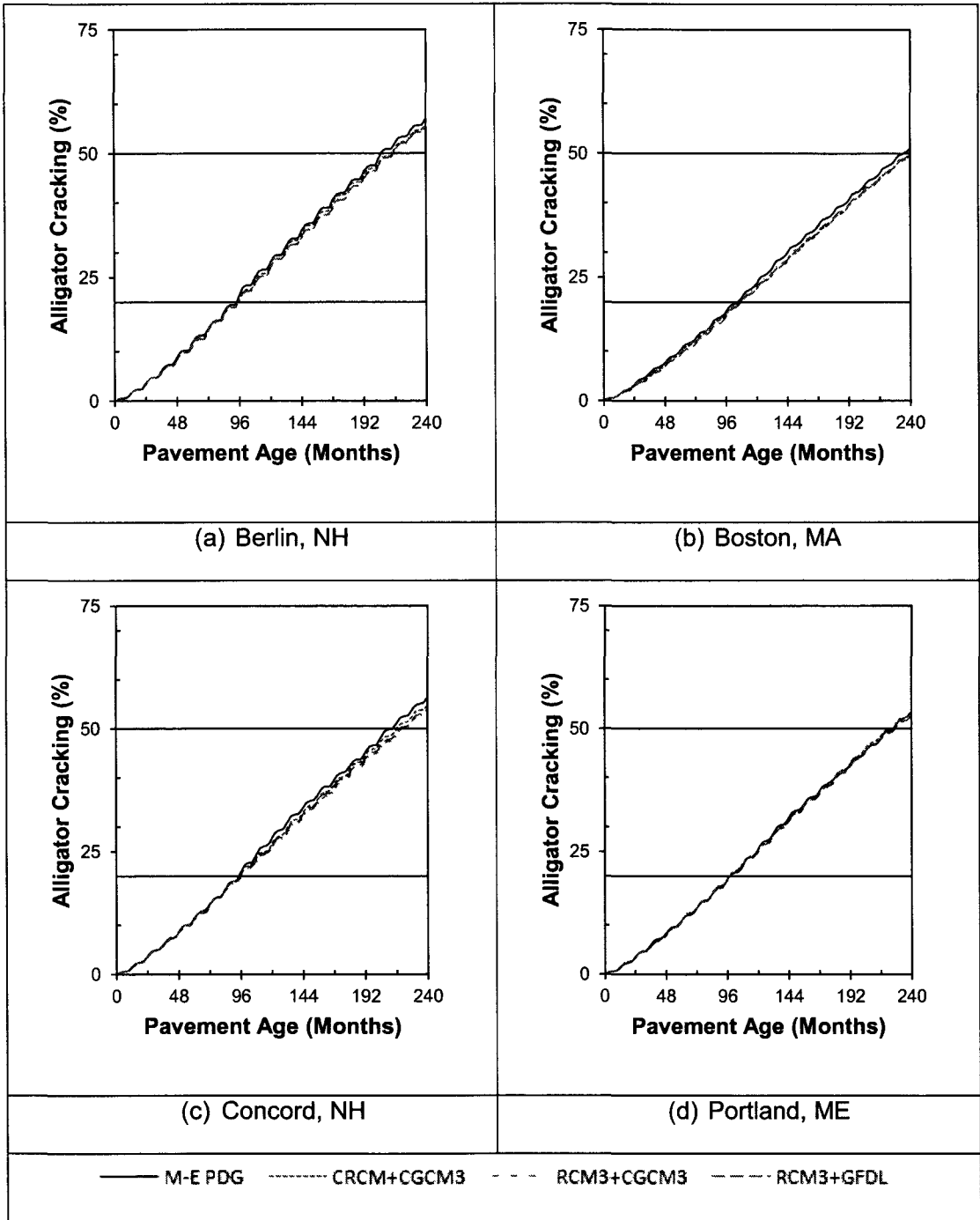


Figure 39 - Hindcast Model Secondary Alligator Cracking

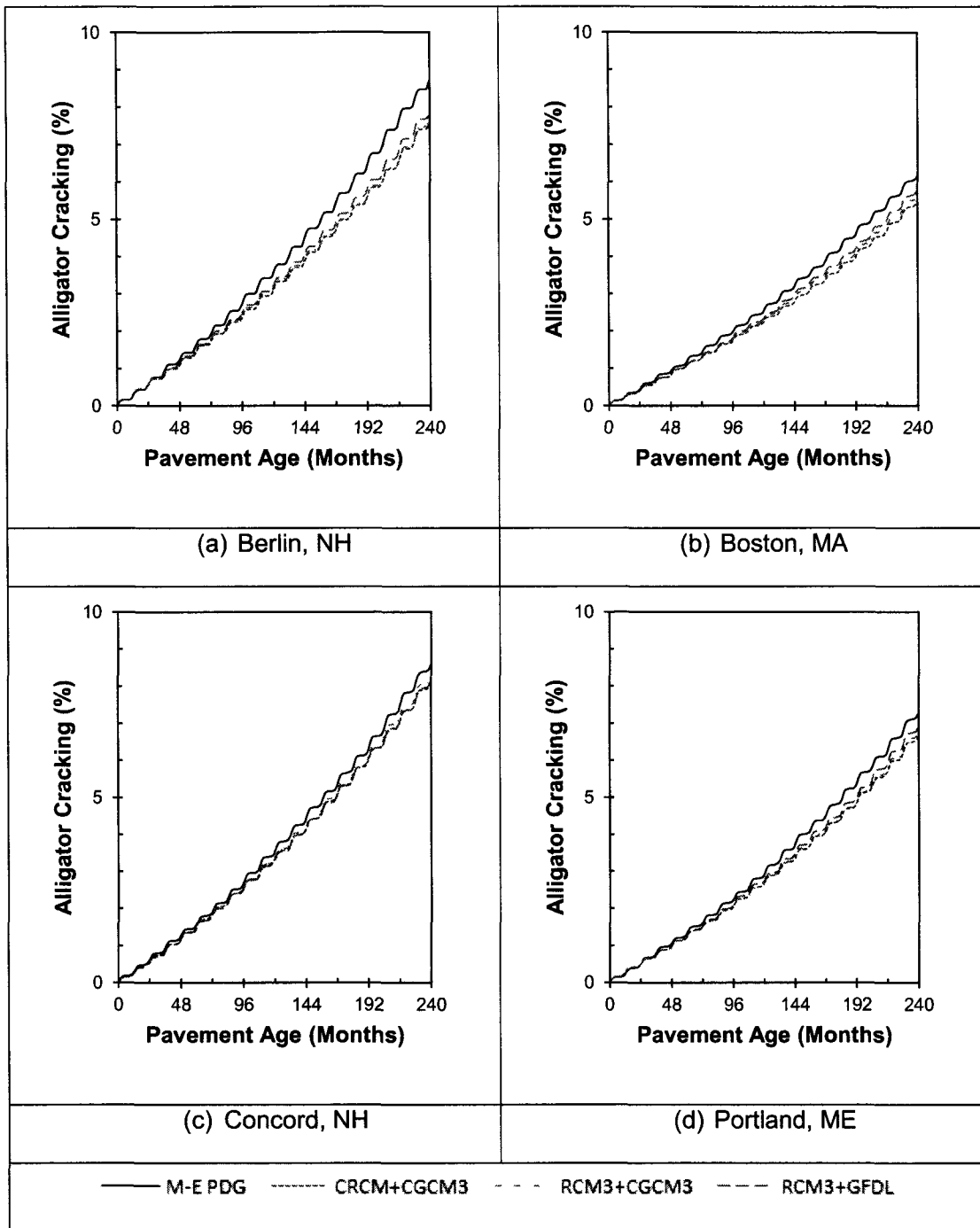


Figure 40 - Hindcast Model Interstate Alligator Cracking

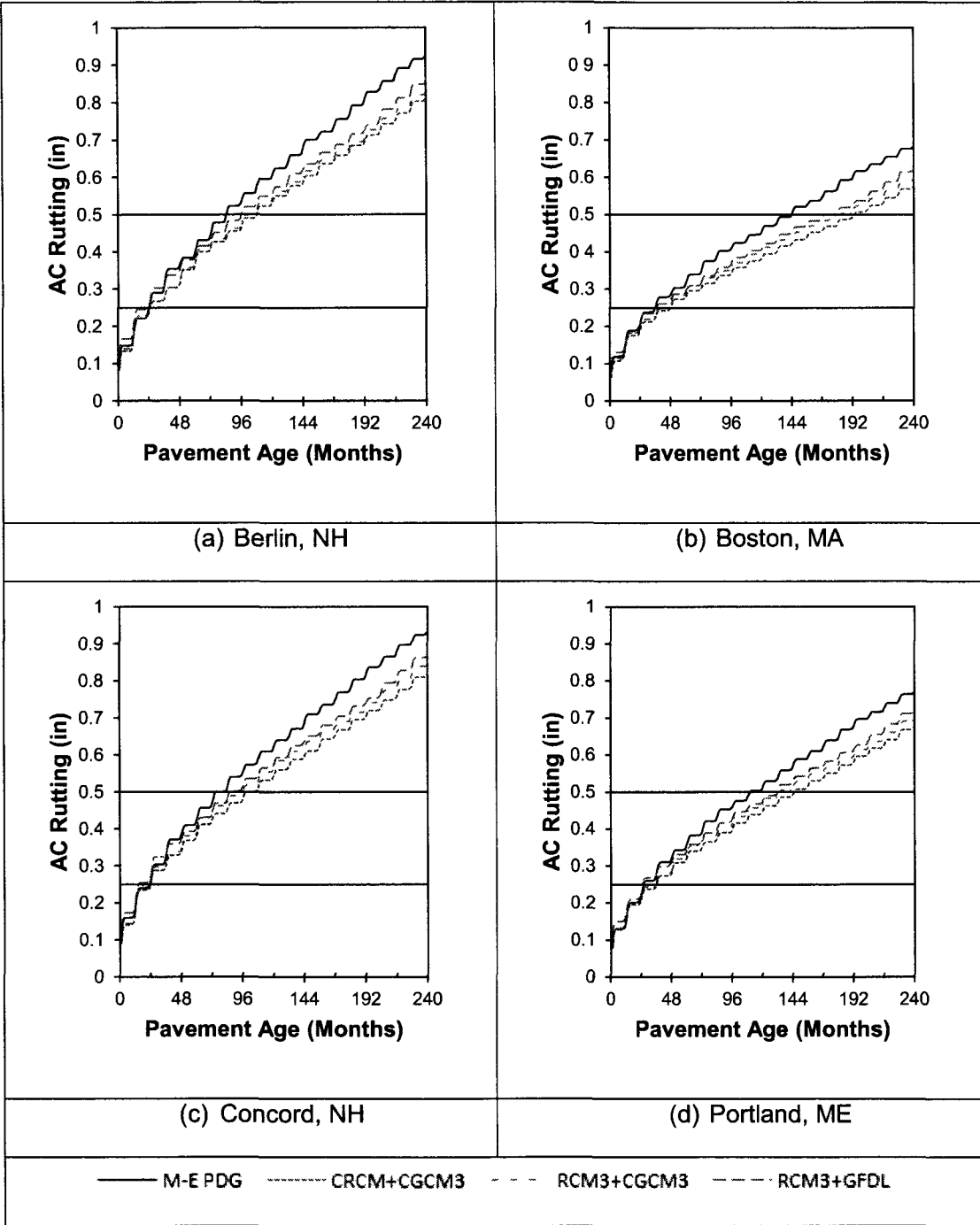


Figure 41 - Hindcast Model Secondary AC Rutting

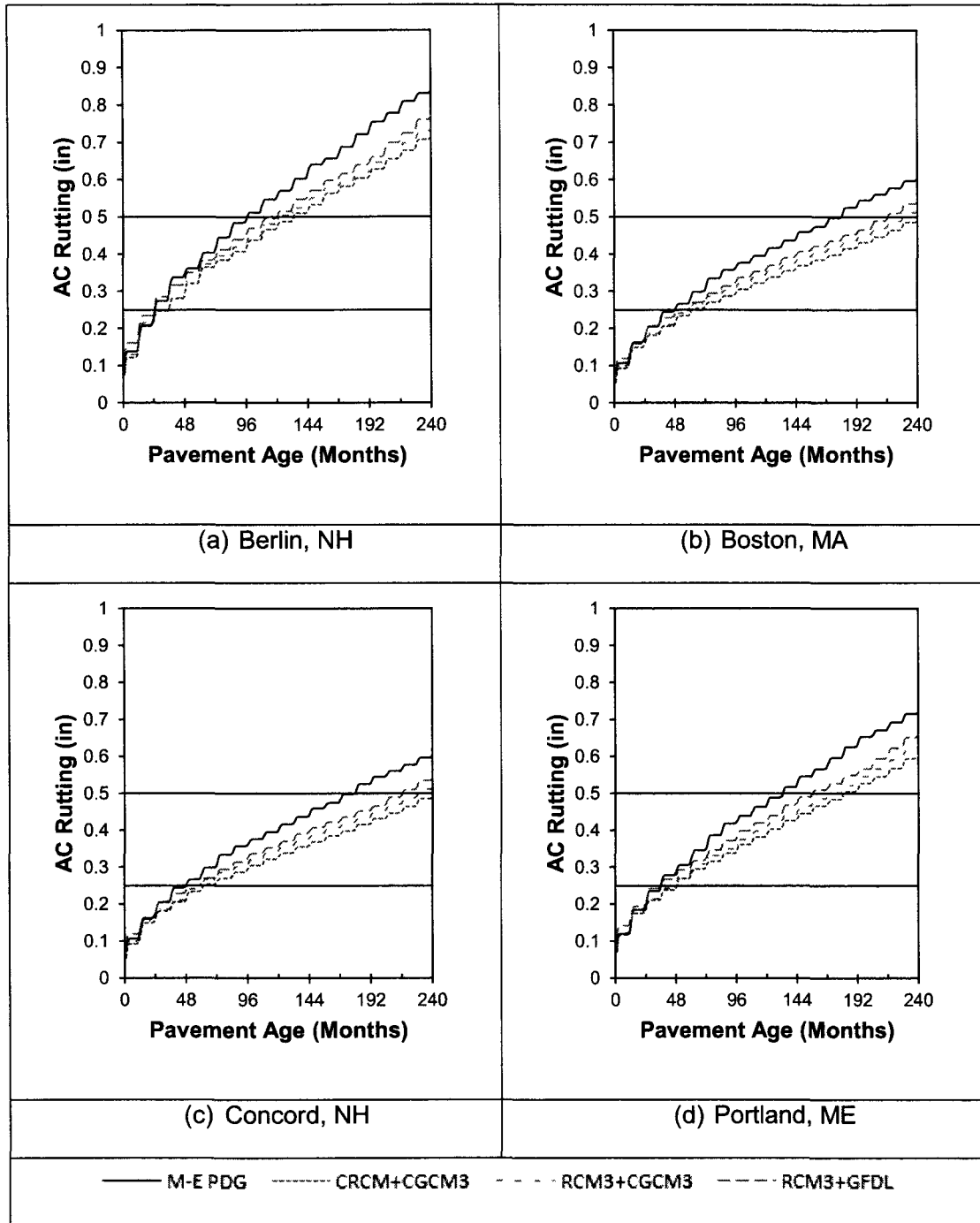


Figure 42 - Hindcast Model Interstate AC Rutting

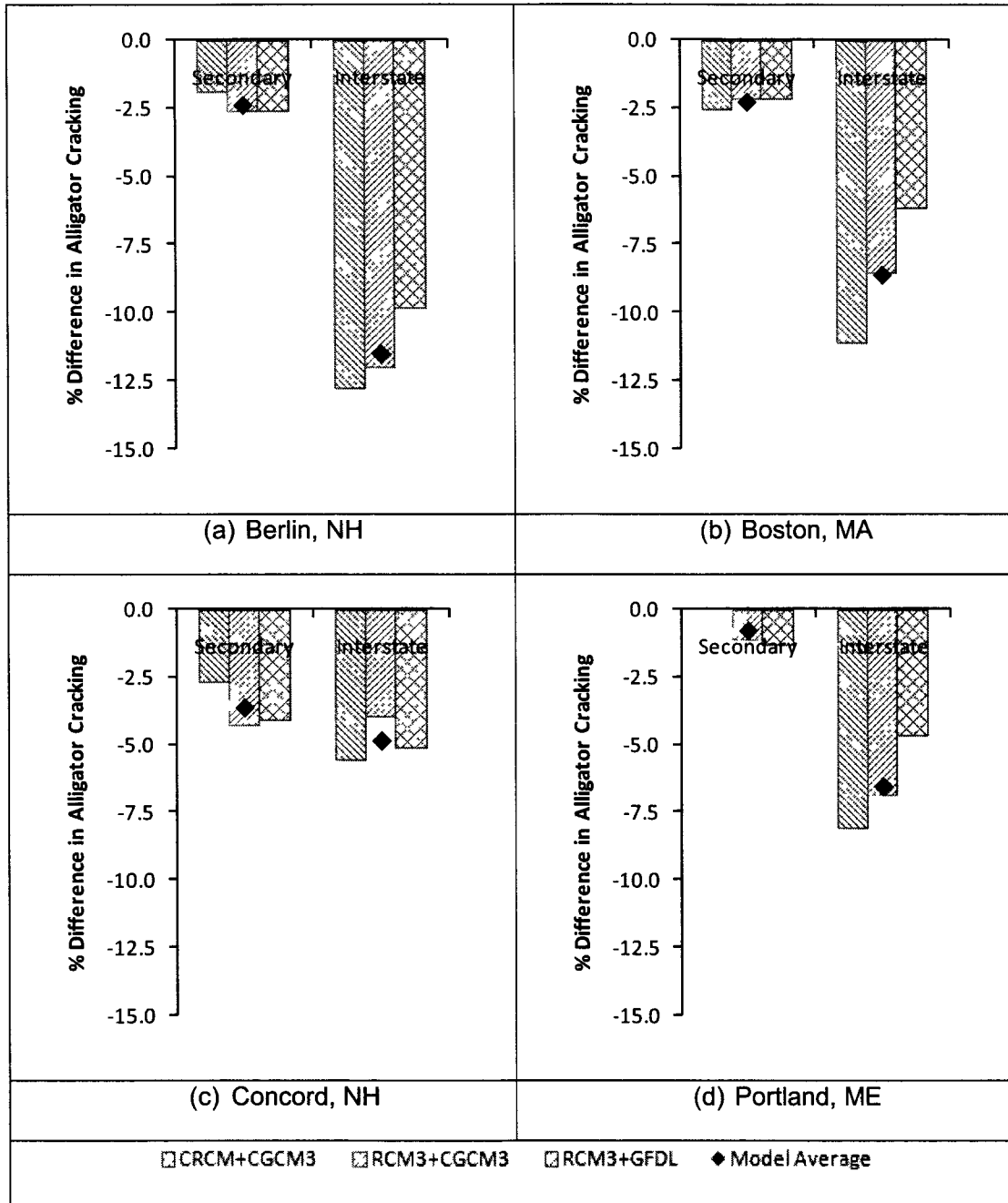


Figure 43 - Percent Difference in Alligator Cracking from Baseline for the Hindcast Model Period

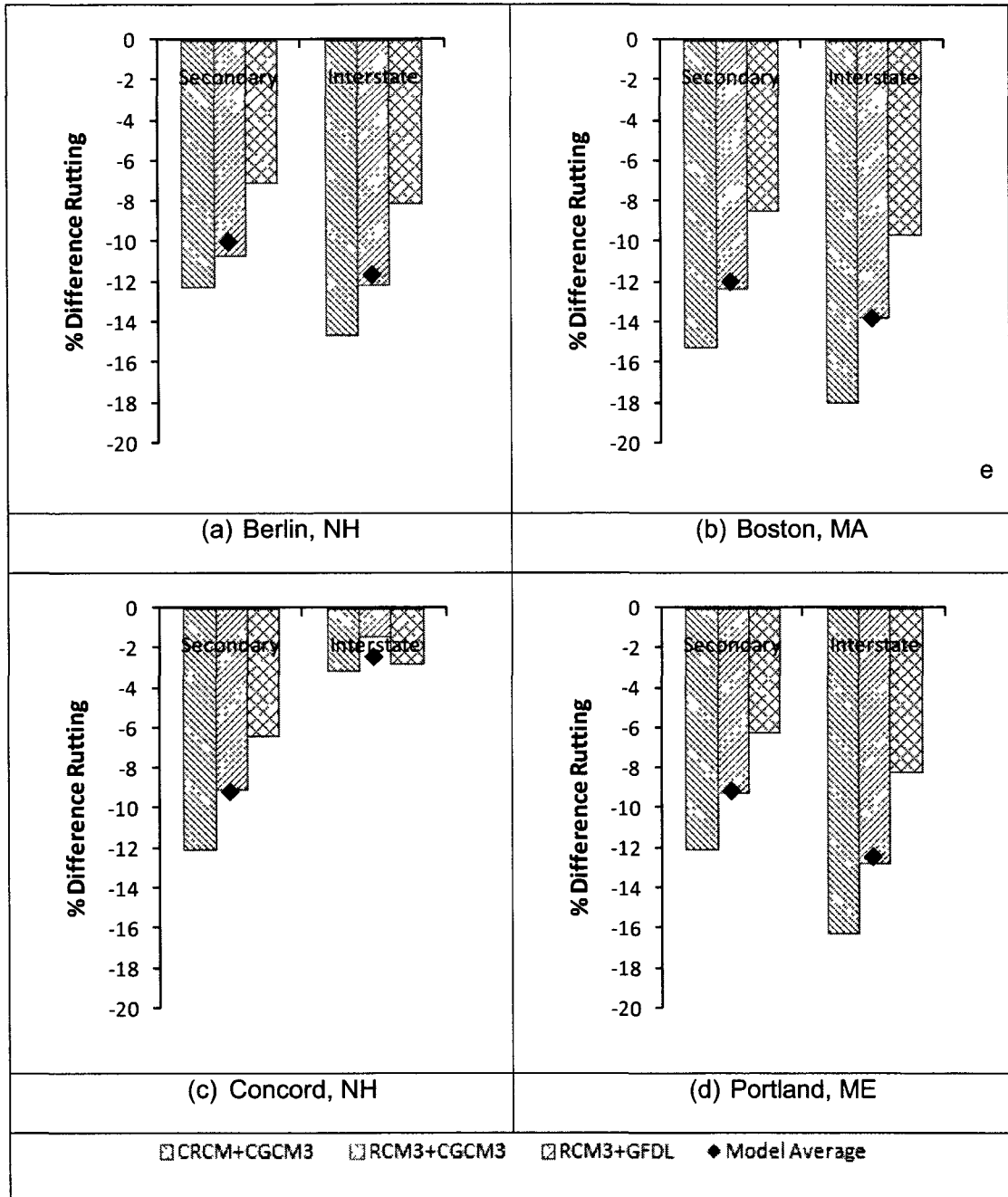


Figure 44 - Percent Difference in AC Rutting from Baseline for the Hindcast Model Period

Future Model Results

Table 12 shows the predicted magnitude of alligator cracking and AC rutting at the end of the 20 year design life for both pavement structures by location from the M-E PDG analysis using the historic ME-PDG climate files and the future temperature scenarios from the three AOGCM+RCM forecasts. Figures 45 to 48 show the accumulation of distress over the design life of the pavement. In Figures 45 to 48, horizontal lines at 20% and 50%, and 0.25 inch and 0.50 inch indicate acceptable levels of distress for alligator cracking and AC rutting, respectively. Table 13 summarizes the pavement age in months at failure. Figure 49 and Figure 51 present the percent difference from baseline in the predicted amount of distress using the three hindcast climate scenarios.

Alligator Cracking

Using the future model temperature data, the predicted alligator cracking is less than baseline for 11 of 12 model scenarios for the secondary pavement (Table 12). The trend in secondary alligator cracking for the future model temperature data is nearly identical to baseline for the coastal locations, and slightly lower for the inland locations (Figure 45). Future model interstate alligator cracking is similar to baseline at all sites (Figure 46). The age at which the pavement reached 20% and 50% alligator cracking for the secondary case was equal or later than baseline for the future model temperature data (Table 13). With the maximum at difference of 12 months (RCM3+GFDL at Berlin, NH) Neither baseline nor future model temperature data exceeded the acceptable levels of distress for alligator cracking for the interstate pavement. The difference in alligator cracking is predicted to be less than 5.5% for both secondary and interstate pavements across all scenarios (Figure 49). In ten of the 12 secondary cases and in five of 12 interstate cases, alligator cracking becomes less severe under the under the future scenario. For the two secondary cases in which alligator cracking was greater for the

future temperature data, the change was less than 1%. Both coastal locations (Boston, MA and Portland, ME) exhibited an increase in interstate alligator cracking. For the inland cases all but one scenario had less alligator cracking for the future period. The GFDL AOGCM scenarios predict greater cracking than the CGCM3 AOGCM temperatures. No pattern was evident for the secondary cases.

AC Rutting

AC rutting is predicted to increase for both secondary and interstate pavements for all locations and scenarios (Table 12 and Figure 50). The GFDL AOGCM consistently predicts the largest amount of AC rutting. The future model temperature data shows a higher rate of AC rutting particularly later in the pavements lifetime (Figure 47 and Figure 48). For secondary AC rutting, all the future models exceed the acceptable levels of distress at the same time or earlier than baseline, with nine of the 12 reaching 0.25 inches and 11 of 12 reaching 0.50 inches earlier than baseline (Table 13). Many reach the threshold close to a year earlier. For interstate AC rutting, 11 of 12 models reached 0.25 inches at the same time or earlier than baseline, the exception being the RCM3+CGCM3 model for Boston, MA exceeding 0.25 inches a month later than baseline. All models exceeded 0.50 inches for the interstate pavement at the same time or up to 21 months earlier than baseline. The increase in AC rutting ranged from 0.036 to 0.134 inches (approximately 4-16%) (Figure 50). Many state agencies would consider the 0.036 inch increase to be insignificant, but the increases approaching and above 0.1 inch could be significant depending upon the total magnitude and the specific location. The RCM3+GFDL model scenario showed the largest change in rutting for secondary and interstate cases across all locations. Relatively modest differences were found for rutting between the two RCMs run using the CGCM3 AOGCM input. The greatest amount of rutting was predicted for Concord, NH while Boston, MA had the least. The

interior locations (Berlin and Concord) show higher increases in rutting for the interstate pavement. There does not appear to be an apparent trend for the secondary pavement structure.

Table 12 - Predicted Distresses for the Future Climate Scenarios

	Alligator Cracking (%)		AC Rutting (in)	
	Secondary	Interstate	Secondary	Interstate
Berlin, NH (M-E PDG)	57.0	8.73	0.927	0.838
CRCM+CGCM3	55.2	8.48	0.965	0.925
RCM3+CGCM3	55.2	8.60	0.977	0.934
RCM3+GFDL	54.7	8.68	1.003	0.972
Boston, MA (M-E PDG)	51.1	6.18	0.681	0.600
CRCM+CGCM3	50.0	6.35	0.738	0.645
RCM3+CGCM3	50.7	6.40	0.737	0.642
RCM3+GFDL	50.8	6.49	0.753	0.661
Concord, NH (M-E PDG)	56.3	8.62	0.933	0.900
CRCM+CGCM3	54.2	8.46	0.982	0.969
RCM3+CGCM3	54.6	8.57	0.994	0.980
RCM3+GFDL	54.2	8.73	1.021	1.012
Portland, ME (M-E PDG)	53.4	7.27	0.769	0.718
CRCM+CGCM3	53.2	7.45	0.805	0.760
RCM3+CGCM3	53.9	7.54	0.810	0.766
RCM3+GFDL	53.6	7.67	0.834	0.792

Table 13 - Future Model Pavement Age (in Months) at Failure

	Alligator Cracking				AC Rutting			
	20%		50%		0.25 in		0.50 in	
	Secondary	Interstate	Secondary	Interstate	Secondary	Interstate	Secondary	Interstate
Berlin, NH (M-E PDG)	94	--	206	--	25	25	85	97
CRCM+CGCM3	96	--	216	--	25	25	85	97
RCM3+CGCM3	96	--	217	--	25	25	84	96
RCM3+GFDL	96	--	218	--	24	24	75	85
Boston, MA (M-E PDG)	105	--	236	--	36	48	144	180
CRCM+CGCM3	108	--	--	--	35	38	136	159
RCM3+CGCM3	106	--	238	--	35	49	135	167
RCM3+GFDL	105	--	238	--	26	38	123	158
Concord, NH (M-E PDG)	95	--	214	--	23	25	82	85
CRCM+CGCM3	96	--	218	--	15	24	74	85
RCM3+CGCM3	96	--	218	--	23	25	74	84
RCM3+GFDL	97	--	221	--	14	16	74	75
Portland, ME (M-E PDG)	98	--	227	--	26	36	111	133
CRCM+CGCM3	97	--	226	--	25	36	110	132
RCM3+CGCM3	97	--	223	--	25	27	109	122
RCM3+GFDL	98	--	226	--	25	26	100	118

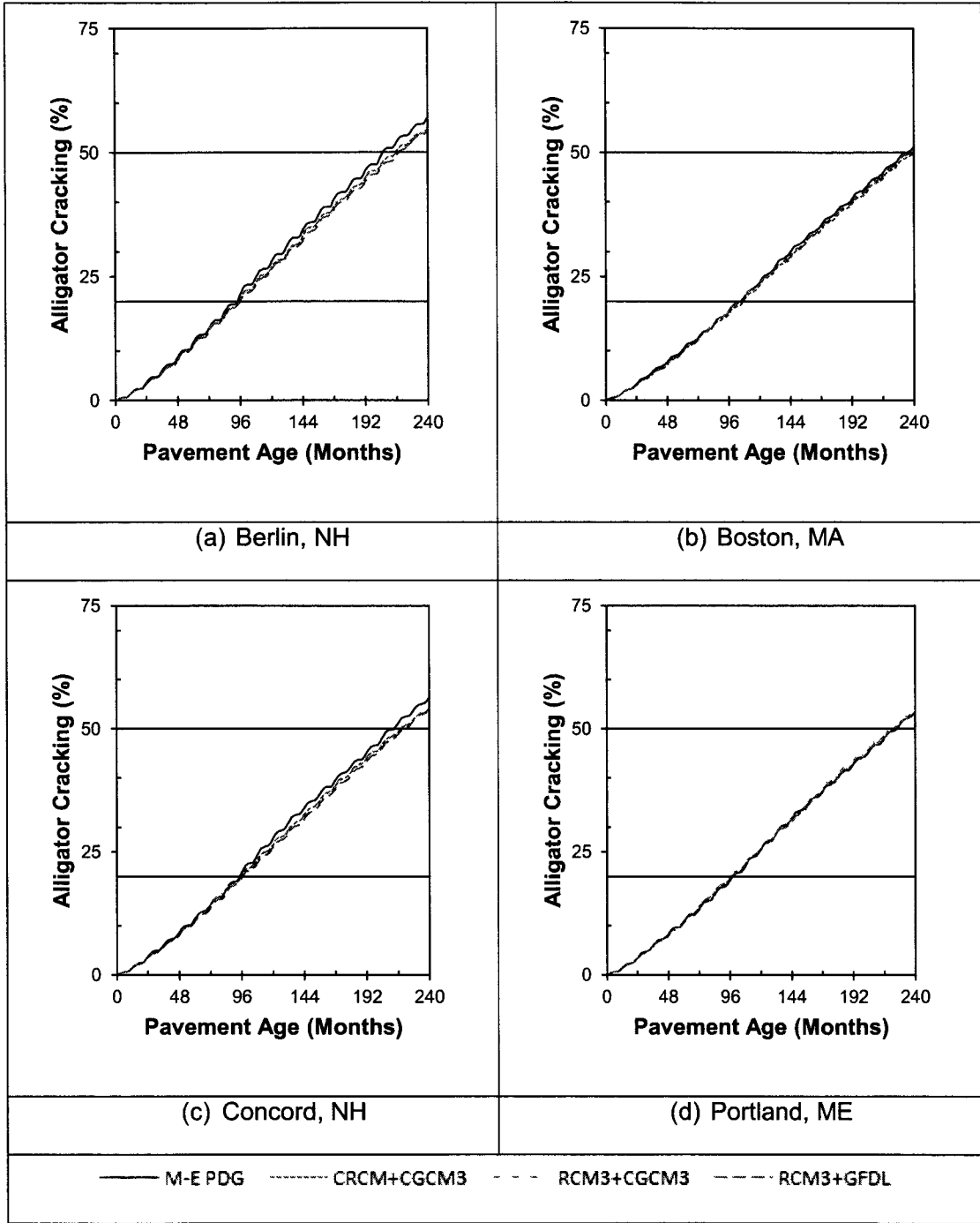


Figure 45 - Future Model Secondary Alligator Cracking

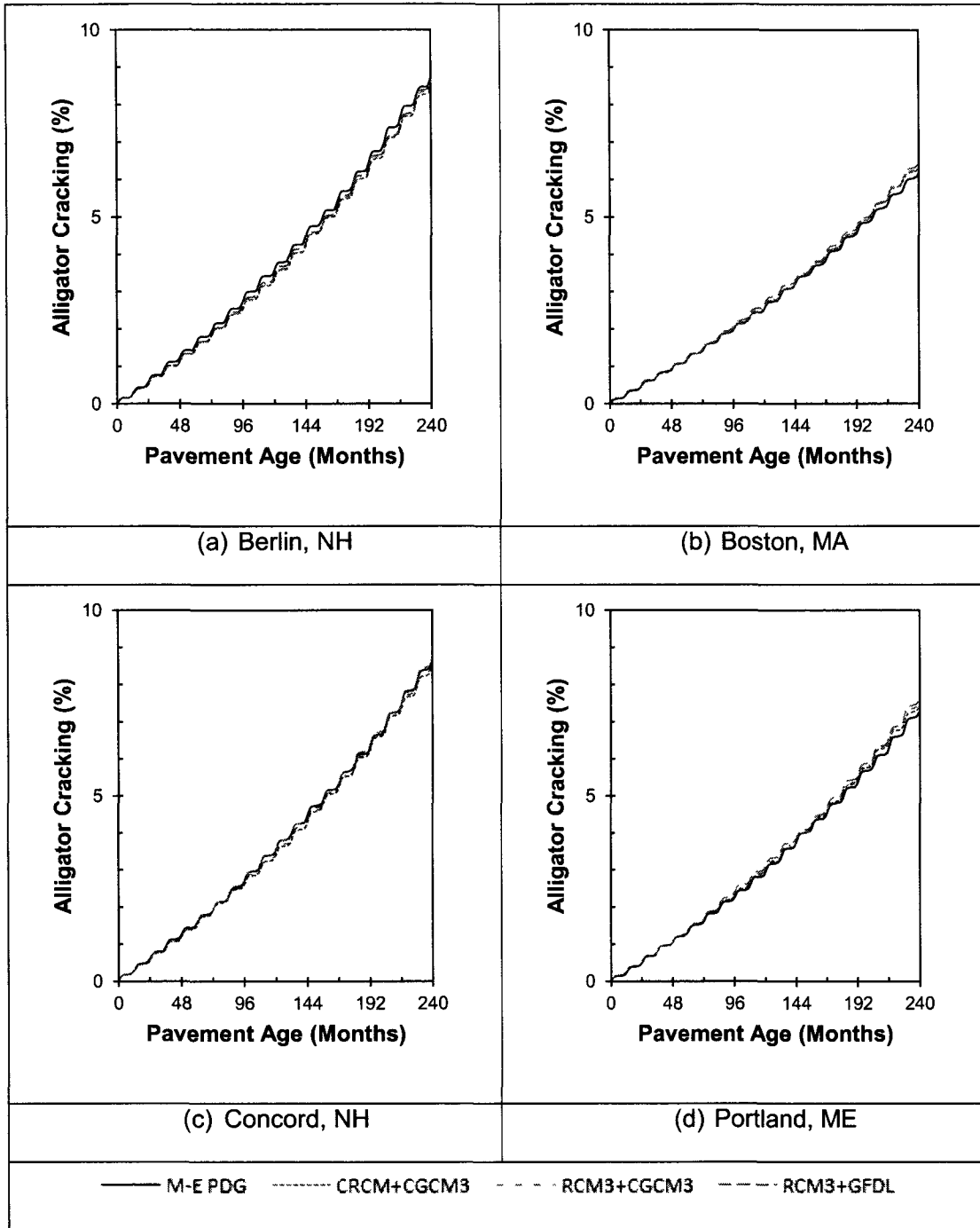


Figure 46 - Future Model Interstate Alligator Cracking

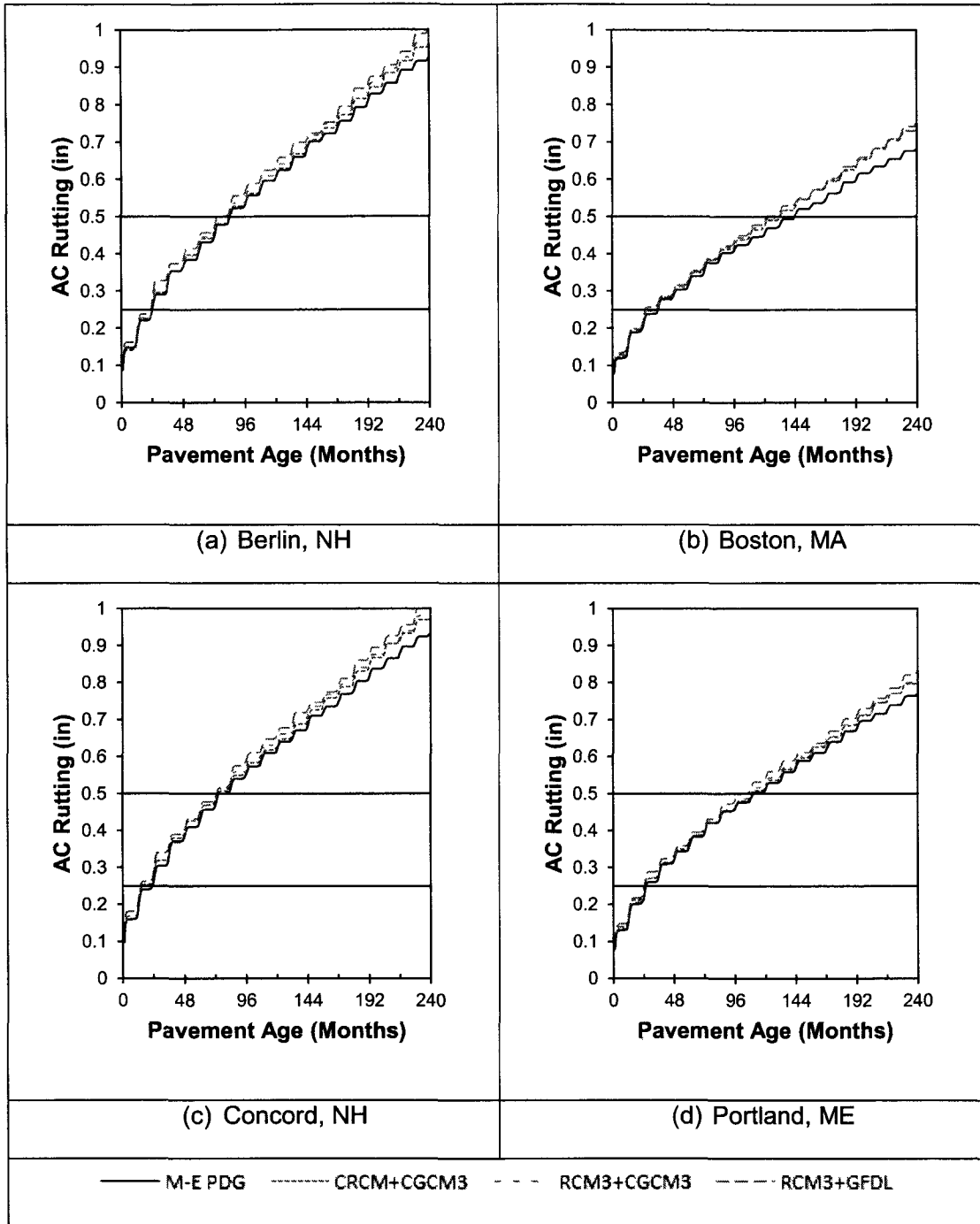


Figure 47 - Future Model Secondary AC Rutting

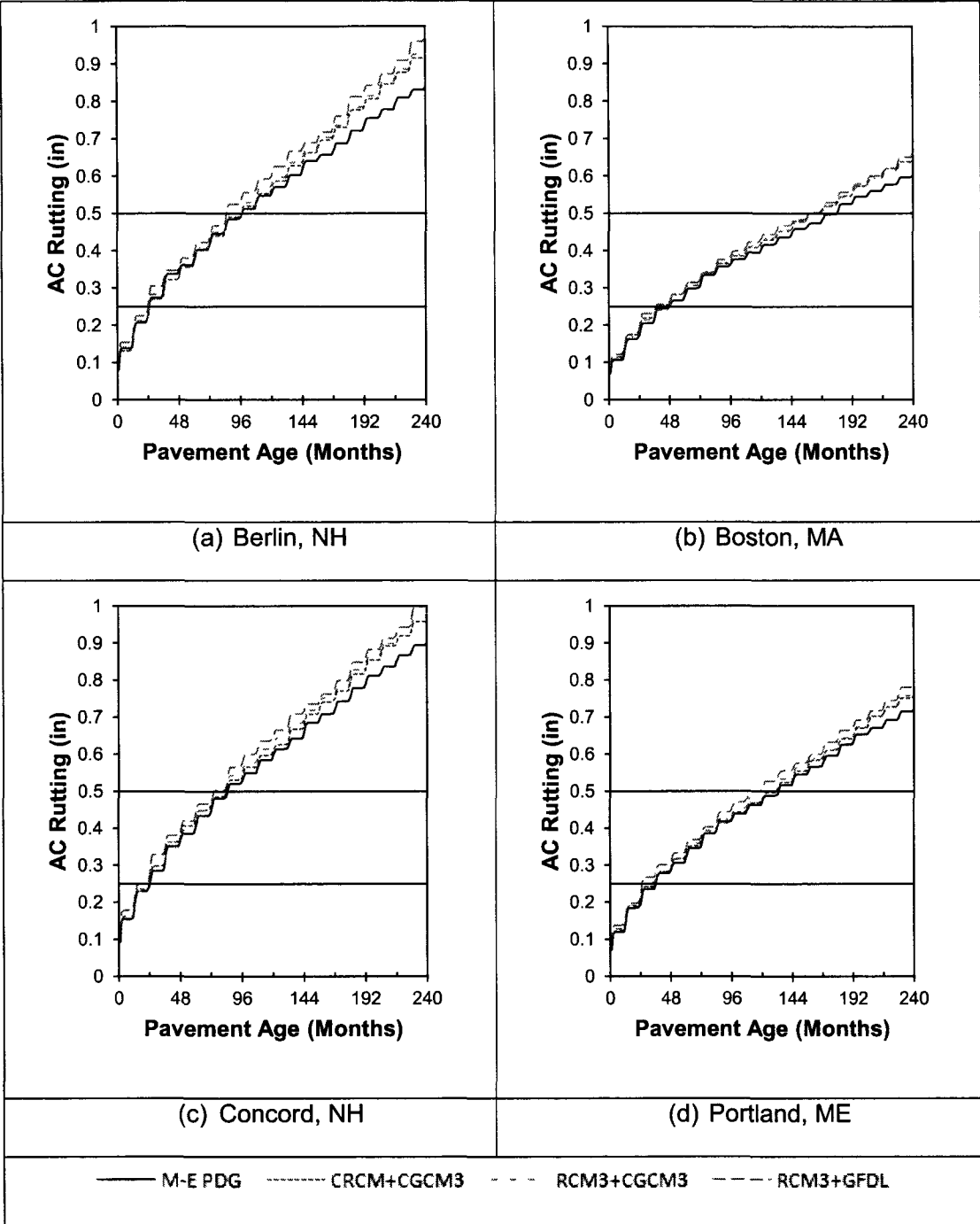


Figure 48 - Future Model Interstate AC Rutting

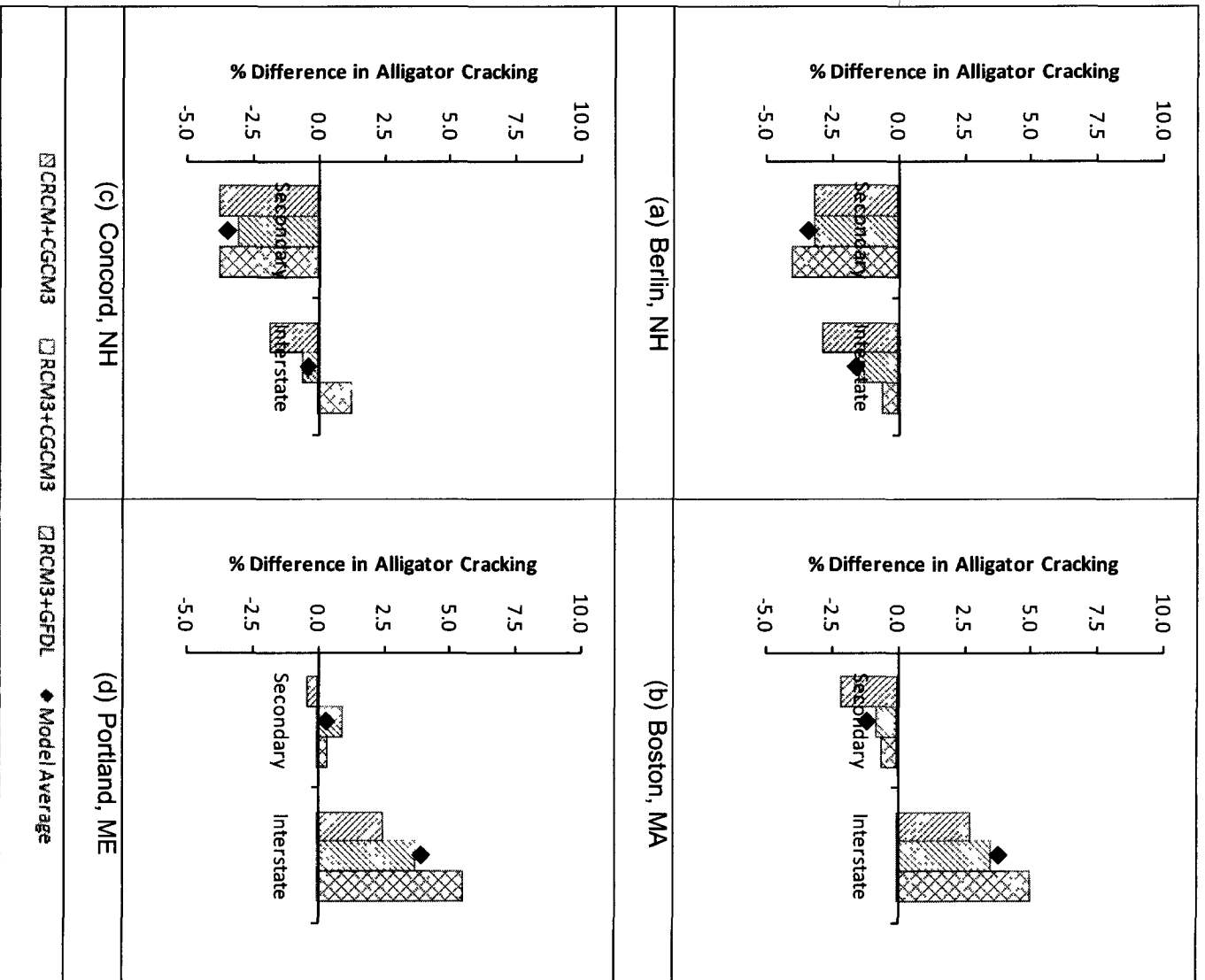


Figure 49 - Percent Difference in Alligator Cracking from Baseline for the Future Model Period

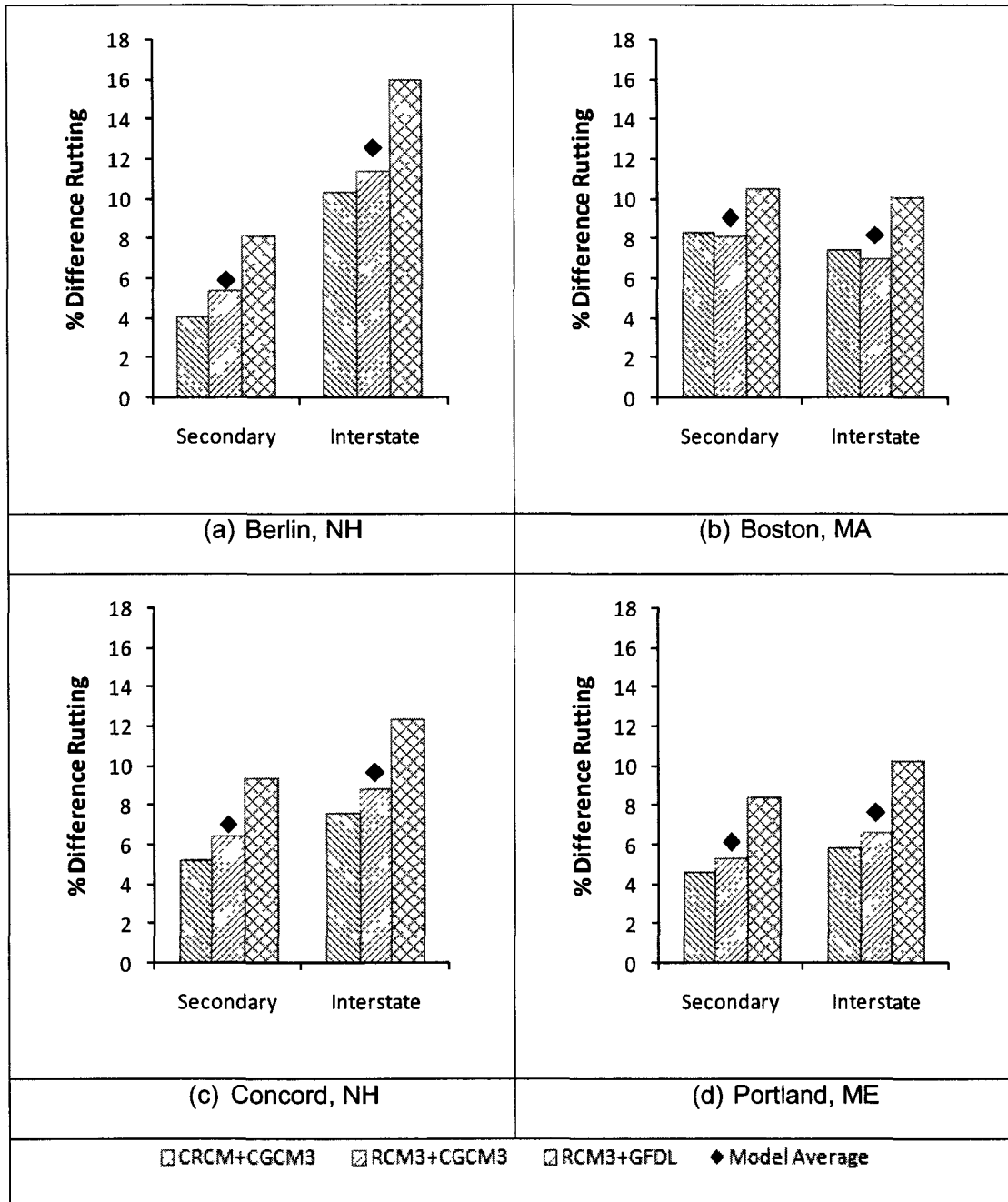


Figure 50 - Percent Difference in AC Rutting from Baseline for the Future Model Period

Future Model versus Hindcast Model

The final analysis compares the models ability to reproduce the observed conditions, comparing the model hindcast and future periods provide a comparison in which both scenarios are drawn from the same source. Thus, the unbiased impacts of the forecast changes are tested within the M-E PDG framework.

Table 14 presents the difference in distresses between the model periods. Figures 51 and 52 present the percent difference between the model periods in the predicted amount of distress using the three future climate scenarios. Table 15 present the difference in time to distress between the model periods.

Alligator Cracking

The difference in alligator cracking between the future and hindcast model periods is predicted to be less than 2.1% for all secondary cases (Table 14). Five of the 12 secondary cases show alligator cracking lessening under the future model period. Three of these five secondary cases occurred at the Concord, NH location. Alligator cracking was more severe for the interstate case with increases ranging from 3.6% to 15.7%. The large percent differences (Figure 51) are due to the small relative percent of cracking (Table 14). Concord, NH experienced the smallest change in interstate cracking. No pattern was apparent for either secondary or interstate differences in alligator cracking.

The difference in time to failure for alligator cracking between the future and hindcast model temperature data is at most five months (Table 15). No location failed before the design life for the interstate pavement under both hindcast and future scenarios. The time to failure for alligator cracking improved or stayed the same for Berlin, NH. No

location saw the time to failure worsen across all models and no pattern was evident within the models.

AC Rutting

AC rutting, is predicted to increase under the future model conditions for all cases and locations (Table 14 and Figure 52). The change is greater than 0.1 inches for each case which is enough to be considered significant by many state agencies. The difference ranges from 10.48 to 31.10%. For the secondary cases, the CRCM+CGCM3 model scenario showed the largest difference from the hindcast model period. For the interstate case, the CRCM+CGCM3 model scenario had the largest difference at three of the four locations. The RCM3+GFDL model scenario had the least difference from the hindcast period for all locations under the secondary case, and the least difference for three of the four locations for the interstate case. The RCM3 RCM showed less difference than the CRCM RCM for all locations and cases.

The difference in time to failure for AC rutting between the future and hindcast model temperature data ranges from zero to 81 months (Table 15). The failure time to 0.25 inches did not change for any model in Berlin, NH with secondary pavements, and was less than a year different for interstate pavements at that location. Concord, NH the time to failure at the 0.25 inches level differed by zero to nine months for both interstate and secondary pavements. The coastal locations saw differences from 11 months to 24 months for both secondary and interstate pavements. The exceptions being the RCM3+GFDL model at Portland, ME, which had only a month difference for the secondary case. AC rutting exceeding 0.50 inches changed considerably by location, failure occurred earlier by between 13 to 58 months for the secondary case, and between two to 81 months for the interstate case. The inland locations fared better than

the coastal, exhibiting differences from two months to three years. The coastal locations exhibited changes from two years to over six years.

Table 14 - Differences in Distresses between Model Periods

	Alligator Cracking (%)		Diff. AC Rutting (in)	
	<i>Secondary</i>	<i>Interstate</i>	<i>Secondary</i>	<i>Interstate</i>
Berlin, NH				
CRCM+CGCM3	-0.7	0.9	0.2	0.2
RCM3+CGCM3	-0.3	0.9	0.1	0.2
RCM3+GFDL	-0.8	0.8	0.1	0.2
<i>Model Average</i>	<i>-0.6</i>	<i>0.9</i>	<i>0.1</i>	<i>0.2</i>
Boston, MA				
CRCM+CGCM3	0.2	0.9	0.2	0.2
RCM3+CGCM3	0.7	0.8	0.1	0.1
RCM3+GFDL	0.8	0.7	0.1	0.1
<i>Model Average</i>	<i>0.6</i>	<i>0.8</i>	<i>0.1</i>	<i>0.1</i>
Concord, NH				
CRCM+CGCM3	-0.6	0.3	0.2	0.1
RCM3+CGCM3	0.7	0.3	0.1	0.1
RCM3+GFDL	0.2	0.6	0.1	0.1
<i>Model Average</i>	<i>0.1</i>	<i>0.4</i>	<i>0.2</i>	<i>0.1</i>
Portland, ME				
CRCM+CGCM3	-0.2	0.8	0.1	0.2
RCM3+CGCM3	1.1	0.8	0.1	0.1
RCM3+GFDL	0.9	0.7	0.1	0.1
<i>Model Average</i>	<i>0.6</i>	<i>0.8</i>	<i>0.1</i>	<i>0.1</i>

Table 15 - Difference in Time to Distress (Future - Hindcast) in Months. Negative values indicate distress occurs earlier.

	Alligator Cracking				AC Rutting			
	20%		50%		0.25 in		0.50 in	
	<i>Secondary</i>	<i>Interstate</i>	<i>Secondary</i>	<i>Interstate</i>	<i>Secondary</i>	<i>Interstate</i>	<i>Secondary</i>	<i>Interstate</i>
Berlin, NH								
CRCM+CGCM3	1	--	1	--	0	-11	-24	-36
RCM3+CGCM3	0	--	1	--	0	-11	-24	-26
RCM3+GFDL	1	--	3	--	0	-1	-22	-36
Boston, MA								
CRCM+CGCM3	1	--	--	--	-13	-24	-58	-81
RCM3+CGCM3	0	--	-2	--	-13	-11	-47	-62
RCM3+GFDL	-3	--	-2	--	-11	-13	-55	-59
Concord, NH								
CRCM+CGCM3	0	--	1	--	-9	0	-33	-11
RCM3+CGCM3	0	--	-3	--	0	0	-23	-2
RCM3+GFDL	1	-	2	--	-1	-9	-13	-21
Portland, ME								
CRCM+CGCM3	-1	--	1	--	-12	-13	-36	-49
RCM3+CGCM3	-1	--	-5	--	-11	-22	-25	-48
RCM3+GFDL	0	--	-2	--	-1	-11	-33	-39

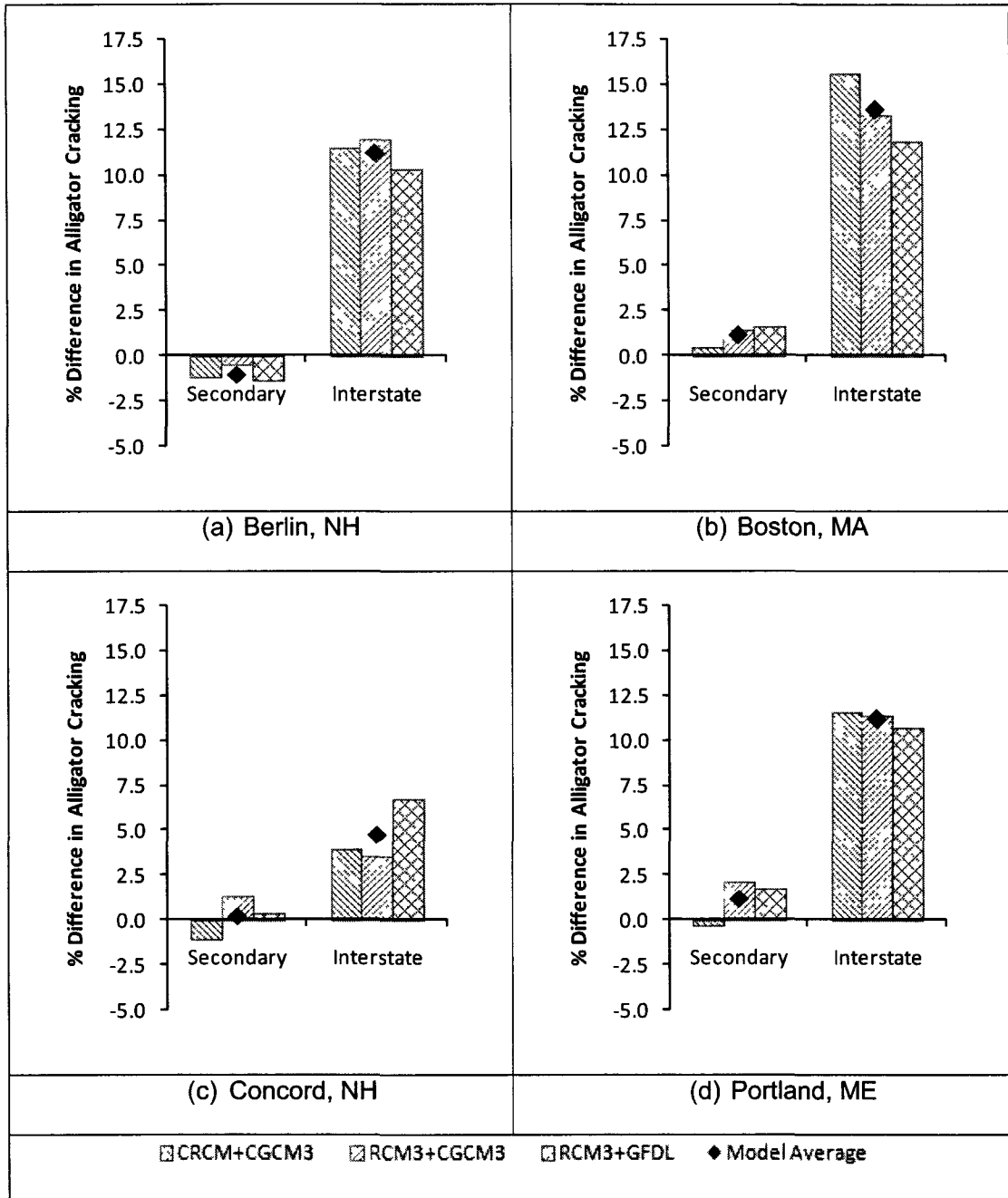


Figure 51 - Percent Difference in Alligator Cracking between Model Periods

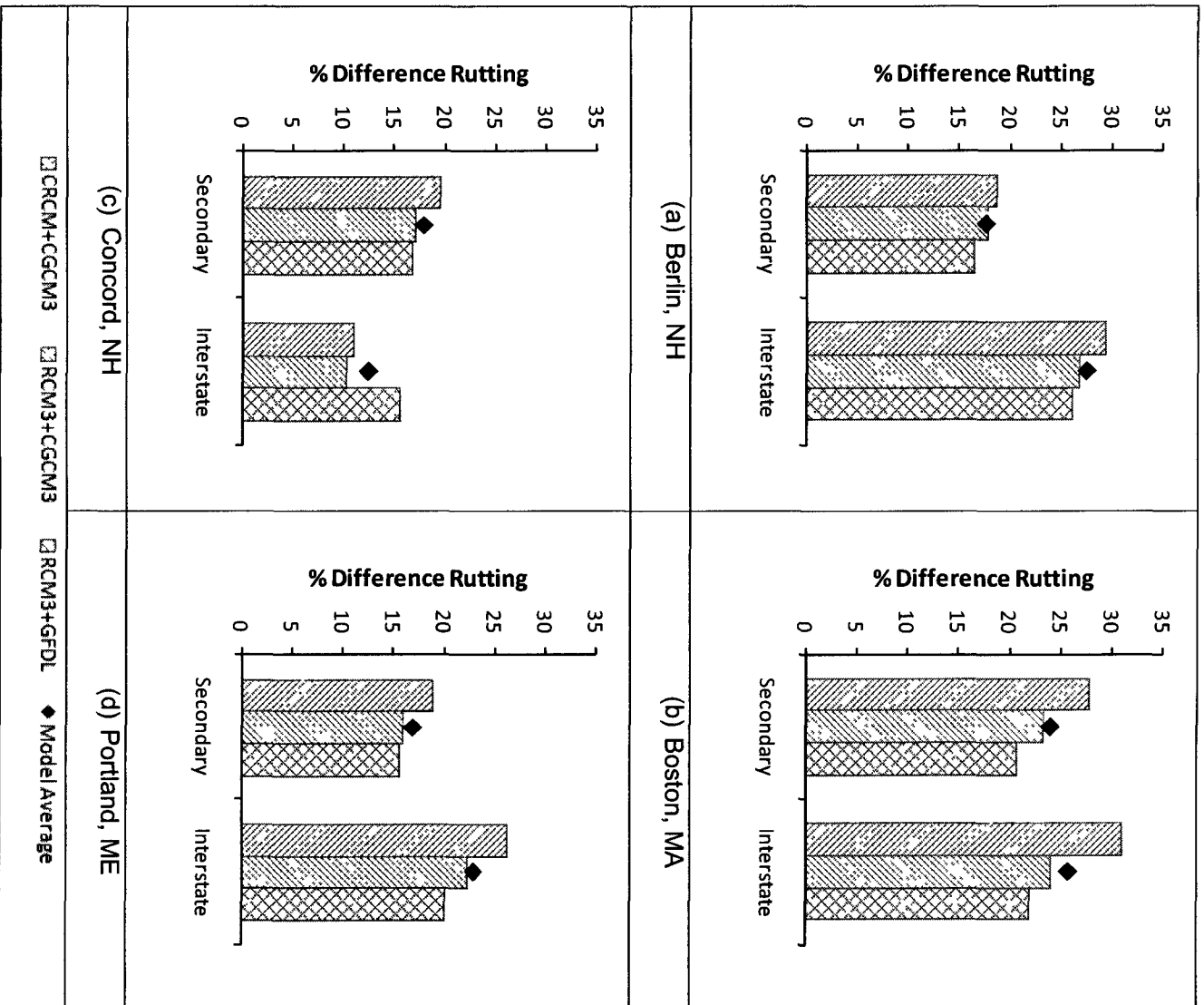


Figure 52 - Percent Difference in AC Rutting between Model Periods

CHAPTER V – SUMMARY

Conclusion

This thesis presents a methodology by which the implications of forecasted climate change on pavement deterioration processes can be assessed. This work focuses on the preparation and use of climate model datasets as inputs into the Mechanistic-Empirical Pavement Design Guide (M-E PDG) model to simulate pavement performance and deterioration over time. The methodology is illustrated using model temperature data from three NARCCAP AOGCM+RCM scenarios.

The model hindcast temperature was shown to match the observed temperature values reasonably well, under predicting the mean annual temperature by no more than 1.3°F. The largest deviation in the hindcast temperature occurred in the months of August and September. Reviewing the non-downscaled data and downscaled data (Figure 3, Figure 37) showed the peak mean monthly temperatures to occur during the same time. Thus the discrepancy may be in part due to model parameterization.

The future model temperature matched the best estimates of the average annual temperature change (3.2 to 7°F) (IPCC, 2007). Here again, the months of August and September appeared to be problematic, as they showed considerably lower increases in temperature change than the other months. This may be due to the extremes not properly being accounted for within the models and/or the CDF-transformation.

The hindcast model temperature had a moderate difference in AC rutting. For alligator cracking, the secondary case exhibited a negligible change, while the interstate case

showed a modest departure from that of the observed temperature data. The CRCM+CGCM3 model showed the poorest reproduction of observed conditions with regard to interstate alligator cracking. Yet, for secondary alligator cracking at Portland, ME the CRCM+CGCM3 model matched the observed conditions with no difference. The CRCM+CGCM3 model also had the greatest difference from baseline for both secondary and interstate AC rutting under the hindcast model period. While, no model exactly reproduced the observed conditions for using the hindcast model temperature data, one could conclude that for the area of interest the CRCM+CGCM3 model has the weakest results.

The potential impact of future temperature based on changes from observed temperature values on pavement performance was also shown to be modest for AC rutting and negligible for alligator cracking from this work. No trend is apparent with regards to location. The interior locations showed larger changes in interstate rutting, while the coastal locations showed greater increases in alligator cracking, yet no pattern was evident with regards to the distresses for the secondary case. For both distresses, the RCM3+GFDL model produced the largest overall change.

When the model periods are paired, the differences in AC rutting become much greater for all locations and cases. These differences occur at the same time or earlier. The change in the magnitude and time to failure for alligator cracking remains negligible for the secondary case and modest for the interstate case.

With the exception of interstate cracking, the pavement exceeds the acceptable levels of distress for baseline, hindcast, and future model conditions. The failure of the pavement under baseline conditions suggests that the pavement, both secondary and interstate, was underdesigned for the given traffic and climatic conditions. The hindcast conditions'

later failures compared to that of the baseline are likely due to the models decreased monthly temperatures. The future models equalling or lasting longer than baseline at 20% and 50% alligator cracking for the secondary case was due to the increase in temperature. It is expected that alligator cracking will decrease with an increase in temperature due to the increase in the asphalts' flexibility. AC rutting exceeded failure thresholds failing sooner in the future model than the baseline agrees with the modest increase in AC rutting for all locations. AC rutting was non-negligible for both the comparison of future model temperature to observed temperature and the paired model period differences. Furthermore, the difference in time to failure for AC rutting between the future and hindcast model temperature data indicates that road would require maintenance six years earlier. This suggests that climate change needs to be considered for pavement design and management where AC rutting potential exists.

The only other quantitative analysis of climate change impacts on pavement performance was conducted by Mills et al. (2007a, 2007b). In agreement with Mills et al., this work concludes that forecasted temperature changes and the resulting higher pavements temperatures increase the potential for rutting. Additionally, the M-E PDG results here and in Mills et al., were not universal, but nonetheless suggests that rutting and cracking will increase due to climate change.

Ultimately, the results of this work were based on many assumptions, including the pavement design as well as the climate scenarios. While changes in emissions scenarios would likely change the results, considering a nonstationary climate is shown to be important.

Future Work

No model or location stands out as exemplary. This consistency indicates that limited consideration of model to model variation is needed in order to fully assess the implications of climate change on pavement design and performance. Thus, a consistent approach for converting variables is recommended. This study uses hourly climatic files with RCM+AOGCM temperatures and the remaining variables (percent sunshine, precipitation, relative humidity, and wind) were not changed. Forecasted modifications to all variables are required to completely assess net impacts. Furthermore, the decoupling of the interactions among the variables potentially mutes the changes that temperature has on the performance of pavements in the future. Additionally, a greater range of climate scenarios across more locations would enhance confidence in the results. Modeling more pavement designs across a wider geographical area would provide designers and managers with insight into which pavements and locations should consider climate change effects and how to modify designs to minimize distress. The uncertainty associated with each scenario and its impact on the various pavement deterioration processes also needs to be considered as the work progresses. Quantifying the uncertainty will allow transportation managers and pavement designers to better understand the potential impacts of climate change on the future of pavement performance.

LIST OF REFERENCES

Akhtar, M., N. Ahmad, et al. Use of regional climate model simulations as input for hydrological models for the Hindukush-Karakorum-Himalaya region. *Hydrology and Earth System Sciences*, 2009, 13(7), pp. 1075-1089.

Fowler, H. J., S. Blenkinsop, et al. Linking climate change modeling to impacts studies: recent advances in downscaling techniques for hydrological modeling. *International Journal of Climatology*, 2007, 27(12), pp. 1547-1578.

Intergovernmental Panel on Climate Change. "Summary for Policymakers." *Climate Change 2007: The Physical Science Basis. Contribution of Working Group I to the Fourth Assessment report of the Intergovernmental Panel on Climate Change*, S. Solomon et al., eds., Cambridge University Press, Cambridge, U.K., (<http://www.ipcc.ch>), 2007.

Johanneck, L. and L. Khazanovich (2010). "Comprehensive Evaluation of Effect of Climate in Mechanistic-Empirical Pavement Design Guide Predictions." *Transportation Research Record*(2170): 45-55.

Michelangeli, P. A., M. Vrac, et al. Probabilistic downscaling approaches: Application to wind cumulative distribution functions. *Geophysical Research Letters* 36, 2009.

Mills, B., S. L. Tighe, et al. *The Road Well-Traveled: Implications of Climate Change for Pavement Infrastructure in Southern Canada*. Waterloo, Adaptation and Impacts Research Division, Environment Canada, and University of Waterloo, 2007.

Mills, B. N., S. L. Tighe, et al. Climate Change Implications for Flexible Pavement Design and Performance in Southern Canada. *Journal of Transportation Engineering-ASCE* 135(10), 2007, pp. 773-782.

National Research Council. *Potential Impacts of Climate Change on U.S. Transportation: Special Report 290*. Committee on Climate Change and U.S. Transportation. TRB. The National Academies Press, Washington, DC, 2008.

Rivington, M., D. Miller, et al. Downscaling regional climate model estimates of daily precipitation, temperature and solar radiation data. *Climate Research*, 2008, 35(3), pp. 181-202.

Transportation Research Board. *A Transportation Research Program for Mitigating and Adapting to Climate Change and Conserving Energy*. TRB, National Research Council, Washington, D.C., 2009.

Transportation Research Board. *Guide for Mechanistic-Empirical Design of New and Rehabilitated Structures*. NCHRP 36 Report I-37A. TRB, National Research Council, Washington, D. C., 2004

Yoder, Eldon J., and Matthew W. Witczak. Principles of Pavement Design. New York: Wiley, 1975.

APPENDIX A

To concatenated the individual netCDF files to form a single file for a period (either hindcast or future) for each variable. The following procedure was used.

Begin by opening Cygin. Point the environment variable UDUNITS2_XML_PATH to the udunits2.xml file with,

```
export UDUNITS2_XML_PATH='/usr/share/udunits/udunits2.xml'
```

Using the netCDF operator **ncrcat**, concatenate the individual file spanning five years to a single period. The syntax is as follows,

```
./ncrcat [input-files] [output-file]
```

For ease of use the input file should be put into the present working directory, and output files saved there as well.

APPENDIX B

MATLAB code used to extract the sub-region of from the concatenated netCDF files.

```
% Before One Starts Specify the Limits of the Data (x, y, time)
tic;
%% NetCDF Import
ncid=netcdf.open('filename','NC_NOWRITE');
varid=netcdf.inqVarID(ncid,'huss');
% Get NetCDF Data & Subdivide
data = netcdf.getVar(ncid,varid);
huss = data(:, :, :);
% Close NetCDF % Clear Variable Data
clearvars data varid
netcdf.close(ncid)
%% NetCDF Import
ncid=netcdf.open('filename','NC_NOWRITE');
varid=netcdf.inqVarID(ncid,'rsds');
% Get NetCDF Data & Subdivide
data = netcdf.getVar(ncid,varid);
rsds = data(:, :, :);
% Close NetCDF % Clear Variable Data
clearvars data varid
netcdf.close(ncid)
%% NetCDF Import
ncid=netcdf.open('filename','NC_NOWRITE');
varid=netcdf.inqVarID(ncid,'pr');
% Get NetCDF Data & Subdivide
data = netcdf.getVar(ncid,varid);
pr = data(:, :, :);
% Close NetCDF % Clear Variable Data
clearvars data varid
netcdf.close(ncid)
%% NetCDF Import
ncid=netcdf.open('filename','NC_NOWRITE');
varid=netcdf.inqVarID(ncid,'ps');
% Get NetCDF Data & Subdivide
data = netcdf.getVar(ncid,varid);
ps = data(:, :, :);
% Close NetCDF % Clear Variable Data
clearvars data varid
netcdf.close(ncid)
%% NetCDF Import
ncid=netcdf.open('filename','NC_NOWRITE');
varid=netcdf.inqVarID(ncid,'tas');
% Get NetCDF Data & Subdivide
data = netcdf.getVar(ncid,varid);
tas = data(:, :, :);
% Close NetCDF % Clear Variable Data
clearvars data varid
```

```

netcdf.close(ncid)
ncid=netcdf.open('...');
varid=netcdf.inqVarID(ncid,'...');
data = netcdf.getVar(ncid,varid);
uas = data(:, :, :);
clearvars data
netcdf.close(ncid)
ncid=netcdf.open('... WRITE');
varid=netcdf.inqVarID(ncid,'...');
data = netcdf.getVar(ncid,varid);
vas = data(:, :, :);
clearvars data
netcdf.close(ncid)
ncid=netcdf.open('... WRITE');
varid=netcdf.inqVarID(ncid,'...');
data = netcdf.getVar(ncid,varid);
lon = data(:, :);
clearvars data
varid=netcdf.inqVarID(ncid,'...');
data = netcdf.getVar(ncid,varid);
lat = data(:, :);
clearvars data
varid=netcdf.inqVarID(ncid,'...');
data = netcdf.getVar(ncid,varid);
time = data;
clearvars data
save('...')
toc;

```

APPENDIX C

MATLAB code used to extract the model point and convert NARCCAP variables into M-E PDG variables. Shown code is using the RCM+GFDL future scenario and model point 109, 48 as an example. Note: the difference in indexing with respect to the extracted region. Model point 109, 48 refers to the point in relation to complete NARCCAP region, point 16, 12 refers to the point's position in relation to the extracted region. This difference is due to the re-indexing upon extracting.

```
tic;
    Ft. Variables from Extracted Region
load RCM3_rc11_Future.mat
huss = huss(16, 12, :);
rsds = rsds(16, 12, :);
pr = pr(16, 12, :);
ps = ps(16, 12, :);
tas = tas(16, 12, :);
uas = uas(16, 12, :);
vas = vas(16, 12, :);
lat = lat(16, 12);
lon = lon(16, 12);
save PCM_rc11_Future_109_48.mat time lat lon huss rsds pr ps tas uas vas
%a
% Data, all the variables
% Fill Missing Value = 1e20 => NaN
% Typical Test to check the no. of Fill Missing Places
huss(huss == 1e20) = NaN;
NaNCount_huss = sum(sum(sum(isnan(huss))));
pr(pr == 1e20) = NaN;
NaNCount_pr = sum(sum(sum(isnan(pr))));
ps(ps == 1e20) = NaN;
NaNCount_ps = sum(sum(sum(isnan(ps))));
rsds(rsds == 1e20) = NaN;
NaNCount_rsds = sum(sum(sum(isnan(rsds))));
tas(tas == 1e20) = NaN;
NaNCount_tas = sum(sum(sum(isnan(tas))));
uas(uas == 1e20) = NaN;
NaNCount_uas = sum(sum(sum(isnan(uas))));
vas(vas == 1e20) = NaN;
NaNCount_vas = sum(sum(sum(isnan(vas))));
% calculate Variable Space
variable = zeros([size(lat, 1), size(lat, 2), 3*length(time)]);
time_lhr = zeros([size(lat, 1), size(lat, 2), 3*length(time)]);
huss_lhr = zeros([size(lat, 1), size(lat, 2), 3*length(time)]);
```

```

pr_1hr = zeros([size(lat, 1), size(lat, 2), 3*length(time)]);
ps_1hr = zeros([size(lat, 1), size(lat, 2), 3*length(time)]);
rsds_1hr = zeros([size(lat, 1), size(lat, 2), 3*length(time)]);
tas_1hr = zeros([size(lat, 1), size(lat, 2), 3*length(time)]);
uas_1hr = zeros([size(lat, 1), size(lat, 2), 3*length(time)]);
vas_1hr = zeros([size(lat, 1), size(lat, 2), 3*length(time)]);
Sp = zeros([size(lat, 1), size(lat, 2), 3*length(time)]);
Omega = zeros([size(lat, 1), size(lat, 2), 3*length(time)]);
Omega_1 = zeros([size(lat, 1), size(lat, 2), 3*length(time)]);
Omega_2 = zeros([size(lat, 1), size(lat, 2), 3*length(time)]);
Omega_S = zeros([size(lat, 1), size(lat, 2), 3*length(time)]);
Ra = zeros([size(lat, 1), size(lat, 2), 3*length(time)]);
Ra_Avg = zeros([size(lat, 1), size(lat, 2), 3*length(time)]);
Rso = zeros([size(lat, 1), size(lat, 2), 3*length(time)]);
RH = zeros([size(lat, 1), size(lat, 2), 3*length(time)]);
e = zeros([size(lat, 1), size(lat, 2), 3*length(time)]);
es = zeros([size(lat, 1), size(lat, 2), 3*length(time)]);
Pr = zeros([size(lat, 1), size(lat, 2), 3*length(time)]);
T = zeros([size(lat, 1), size(lat, 2), 3*length(time)]);
W = zeros([size(lat, 1), size(lat, 2), 3*length(time)]);
    Convert 3-hour time steps to 1-hour time steps
    NCEP Primary 3-hourly 1000 hPa (2-D) Tab 0.2 --> hourly
    TIME
x = datenum('0000-01-01 01:00:00', 'YY-MM-DD HH:MM:SS');
for i = 1:length(time);
    time_1hr(3*(i-1)+1) = time(i) - x;
    time_1hr(3*(i-1)+2) = time(i);
    time_1hr(3*(i-1)+3) = time(i) + x;
end
    Day: 01-01-00 00:00:00 --> 01-01-00
    Time: Since 01-01-01 00:00:00 --> 01-01-00
time_1hr = time_1hr + datenum('2003-01-01 00:00:00', 'YYYY-MM-DD
HH:MM:SS');
Time_1hr = cellstr(datestr(time_1hr, 'YYYY-MM-DD HH:MM:SS'));
    Create humidity, rhus (0.00-1)
for i = 1:length(time);
    rhus_1hr(:, :, (3*(i-1)+1)) = rhus(i);
    rhus_1hr(:, :, (3*(i-1)+2)) = rhus(i);
    rhus_1hr(:, :, (3*(i-1)+3)) = rhus(i);
end
    Precipitation, pr (0.00-2.00)
for i = 1:length(time);
    if i == 1
        pr_1hr(:, :, (3*(i-1)+1)) = pr(i);
        pr_1hr(:, :, (3*(i-1)+2)) = pr(i);
    else
        pr_1hr(:, :, (3*(i-1)+0)) = pr(i);
        pr_1hr(:, :, (3*(i-1)+1)) = pr(i);
        pr_1hr(:, :, (3*(i-1)+2)) = pr(i);
    end
end
    Surface pressure, ps (10)
for i = 1:length(time);
    ps_1hr(:, :, (3*(i-1)+1)) = ps(i);
    ps_1hr(:, :, (3*(i-1)+2)) = ps(i);
    ps_1hr(:, :, (3*(i-1)+3)) = ps(i);
end

```

```

for i = 1:length(time);
    if i == 1
        rsds_lhr(:, :, (3*(i-1)+1)) = rsds(1);
        rsds_lhr(:, :, (3*(i-1)+2)) = rsds(1);
    else
        rsds_lhr(:, :, (3*(i-1)+0)) = rsds(1);
        rsds_lhr(:, :, (3*(i-1)+1)) = rsds(1);
        rsds_lhr(:, :, (3*(i-1)+2)) = rsds(1);
    end
end

% Temperature, tas (K)
for i = 1:length(time);
    tas_lhr(:, :, (3*(i-1)+1)) = tas(1);
    tas_lhr(:, :, (3*(i-1)+2)) = tas(1);
    tas_lhr(:, :, (3*(i-1)+3)) = tas(1);
end

% Uul Surface Wind Speed, uas (m s^-1)
for i = 1:length(time);
    uas_lhr(:, :, (3*(i-1)+1)) = uas(1);
    uas_lhr(:, :, (3*(i-1)+2)) = uas(1);
    uas_lhr(:, :, (3*(i-1)+3)) = uas(1);
end

% Meridional Surface Wind Speed, vas (m s^-1)
for i = 1:length(time);
    vas_lhr(:, :, (3*(i-1)+1)) = vas(1);
    vas_lhr(:, :, (3*(i-1)+2)) = vas(1);
    vas_lhr(:, :, (3*(i-1)+3)) = vas(1);
end

% Latent Heat Flux, huss (W m^-2)
clearvars huss pr es es es
% Create NARCCOS2 variables for NCEP2 analysis
% Total cloud radiative forcing
% Surface evaporation, es (W m^-2)
% Surface precipitation, pr (W m^-2)
e = huss_lhr.*(ps_lhr/0.622);
es = 611*exp((17.27.*(tas_lhr-273.15))./(237.3 + (tas_lhr-273.15)));
RH = (e./es)*100;
RH(RH >= 100)=100;
RH = reshape(RH, length(time_lhr), 1);
% Surface precipitation, pr (W m^-2)
pr = pr_lhr*3600*0.0393700787;
pr(pr < 0)=0;
pr = reshape(pr, length(time_lhr), 1);
% Surface evaporation, es (W m^-2)
inputDate = time_lhr;
[day, fraction] = date2doy(inputDate);
hour = str2double(cellstr(datestr(time_lhr, 'HH')));
t = hour - 5.5;
t = reshape(t, 1, length(time_lhr));

```



```

Lz = 75;
Lm, Longitude of the Location [degrees R]
Lm = 360 - lon;
Sc, Seasonal Correction for Solar Time
b = (2*pi()*(doy - 81))/364;
Sc = 0.1645*sin(2*b) - 0.1255*cos(b) - 0.025*sin(b);
Omega, Solar Time at Midpoint of Period
for i = 1:length(time_lhr);
Omega(:, :, i) = (pi()/12).*((t(1,i) + 0.06667.*(Lz-Lm) + Sc(1,i)) - 12);
end
Omega_1, Solar Time at the Beginning of the Period
Omega_1 = Omega - (pi()*1)/24;
Omega_2, Solar Time at the End of the Period
Omega_2 = Omega + (pi()*1)/24;
Lat, (Degree) to Lat. (Radian)
Lat = (pi/180)*lat;
Solar Constant, G (MJ m^-2 min^-1)
G = 0.0820;
Inverse relative distance Earth-Sun, dr
dr = 1 + 0.033*cos(((2*pi())/365)*doy);
Solar Declination, delta (Radian)
delta = 0.409*sin(((2*pi())/365)*doy - 1.39);
Omega_S, Sunset Solar Angle
for i = 1:length(time_lhr);
Omega_S(:, :, i) = acos(-tan(Lat).*tan(delta(1,i)));
end
Extraterrestrial Radiation, Pa (MJ m^-2 hour^-1)
for i = 1:length(time_lhr);
Ra(:, :, i) = (12*60/pi())*G*dr(1,i).*((Omega_2(:, :, i)-
Omega_1(:, :, i)).*sin(Lat).*sin(delta(1,i))) +
(cos(Lat).*cos(delta(1,i)).*(sin(Omega_2(:, :, i))-
sin(Omega_1(:, :, i))));
end
if Omega > Omega_S or Omega < -Omega_S by definition Pa = 0
for i = 1:length(time_lhr);
if ((Omega(:, :, i) > Omega_S(:, :, i)) || (Omega(:, :, i) < -
Omega_S(:, :, i)));
Ra(:, :, i) = 0;
end
end
Average Extraterrestrial Radiation, Pa Avg (MJ m^-2 hour^-1)
for i = 1:length(time_lhr);
if i <= 2 && (hour(i, :) == 3 || hour(i, :) == 6 || hour(i, :) == 9 ||
hour(i, :) == 12 || hour(i, :) == 15 || hour(i, :) == 18 || hour(i, :) ==
21 || hour(i, :) == 0);
Ra_Avg(:, :, (i-1)) = (Ra(i) + Ra(i-1))/2;
Ra_Avg(:, :, i) = (Ra(i) + Ra(i-1))/2;
elseif i > 2 && (hour(i, :) == 3 || hour(i, :) == 6 || hour(i, :) == 9
|| hour(i, :) == 12 || hour(i, :) == 15 || hour(i, :) == 18 || hour(i, :)
== 21 || hour(i, :) == 0);
Ra_Avg(:, :, (i-2)) = (Ra(i) + Ra(i-1) + Ra (i-2))/3;
Ra_Avg(:, :, (i-1)) = (Ra(i) + Ra(i-1) + Ra (i-2))/3;
Ra_Avg(:, :, i) = (Ra(i) + Ra(i-1) + Ra (i-2))/3;
end
end
Daily solar radiation, kJ m^-2 hour^-1
a = 0.25;

```

```

b = 0.50;
Rso = (a+b).*Ra_Avg;
% Convert Rso (W m^-2) to (kWh m^-2)
Rso = (1/0.0036).*Rso;
% Convert Rso to Sp (kWh m^-2)
Sp = (rsds_1hr./Rso)*100;
for i = 1:length(time_1hr);
    if Ra(:, :, i) == 0 && rsds_1hr(:, :, i) == 0;
        Sp(:, :, i) = 0;
    elseif Ra(:, :, i) == 0 && rsds_1hr(:, :, i) ~= 0;
        Sp(:, :, i) = Sp(:, :, (i-1));
    end
end
end
Sp(Sp>=100)=100;
Sp = reshape(Sp, length(time_1hr), 1);
% Temperature, T (F)
% T (K) -- (degree C) --> (degree F)
T = (tas_1hr - 273.15)*(9/5) + 32;
T = reshape(T, length(time_1hr), 1);
% Wind Speed, W (m s^-1)
% uas & vas (m s^-1) --> (m s^-1)
uas_1hr = 2.23693629*uas_1hr;
vas_1hr = 2.23693629*vas_1hr;
W = sqrt((uas_1hr.^2) + (vas_1hr.^2));
W = reshape(W, length(time_1hr), 1);
% Create variables $ W, T, Sp, Pr, RH
% To export the relevant matrix to Excel for Windows (and use the
% default 1000 base system),
Time = time_1hr-datetime('2010-10-13 00');
Time = reshape(Time, length(time_1hr), 1);
% concatenate variables to an array
MEPDG = horzcat(Time, T, W, Sp, Pr, RH);
save('M3_01_E_10_13_08_MEPDG.mat', 'Time', 'T', 'W', 'Sp', 'Pr', 'RH');
toc;

```

APPENDIX D

R script used to execute the package to perform the CDF-transformation. The Downscaled_Data.dat contains the downscaled data produced from the CDF-t method. The Output_Data.dat contains the necessary information to develop the graphs associated with the CDF-t method.

```
library(CDFt) # load package "CDFt"

Data_1 <- read.csv("CDFt_1.csv", skip = 0, sep = ",", dec = ".", header = TRUE) # load data table
Data_2<- read.csv("CDFt_2.csv", skip = 0, sep = ",", dec = ".", header = TRUE) # load data table

### Set Variables

ObsRp = Data_1$ObsRp
DataGp = Data_1$DataGp
DataGf = Data_2$DataGf

### Call CDFt Method

Results = CDFt(ObsRp, DataGp, DataGf, npas = 100, dev = 2)

x <- Results$x
FGp <- Results$FGp
FGf <- Results$FGf
FRp <- Results$FRp
FRf <- Results$FRf

x <- Results$x
DS <- Results$DS

### Write Downscaled Data to Table

write.table(DS, file = "Downscaled_Data.dat", append = FALSE, sep = ",", dec = ".", col.names =
TRUE)

Output = data.frame(x =x, FRp = FRp, FGp = FGp, FRf = FRf, FGf = FGf)

write.table(Output, file = "Output_Data.dat", append = FALSE, sep = ",", dec = ".", col.names =
TRUE)
```

Statistics

CramerVonMisesTwoSamples(ObsRp, DataGp)

CramerVonMisesTwoSamples(ObsRp, DataGf)

CramerVonMisesTwoSamples(ObsRp, DS)

KolmogorovSmirnov(ObsRp, DataGp)

KolmogorovSmirnov(ObsRp, DataGf)

KolmogorovSmirnov(ObsRp, DS)